Use of High Intensity Focused Ultrasound to Destroy Subcutaneous Fat Tissue

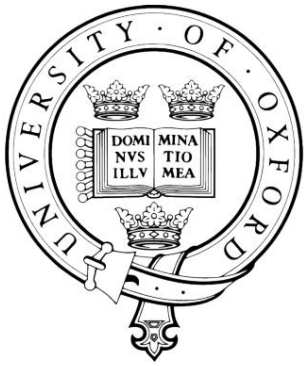

Zoe Kyriakou

Department of Engineering Science

University of Oxford

A thesis submitted for the degree of

Doctor of Philosophy

2010

Acknowledgments

The completion of this dissertation has been one of the most significant academic challenges I have ever had to face. Without the continuous support, patience and understanding of the following people, this study would not have been completed.

First and foremost, I would like to thank my supervisor Pr. Constantin-C. Coussios, for his invaluable guidance and commitment from the initial to the final stages of my research. He greatly inspired me to work in this project. He encouraged me to not only grow as a researcher, but also as an independent thinker. He not only taught me acoustics, but how to look at the "bigger picture" and what re-search is about. These few words cannot suffice to express my gratitude.

I also owe a special thank you to Dr. Manish Arora. I am very grateful for his never-ending willingness to help me with all possible problems that arose over the course of this project.

The interdisciplinary nature of this research called for a variety of advanced histological techniques. I would like to thank Dr. Tahera Ansari and Pr. Paul Sibbons for introducing me to histology and for spending time with me explaining and clarifying many new concepts.

I would also like to thank Sorisa (Barcelona, Spain) for sponsoring the majority of the research presented in this thesis. I am grateful to Dr Albert Amat, and to his colleague Marc Ignasi Corral-Baques for enabling the in vivo experiments presented in Chapter 6.

Mr. James Fisk must also be credited for turning my first draft designs to excellent structures and within very tight time-frames. I would also like to thank Mr. Colin Dawson, Mr. Steve Morris and Mr. David Torjussen for always providing me with fresh tissue, the quality of which was of major importance for the quality of this work.

My graduate studies would not have been such an enjoyable and exceptional experience if it weren't for all the members of the Biomedical Ultrasonics and Biotherapy Laboratory, both present and past, and the unique atmosphere we all shared in the lab. Conversation with other DPhil students and post-doc researchers proved very valuable; in particular those with Dr. Jamie Collin, Bassel Rifai and Natalie Hockham. My friends both in Oxford and in Greece were always a source of support and understanding. I would like to specially thank Dr. Miriam Bazan, Natalie Hockham, Emilie Holland, Xenia Kesoglidou, Bettina Koller, Lia Koudouni, Vithleem Kyriakidou and Eleonora Mylonopoulou, with whom I shared my thoughts, frustrations and considerations but also some of the best and definitely unforgettable moments during my time as a graduate student.

On a more personal note, I would like to express my most heartfelt thanks to my parents, Michali and Popi, for their continuous support and encouragement throughout all these years. Their endless and unconditional love and tolerance have enabled me to not only complete this dissertation successfully and on time but most importantly to fully enjoy my time as a graduate student. I am also very grateful to my brother Vassilis for his endless emotional support and for always being there whenever I need a piece of sound advice or someone to talk to.

Finally and most importantly, I would like to thank Alexandros Antoniadis for his continuous patience, understanding and love and for always having my calm and happiness as his first priority.

Abstract

Given the great promise of High Intensity Focused Ultrasound (HIFU) as a therapeutic modality, the aim of the present study is to develop and optimise a technique that uses externally applied focused ultrasound energy and remote, ultrasound-based treatment monitoring to destroy subcutaneous fat safely, effectively and non-invasively. Based on initial cavitation and temperature measurements performed *ex vivo* in excised porcine fat at four different frequencies (0.5, 1.1, 1.6 & 3.4MHz) over a range of pressure amplitudes and exposure durations, it was concluded that 0.5MHz is the optimal frequency for this application since it is capable of instigating inertial cavitation at relatively modest pressures while enhancing focal heat deposition. Histological assessment of tissue treated above the cavitation threshold at 0.5MHz both *ex* vivo and *in vivo* demonstrated damage to adipocytes and connective tissue. Furthermore, a good correlation was identified between the energy of broadband emissions detected by the passive cavitation detector (PCD) and the focal temperature rise at 0.5MHz during *ex vivo* experimentation, which could be exploited as a tool for non-invasive monitoring of successful treatment delivery. In addition, localisation of cavitation activity by means of passive cavitation detection was achieved and shown to provide a strong indicator of the location of induced histological damage. Based on the specific requirements identified during initial experimentation, an application-specific HIFU transducer, cavitation detector and real-time treatment monitoring software was developed and tested *ex vivo.* This treatment system was found capable of producing extensive damage to adipocytes and collagen confined to the subcutaneous fat layer at the desired treatment depth, which coincided with the location of cavitation activity as displayed by the real-time treatment monitoring software.

Contents

List of Figures

List of Tables

Nomenclature

B/A	Parameter of non-linearity
I	Intensity
Q	Rate of heating
R	Bubble radius
Z	Characteristic acoustic impedance
c	Speed of sound
f	Frequency
k	Wave number
p	Pressure
$pkpk$	Peak-to-peak
s	Entropy
t	Time
a	Attenuation coefficient
a_{α},	Absorption coefficient
a_s	Scattering coefficients
κ	Compressibility
λ	Wavelength
ρ	Density
τ	Perfusion time constant
ω	Angular frequency

1 Introduction

1.1 Motivation for the project

Surgery is currently the most commonly used technique to remove excessive fat deposits within the human body. The idea of developing a non-invasive technique for lipolysis is not new, since the general trend nowadays is towards clinical applications, therapies and techniques that require minimum intervention to the patient, resulting in minimum discomfort, pain, bleeding, side-effects, post-operative bruising and swelling.

Given the great promise of ultrasound as a therapeutic modality, there are a number of factors that motivated this research, which include (i) the fact that the mechanisms for optimal fat destruction by ultrasound remain poorly understood, (ii) that there is currently no device that works effectively and safely in destroying fat cells non-invasively and (iii) that there are no reliable techniques for monitoring tissue destruction in real-time. The aim of this research is therefore to develop and optimise a technique that uses externally applied ultrasound energy and remote, ultrasound-based treatment monitoring to destroy subcutaneous fat safely, effectively and non-invasively.

1.2 Sonolysis

The idea of using sound waves to selectively destroy excess fat is not new. In particular ultrasound, which refers to sound waves of frequency above 20kHz, has attracted increasing interest as a potential tool for selectively destroying subcutaneous fat. Ultrasound was firstly used as an invasive body contouring technique that selectively destroyed undesired fat tissue and resulted in the lysis of the fat cell membrane (Giuseppe A.Ferraro 2007)(Ferraro 2007), which was then manually remodelled and

removed using a suction surgical device and was known as ultrasound-assisted liposuction (UAL). This technique provided several advantages over traditional liposuction *i.e.* improved contour, decreased revision rate, less surgeon fatigue and less bruising in fibrous areas. In order to decrease the postoperative complications, UAL was improved and modified and the resulting technique became known as external ultrasound-assisted liposuction (XUAL). The damaged tissue was then removed using traditional liposuction. The drawbacks and accompanying risks of these invasive procedures in fat removal, *i.e.* skin burns, hematomas, extensive cutaneous necrosis over the abdomen, pain and discomfort, (Ablaza et al. 1998;Cedidi and Berger 2002;Ferraro et al. 2008;Lawrence and Cox 2000;Mendes 2000;Perez and van Tetering 2003;Rohrich et al. 1998) motivate the search for a safer and truly non-invasive method of lipolysis.

More recently, HIFU has been proposed as a tool for non-invasive lipolysis, with a number of treatment systems being commercially available. The LipoSonix system (Medicis Technologies Corporation, USA) operates at 2MHz and utilizes intensities greater than 1,000W/cm^2, whereas other ultrasound systems available on the market for body sculpting operate at 0.2MHz and at intensities as low as 17.5W/cm^2.

1.3 Thesis outline

Chapter 2 starts by introducing the anatomy of adipose tissue and provides an overview of the fundamental physics governing the propagation of ultrasound in media with various acoustic properties. A brief review of the numerous applications of therapeutic ultrasound is then provided, before describing the generation of acoustic waves. Ultrasound induced bioeffects are then described, with particular emphasis on acoustic

cavitation. Techniques for therapy monitoring in current clinical use are then discussed, alongside novel methods currently under development in the laboratory.

Chapter 3 introduces the reader to the overall experimental rationale and procedure used in developing and optimizing the non-invasive lipolysis technique. It starts by giving an outline of the acoustical experimental setup, describing both the existing facilities that were available in the Oxford biomedical ultrasonics and biotherapy laboratory, as well as the additional devices that were built solely for the purpose of this research. The experimental procedure followed before, during and after each and every experiment is also described in detail.

Chapter 4 covers the preliminary results obtained from experiments performed in the laboratory on *ex vivo* fat and focuses on issues related to data acquisition, post-processing and analysis. The first section is devoted to the full characterization of the high intensity focused ultrasound (HIFU) transducers used in the various phases of this research. A first set of measurements of ultrasound attenuation in subcutaneous fat acquired at four different frequencies under consistent experimental conditions is then presented. Both cavitation and temperature measurements were obtained at four different HIFU frequencies and detailed results are presented hereafter. Based on these results, conclusions were then drawn to enable optimization of the treatment delivery.

Chapter 5 presents preliminary *ex vivo* histological results obtained in the laboratory using excised porcine subcutaneous adipose tissue and a preliminary experimental setup using a spherically focused ultrasound transducer. The first section shows untreated samples that served as control samples. A detailed description of the macroscopic and microscopic damage observed following cavitation inducing exposures is shown in the

next sections, before introducing the conclusions reached from the histological investigation.

Chapter 6 presents acoustic and histological results obtained during *in vivo* experimentation using the preliminary experimental setup with a spherically focused HIFU transducer. The first part describes the portable experimental setup built for these experiments, the way the animal donor was prepared and the treatment plan followed. Acoustic measurements and detailed histological results are then presented, followed by the conclusions reached.

Chapter 7 focuses on techniques developed for treatment monitoring and starts by describing the correlation between the inertial cavitation activity and the focal temperature rise that was found to exist in adipose tissue. Localisation of cavitation activity by means of passive cavitation detection and its correlation with histological damage is then explained, alongside the detailed volumetric tissue analysis performed.

Chapter 8 presents the application-specific HIFU transducer, cavitation detector and real-time treatment monitoring software that was developed for non-invasive lipolysis based on the optimisation of the ultrasound exposure parameters achieved so far. A full characterization of this HIFU transducer is presented and an analysis of the acoustic and histological data obtained in *ex vivo* adipose tissue following ultrasound exposures with this new setup follows.

Chapter 9 summarises all accomplishments and limitations of the present work.

2 Literature Review

The aim of this research is to develop a non-invasive technique to destroy subcutaneous adipose tissue using High Intensity Focused Ultrasound (HIFU) waves generated by a focused transducer positioned outside the human body. An understanding of the physiological properties of the tissue in question and an explanation of the fundamental physics governing the propagation of sound are thus required. This chapter also provides the reader with an overview of the governing principles and applications of therapeutic ultrasound and of the various mechanical and thermal effects which it can induce in tissue. Current methods of monitoring HIFU treatments are also introduced and their applicability to sono-lipolysis is assessed.

2.1 Properties of adipose tissue

2.1.1 Anatomy of adipose tissue

The word ‘adipose tissue’ is used to describe fat tissue, which is scattered throughout the body, forming an organ as regards to both its structure and function. There are two types of mature adipocytes organized in this multidepot organ, white and brown, each having different colour, function and histology (Avram et al. 2005;Cinti 2005). Brown fat is most widely distributed in babies, tends to gradually disappear by the age of one and is specialised for heat production. White adipose tissue provides long term fuel storage at a high energy density, thermal insulation and mechanical protection of underlying tissues. Other primary functions include the uptake, synthesis and storage of lipid and release of fatty acids in response to various stimuli (Trayhurn 2006).

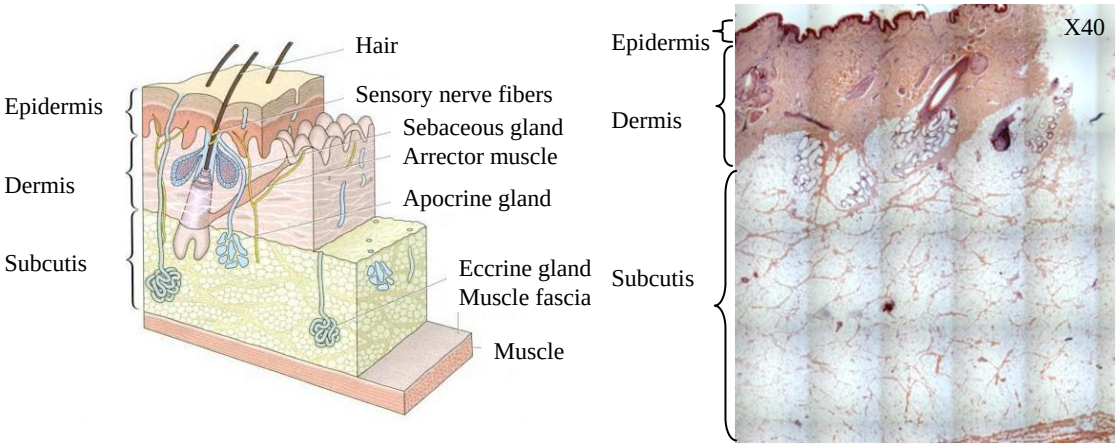

Figure 2-1: Three dimensional diagram of the epidermis, dermis, subcutaneous fat and muscles. Figure adapted from (Sterry et al. 2006) (left). A transverse histological section obtained by scanning a large tissue slide is showing the epidermis on top, the dermis and the subcutaneous fat layer organised in lobules. Each individual scan is magnified by 40 (right).

Subcutaneous adipose tissue is the deepest of the three layers of the skin, as shown in the three dimensional diagram in Figure 2-1 (left). The outer layer is the epidermis with its thickness ranging between 0.05mm and 1.5mm, followed by the dermis with its thickness varying between 0.3mm and 3mm. Subcutaneous tissue is a layer of fat and its thickness varies significantly throughout the body and from human to human. It represents about 80% of all body fat and comprises of white adipocytes, which unless severely depleted, are spherical; an unusual shape for functionally mature animal cells. In people, their diameter ranges between 30-70μm and their volume between 0.1-1nl, thousands of times larger than red blood cells. Lipids within the white adipocytes are organized within one large, unilocular droplet, the size of which can exceed 50μm, and therefore occupy the majority of the intracellular space. The lipid droplet has no internal structure and compresses the cytoplasm and the rather small nucleus towards the cellular membrane. A transverse histological section obtained by scanning a large tissue slide under a light microscope, is showing the epidermis, the dermis and the subcutaneous adipose tissue in Figure 2-1 (right). Adipocytes are all held together by a mesh of fibres that are composed of collagen and receive a vascular and nerve supply. Fatty tissue is homogeneous and

bright cadmium-like yellow. A variation in colour may indicate a pathologic process: white to white/yellow in fat necrosis, paler yellow in lipoma, redish in angio-lipoma (Pond 1998;Sternberg 1992).

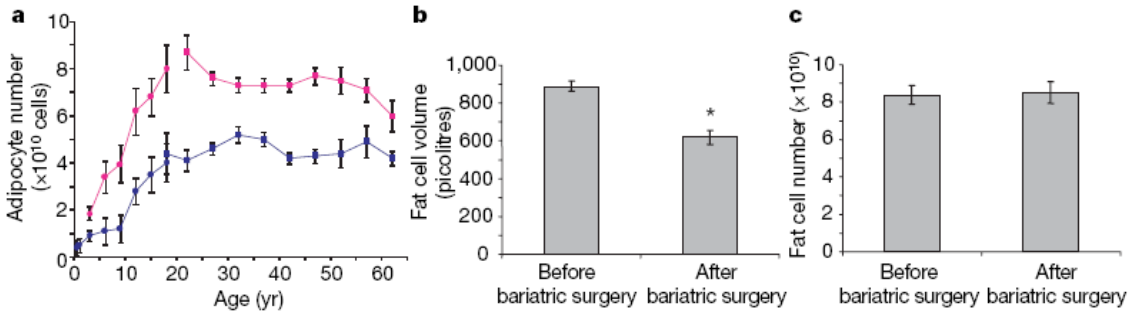

Figure 2-2: a) The adipocyte number increases in childhood and adolescence, with the number levelling off and remaining constant in adulthood in both lean (blue) and obese (pink) individuals. b) Major weight loss by bariatric surgery results in significant decrease in cell volume but c) fails to reduce adipocyte cell number (1-2 years post-surgery). Figure adapted from (Spalding et al. 2008).

The total fat mass of a human body is determined by both the adipocyte number and size. There are thus two kinds of obesity: hypertrophic adiposity, which is characterized by larger-than-normal adipocytes in normal numbers, and hyperplastic adiposity, which is characterized by regular-sized adipocytes of a greater quantity (Zocchi 1992). According to recent research the total adipocyte number in all individuals is increased during childhood and adolescence and remains constant in adulthood. Given that the cell death rate is similar for all individuals; obese adults produce a greater number of new adipocytes every year so that the total number of adipocytes remains constant (Spalding et al. 2008). As shown in Figure 2-2, bariatric surgery results in great weight loss by reducing the size and not the total number of adipocytes in an adult's body.

2.1.2 Histology of adipose tissue

The following section describes the various different histological procedures available in the literature to enable the study of the anatomy of the adipose tissue at a cellular level under a microscope. Such methods refer to appropriate means of fixing, sectioning and staining adipose tissue to evidence salient features that are relevant to the present investigation. The methods specifically chosen for the present work will be then described in greater detail in Chapter 3. Figure 2-3 shows a typical histological section with spherical adipocytes and peripheral nuclei being compressed towards the thin rim of the cytoplasm (Kerr 1999).

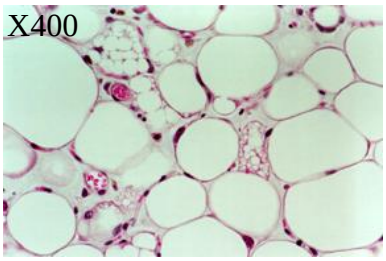

Figure 2-3: Adipocytes in a histological section stained with H&E showing small nuclei being compressed towards the thin rim of cytoplasm and a single fat droplet per cell. Figure adapted from (Kerr 1999).

Fixing is required in order to prevent degradation of the tissue and to maintain the structure of the cell and of the sub-cellular components. This can be done by immersing the sample in 10% neutral buffered formalin (NBF) and then embedding it in paraffin, rendering the sample suitable for sectioning using the microtome.

An alternative option is to freeze the sample from fresh in one of the following two ways: i) drop the tissue into a mould of Optimal Cutting Temperature (OCT) compound and let it freeze inside a dish of iso-pentane positioned over dry ice, a technique that allows the tissue to slowly achieve a uniform low temperature or ii) drop the tissue in

liquid Nitrogen, a method most widely known as ‘snap freezing’. However, snap freezing has the disadvantage of a non-uniform freezing that might result in the break of the micro-structure and was therefore considered inappropriate for our case. Sectioning of frozen samples is done using a microtome operating at low temperature, called cryotome.

Some of the available staining techniques for lipids are presented in Table 2-1 (Bancroft and Cook 1994;Ross et al. 1989;Sternberg 1992;Walgenbach et al. 2001).

Table 2-1: Staining techniques for lipids (Bancroft and Cook 1994;Sternberg 1992).

Stain type	*Specific compound it stains*	*Comments*
Haematoxylin (H)	nucleus- blue	very widely used when paired together (H&E)
Eosin (E)	cytoplasm - pink	
Masson's trichrome	nucleus – black cytoplasm – red/pink collagen fibers & mucus– blue/green	used for connective tissue; available in a variety of 3-colour combinations
Oil-red O	lipids - red nuclei – blue	most common technique for lipids, intense stain and fast procedure
Sudan black	lipids - dark blue to black	restricts its application to single-staining techniques and might non-specifically stain other substances such as coagulated proteins
Picro Sirius	healthy collagen- red under light microscope/ bright orange under polarised light	distinguishes between healthy/ unhealthy collagen,
Congo red stain	Lipo-polysaccharide (LPS)	diagnosis of certain illnesses

2.2 Basics of ultrasound

There are two kinds of waves: transverse waves, where the displacement of the particles in the medium through which the wave travels is perpendicular to the direction of motion

of the wave, and longitudinal waves, where the particles are displaced parallel to the direction of motion of the wave (Leighton TG 1994), like sound waves. The term ultrasound refers to sound waves of frequency in excess of 20kHz, which represents the upper limit of human hearing.

2.2.1 Sound propagation

Propagation of a sound wave through a medium requires that the medium has both mass and elasticity. Elasticity, generally represented in acoustics by the medium compressibility, κ, forces the medium to resist any changes being induced by the propagating acoustic wave and to return to its initial state. Inertia, represented by the mass density, ρ, causes the motion to overshoot, thus requiring a correction in the opposite direction. This results in wave propagation.

The equation governing the propagation of a small amplitude acoustic wave through a non-viscous, homogeneous and linear medium can be derived given three fundamental equations: the continuity equation, which expresses conservation of mass, Euler's equation describing the conservation of momentum and the differential equation of state relating pressure and density changes. Combining these three equations yields the linear wave equation,

$$\nabla^2 p = \frac{1}{c^2}\frac{\partial^2 p}{\partial t^2} \qquad \text{Equation 2-1}$$

where c represents the linear speed of sound that can be related to the density and compressibility as follows:

$$c = \left(\frac{\partial p}{\partial \rho}\right)^{\frac{1}{2}} = \frac{1}{\sqrt{\kappa\rho}} \qquad \text{Equation 2-2}$$

For the majority of the present work, it can safely be assumed that all acoustic waves produced by the sound generating devices during experimentation are essentially planar. It is therefore the plane wave solution to Equation 2-1 that is of interest. The sound pressure of a plane wave travelling in the *x*-direction is given by Equation 2-3 and its acoustic intensity by Equation 2-4, respectively.

$$p(x,t) = Pe^{i(k_o x - \omega t)} \qquad \text{Equation 2-3}$$

$$I = \frac{{p_{rms}}^2}{Z} = \frac{{p_{rms}}^2}{\rho c} \qquad \text{Equation 2-4}$$

where P is the peak pressure amplitude, I the acoustic intensity, k_o the wave number, x the position along the axis of sound propagation, ω *the* angular frequency, t time, Z the characteristic acoustic impedance, ρ the density and c the speed of sound (Morse and Ingard 1968).

2.2.2 Speed of sound

Existing methods for measuring the speed of sound are usually accurate within 1%. In biological tissues where the ultrasound frequencies of interest cover a very wide range, measurements can be quite inaccurate (Hill et al. 1986), especially when the tissue in question is very small and fragile, such as the thin septa that separate fat lobules within the adipose tissue.

It has been shown that the speed of sound within a soft tissue is very well correlated with its density (Mast T. D. 2000), which in other words means that tissues with a high concentration of collagen or other proteins have a relatively high density and therefore speed of sound, whereas tissues with greater fat content have a relatively lower density and speed of sound. As shown in Figure 2-4, most liquids and soft tissues have a sound

speed higher than that of water: this is not true for fat, which has lower speed of sound than water due in part to the low density of lipids.

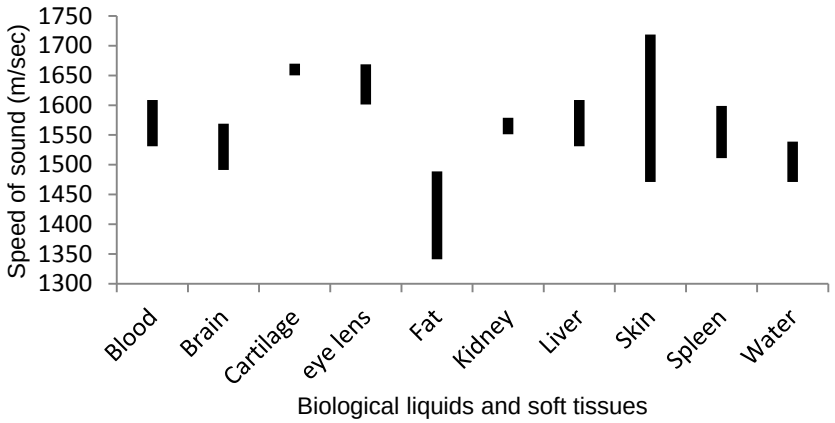

Figure 2-4: Ranges of values for the speed of sound in various biological media. Figure adapted from (Hill et al. 1986).

For biological tissues, sound speed varies little with frequency and increases with increasing hydrostatic pressure. Furthermore, it is interesting to note that the speed of sound in most tissues increases with increasing temperature, though the converse is true for fat, which behaves more like non-aqueous liquids, presumably because of its low water content (Hill et al. 1986).

2.2.3 Nonlinearity of the acoustic medium

"Nonlinearity is a property of a medium by which the shape and amplitude of a signal at a location are no longer proportional to the input excitation" (Szabo 2004).

In general, any thermodynamic quantity can be expressed as a function of another two. If pressure p is expressed as a function of density ρ and entropy s, a Taylor series expansion along the isentrope $s=s_0$ yields

$$P - P_0 = \left(\frac{\partial P}{\partial \rho}\right)_{s,0} (\rho - \rho_0) + \frac{1}{2!}\left(\frac{\partial^2 P}{\partial \rho^2}\right)_{s,0} (\rho - \rho_0)^2 + \ldots \qquad \text{Equation 2-5}$$

where P and ρ are the pressure and density respectively, P_0 and ρ_0 are their ambient values and s is specific entropy. The nonlinearity of a medium is generally described by the parameter *B/A*, which is proportional to the ratio of coefficients of the quadratic and linear terms in this Taylor series (Hamilton and Blackstock 1998). The *B/A* parameter is indicative of the magnitude of the departure from linearity and its significance is its effect on sound speed, as shown by Equation 2-2. A linear medium is one whose *B/A* value is equal to zero (Hill et al. 1986). Most commonly, the coefficient of nonlinearity β is used, which is defined as

$$\beta = 1 + \frac{B}{2A} \qquad \text{Equation 2-6}$$

The speed of sound increases with increasing hydrostatic pressure, which leads to the non-linear behaviour of sound propagation. As a single-frequency plane wave propagates through a non-linear medium, distortion begins because the particle velocity in the compressional phase of the wave is greater than in the rarefactional phase. Distortion is a cumulative event that leads to the formation of a shock wave, which is rich in harmonics of the excitation frequency. The shock formation results in the leakage of energy from the fundamental frequency to its higher harmonics. The extent to which such leakage occurs depends on the amplitude of the incident wave, on the nonlinearity of the medium and on the distance travelled by the wave into the medium (Hamilton and Blackstock 1998;Muir and Carstensen 1980). In other words, the larger the *B/A* parameter of the propagating medium the earlier the shock wave is formed and the more the wave is distorted at a particular distance from the source. The non-linearities will be observed earlier for sound waves of high frequency than for those of low frequency, because of the

cumulative build up of the effects over the distance measured in wavelengths (Hill et al. 1986). An illustration of a high intensity sound wave transmission, distortion, harmonic generation and shock formation, followed by the effect of increased absorption is shown in Figure 2-5.

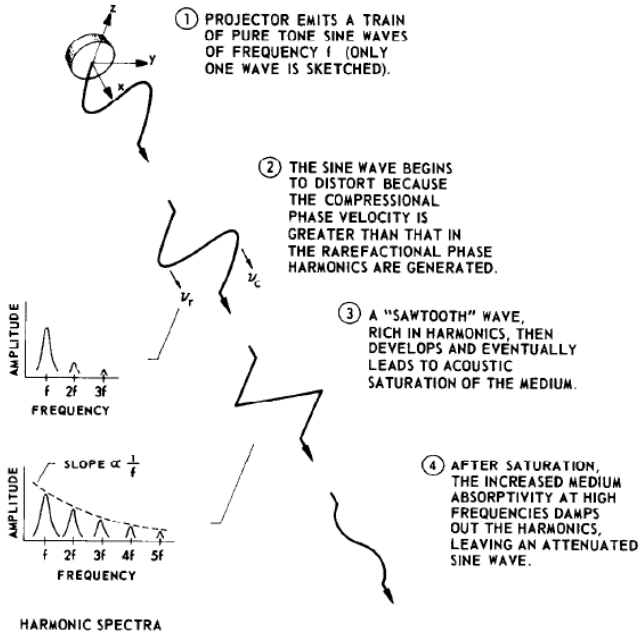

Figure 2-5: Illustration of a high intensity sound wave transmission, distortion, harmonic generation, shock formation and the effect of increased absorption. Figure adapted from (Muir and Carstensen 1980)

In the context of therapeutic ultrasound, non-linear effects become increasingly significant as the depth of treatment is increased, or if a region of high intensity happens to be coincident with a layer of fatty tissue, since it was found that among the soft tissues measured, fat is a very nonlinear tissue and has a *B/A* value which appears to be significantly higher than the values for non-fatty soft tissues and distilled water, mainly due to its low water content (Law et al. 1985;Sehgal et al. 1984).

Measurements have shown that the average value of *B/A* for fat ranges between 10-12, increases with increasing temperature and its magnitude varies among fat tissues taken from different parts of the body (Errabolu et al. 1988). Examples of *B/A* values for a number of propagating media are provided in Table 2-2.

Table 2-2: B/A for water and a number of soft tissues (Law et al. 1985)

Propagating Medium	*B/A*
Water	5.5
Beef liver	7.5
Beef brain	7.6
Beef heart	7.4
Pig muscle	7.5
Pig fatty tissue	11

2.2.4 Attenuation in an acoustic medium

In acoustics, the term attenuation is referring to two different effects: absorption and scattering. When an acoustic wave propagates through a homogeneous medium, changes in the acoustic pressure lead to shear motion of particles in the medium and thus to temperature rise due to viscosity. Therefore, part of the mechanical energy carried by the acoustic wave is converted into heat by viscous absorption. In inhomogeneous media such as biological tissue, regions of different acoustic properties (density and compressibility) scatter the incident wave in all directions, resulting in further loss of part of the incident energy. The loss of the incident energy is characterised by the

attenuation coefficient of the medium, α, given by the sum of the absorption, α_α, and scattering coefficients, α_s (ter Haar G. and Coussios 2007).

This loss in pressure amplitude p as a wave travels in the positive x-direction is characterised by the frequency-dependent attenuation coefficient of a medium α and can be described by an exponential law as a function of the propagation distance x, given in Equation 2-7,

$$p(x,t) = Pe^{i(k_o x - \omega t)}e^{-\alpha x} \qquad \text{Equation 2-7}$$

where P is the peak pressure, k_o the wave number, x the position along the propagation axis, ω the angular frequency, t time and α the attenuation coefficient of the medium.

Both absorption and scattering are frequency dependent, as the wavelength changes in relation to the scale of the tissue structure. These losses increase as a power law with increasing frequency, defined as

$$a = a\left(f\right)^{\gamma} \qquad \text{Equation 2-8}$$

where α and γ are tissue specific constants (Chivers and Hill 1975;Hill et al. 1986).

This frequency dependence of attenuation is particularly important for ultrasound-induced heating, as the rate of heat deposition for a harmonic plane is proportional to the product of the tissue absorption coefficient and the acoustic intensity. Because absorption generally dominates scattering in most biological tissues, the rate of heat deposition caused by a harmonic plane wave in tissue is generally well approximated by the equation

$$Q = 2aI \qquad \text{Equation 2-9}$$

where α represents the attenuation coefficient in *Np/m* and *I* the acoustic intensity.

The higher the excitation frequency the more the wave gets attenuated; which means that higher heat deposition is achieved while the penetration depth is decreased. Therefore, the choice of clinical HIFU frequencies constitutes a compromise between the desired treatment depth, limited by attenuation, and the maximum achievable rate of heating, determined by absorption (Hill 1994;ter Haar G. and Coussios 2007).

The higher the operating frequency or the distance travelled by the ultrasonic wave inside the tissue the greater the absorption. In other words, absorption acts as a low-pass filter and reduces the amplitude of the propagating signal. If the pressure amplitude of a single-frequency sound wave is greatly increased, it can then become nonlinear, for as previously described at finite amplitudes the speed of sound is a function of the local pressure. Absorption and nonlinearity are therefore always involved interactively in competition by reducing and creating harmonics and distortion respectively. At great distances from the source, the increased attenuation of the higher frequencies leaves an attenuated sine wave of the fundamental frequency as illustrated in Figure 2-5 (bottom) (Coussios and Roy 2008;Leighton TG 1994).

Unlike most tissues, the attenuation coefficient of adipose tissue decreases with increasing temperature (ter Haar G. and Coussios 2007). Table 2-3 summarises the values for attenuation coefficient in fat that are available in the literature and suggests that these are very inconsistent.

Table 2-3: Values for the attenuation coefficient in fat available in the literature and reproduced from (Chivers and Parry 1978;Goss et al. 1978). NR stands for not reported and * means that data have been interpolated from a graph.

Species	*Preparation*	*Temperature (°C)*	*Frequency (MHz)*	*Attenuation (dB/cm)*
Human[1]	Fresh	NR	0.8	0.44
Human[1]	Fresh or refrigerated	37	1	0.6 ± 0.2
			3	1.6 ± 0.2
			5	2.3 ± 0.7
Human[1]	Melted	15	0.87	0.39
		18	1.7	0.8
			3.4	1.4
Human[1]	Formalin fixed	18.2 ± 2	1*	0.8*
			2*	1.7*
			4*	4.2*
			5.6*	6.1*
Man[2]	Fresh	37	5.9	20
			6.2	19.1
			7.5	28.6
			7.7	21.7
Man[2]	*In vivo*	NR	6	15.6
Pig[1]	Fresh	32 ± 0.1	1	1.8 ± 0.1
Pig[1]	Fresh	37	1.6*	0.6
			2.5*	1.5
			4*	3
			6*	4.9
			7*	7
Pig[1]	NR	NR	2	10*
			4	16*
			7	32*
			10	50*

2.3 Therapeutic Ultrasound

Ultrasound is nowadays rapidly emerging as a promising tool for non-invasive therapy and drug-delivery. With the aiming of causing tissue necrosis, therapeutic ultrasound

delivers a great amount of energy to the targeted tissue inducing irreversible biological damage (ter Haar G. 1995). In order to achieve this, greater peak intensities of the order of thousands of watts per cm^2 are used and longer pulse durations that last for seconds are sent, instead of tens of watts per cm^2 and milliseconds, used in imaging modalities, where the desired result is to image the tissue in question without inducing any biological damage to it. Some of the therapeutic applications already studied by researchers include rapid and localized heating (Kennedy J.E. 2005), mechanical tissue damage and homogenization (Hall and Fowlkes 2007;Roberts et al. 2006), the dissolution of blood clots (Datta et al. 2006), the locally enhanced and time-released activity of drugs (Jeffers et al. 1991) and the non-invasive disruption of the blood-brain barrier (Hynynen 2001;Hynynen 2008).

2.3.1 High Intensity Focused Ultrasound (HIFU)

High-intensity focused ultrasound (HIFU) refers to the generation of high intensity acoustic waves of pressure amplitudes generally in excess of 1MPa peak-to-peak (pkpk) and frequency in the region of 0.2-8MHz. High intensity beams can be focused at a depth within the tissue and selectively deliver great amounts of energy to the targeted small volume of tissue, while leaving overlying and surrounding tissue relatively unaffected. The volume of destroyed tissue is referred to as a lesion. HIFU is gaining clinical acceptance since the application is non-invasive as long as the source is positioned outside the body (Mitragotri 2005). The principle of HIFU is shown in Figure 2-6 (centre).

HIFU was first suggested as a possible therapeutic modality in 1942 (Lynn et al. 1942) but it was only in the 1970s when imaging techniques such as magnetic resonance

imaging (MRI) and diagnostic ultrasound became sufficiently advanced to allow full observation of the result that therapeutic ultrasound attracted more interest. Since then it has been developed to treat pathological conditions such as malignant cancers of the liver, kidney and breast, uterine fibroids and to enhance transdermal drug delivery while potential applications are also being explored in a number of fields including neurosurgery, ophthalmology, oncology and urology. Applications include sites that are fairly superficial, *e.g.* breast and others that are relatively deep, *e.g.* pancreas, fibroid (ter Haar G. 1995;ter Haar G. and Coussios 2007).

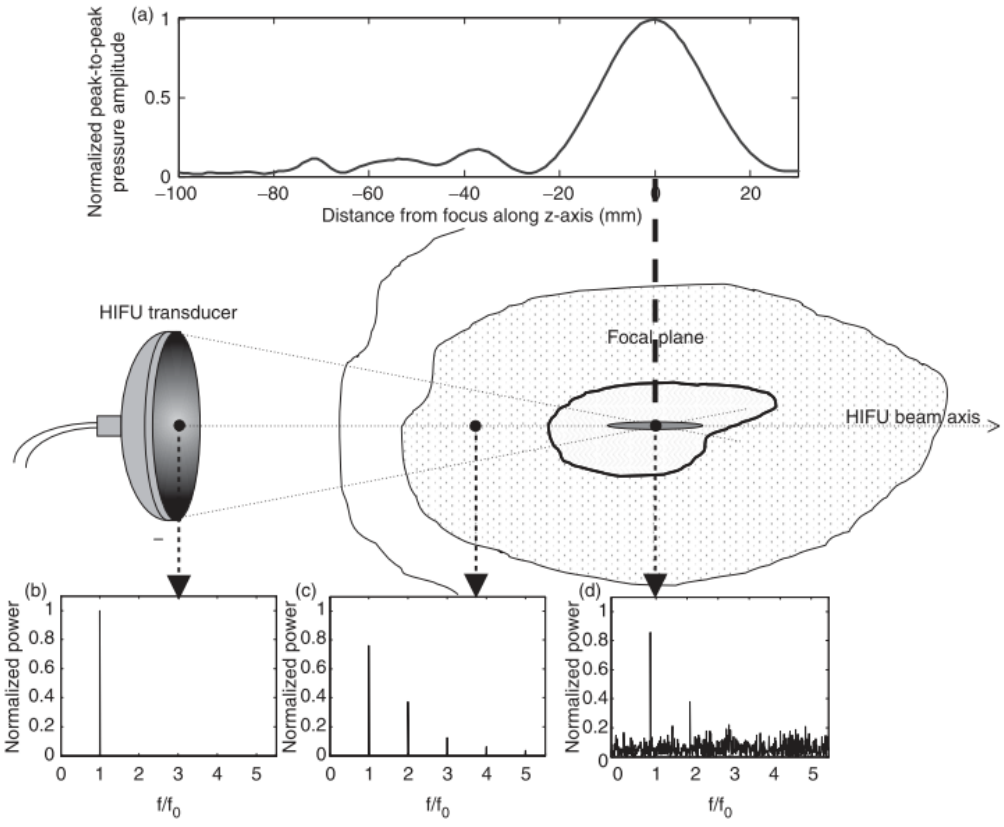

Figure 2-6: Superposition onto the HIFU treatment geometry of a typical axial HIFU pressure profile (a) and of a diagrammatic representation of the frequency-content of the HIFU wave (b-d) as it propagates through tissues. (a) Representative axial pressure distribution for a typical HIFU transducer. The large peak defines the focal region of the HIFU transducer, within which damage is expected to occur. The HIFU transducer is generally excited sinusoidally with a single frequency, f_0, resulting in a monochromatic wave (b). As this wave travels through a nonlinear medium, superharmonic leakage occurs (c) and energy at these higher harmonics is readily absorbed and converted into heat. Finally, if inertial cavitation occurs (generally, but not necessarily in the focal region), the collapsing micro-bubbles convert part of the incident energy into broadband noise emissions (d), which are very rapidly and very locally absorbed and converted into heat. Figure adapted from (ter Haar G. and Coussios 2007).

HIFU has a unique advantage in that it is the only truly non-invasive ablative technique. In addition, HIFU can destroy a region of tissue of any shape, because the source can freely move with respect to the patient and the tissue. However, some of its limitations are the relatively long treatment time required, the lack of a fully accepted real-time monitoring method to assess the tissue change induced and the remaining risk of causing unwanted damage to overlying tissue (Coussios and Roy 2008;ter Haar G. and Coussios C.C. 2007).

2.3.2 Generation of acoustic fields

The generation of acoustic waves at any frequency is simply the case of producing a mechanical oscillation at this frequency and of coupling that oscillation to the desired medium so that displacements are generated in that medium, leading to an acoustic wave. Piezoelectric materials produce mechanical oscillations in response to an electric excitation and *vice versa*, and are therefore widely used to generate ultrasound waves. In biomedical acoustics, the term transducer is used to refer to these devices that convert electrical to mechanical energy and hence generate acoustic waves (Leighton TG 1994).

A medium can be exposed to ultrasonic energy using a focused or an un-focused transducer. In a manner similar to an optical lens, a focused transducer will concentrate the ultrasound energy over a small region, which is the point of maximum pressure and most commonly referred to as the acoustic focus. The size of the acoustic focus depends on the ratio of the aperture of the transducer to the acoustic wavelength, the focus being smaller the larger the ratio, or in other words the same transducer will be more tightly focused and therefore more directional when operating at a higher frequency. Usually an

effective aperture is equivalent to 30 acoustic wavelengths in the propagation medium, in order to achieve directivity (Hill et al. 1986).

The distance between the radiating surface of the transducer and its acoustic focus is defined as the focal length. The on-axis pressure field in between the radiating surface of the transducer and the acoustic focus displays several maxima and minima, as shown in Figure 2-6 (top), whereas at distances greater than the focal length, in the far field, the pressure drops monotonically attaining 1/z behaviour, with *z* being the distance travelled (Hill et al. 1986;Leighton TG 1994;O'Neil 1949). The beam width (BW) is defined as the distance, off-axis, between the points with magnitude 6dB below the maximum intensity. For a spherically focused HIFU transducer the BW is given by Equation 2-10 (Kino 1987)

$$BW = 1.02\frac{Fc}{fD} \qquad \text{Equation 2-10}$$

where c is the speed of sound, f the excitation frequency, F the focal length and D the diameter of the transducer.

Focusing of the ultrasound beam can be very simply achieved by using a single element curved-surface source, in which case the focal length is fixed. Fixed focal-length transducers can also be achieved by using acoustic lenses or acoustic mirrors in combination with a plane single-element transducer. There is also the potential of using multi-element transducers with the elements arranged in a way such as to form the surface of a curved transducer and phasing the drive signal according to the desired focal volume that needs to be generated. This beam steering can therefore be achieved by adjusting the excitation delays to the elements thus requiring no mechanical movements (Hamilton and Blackstock 1998;Hill et al. 1986;ter Haar G. and Coussios 2007).

2.3.3 Detection and measurement of acoustic fields

Hydrophones are devices used to detect sound and also make use of the piezoelectric effect. These are a unique type of transducer designed to measure absolute pressure values, ideally over a wide frequency range and using element sizes that are considerably smaller than the wavelength. Hydrophones take a real-time measurement of the acoustic pressure against time and are used to take readings at several positions in the sound field to determine its spatial profile. These pressure data are linearly transformed into a time-varying voltage, using the frequency-dependent sensitivity (mV/MPa) of the hydrophone, which is obtained by calibrating the sensor using non-acoustic methods. In practice, for accurate readings, the active area of the hydrophone must be significantly smaller than any spatial variation of the field, and in particular, it should be smaller than the acoustic wavelength, so as to minimise the disturbance to the measured field caused by the presence of the hydrophone itself. Using element sizes that are smaller than the wavelength is also important in terms of minimizing spatial averaging of the sound pressure experienced over the area of the active element.

Figure 2-7: A membrane hydrophone (left) and a set of needle hydrophones of different element size each one of which can be screw-connected to the preamplifier base unit (centre). Illustration by courtesy of Precision Acoustics Ltd, Dorchester, Dorset, UK, (left & centre). A robust needle hydrophone that can be inserted in tissue and thus provide *in situ* pressure measurements (right). Illustration courtesy of ONDA Corporation, Sunnyvale, USA.

The response of the hydrophone placed within a sound field is usually directional, in that it has different sensitivity to sound arriving from different directions. The smaller the size of the hydrophone in relation to the wavelength the less directional the instrument is. As a rough guide, the response is generally adequately omnidirectional if the element's dimension is less than a tenth of the wavelength ($\lambda/10$).

To study sound fields in the MHz frequency range, there are two major types of probes: membrane and needle hydrophones, as shown in Figure 2-7. Membrane hydrophones exhibit a flat response over the range of frequencies used in medical applications but have a reduced signal-to-noise ratio and are very fragile and prone to damage. Needle hydrophones have very good directivity and signal-to-noise ratio, but their frequency response is strongly dependent on the tip diameter and thus varies greatly over a broad range of frequencies. Special needle hydrophones can also be embedded in tissue giving extremely valuable measurements of the acoustic field *in situ*. The sensitive element of both types of hydrophones is made of polyvinylidene fluoride (PVDF), a strongly piezoelectric polymer (Hill et al. 1986;Leighton TG 1994).

2.4 Ultrasound-induced bioeffects on tissue

A high intensity ultrasound wave generated by a focused transducer outside the body can produce tissue damage *via* two main mechanisms: thermal and mechanical. Rapid temperature rises can result from direct absorption of the incident ultrasonic energy. Mechanical effects refer to acoustic radiation force, shock wave formation and bubble formation and pulsation due to the incident ultrasonic wave. In this work, bubble formation is defined as acoustic nucleation, whereas any activity of the bubbles in the medium exposed to an ultrasonic field is defined as acoustic cavitation (Coakley and

Nyborg, 1978). Acoustic cavitation is also the most important physical mechanism by which ultrasound interacts with tissue. Thresholds for biological responses are time-dependent for thermal effects and time-independent for mechanical effects. However, the extent of the resulting biological effect is dependent on the exposure duration for both mechanisms, once a threshold value has been exceeded (Barnett et al. 1994).

2.4.1 Thermal effects

When an ultrasound wave propagates through a particular tissue layer, the pressure fluctuations induced lead to a shearing motion of tissue at a microscopic level, which results in frictional heating. Part of the mechanical energy carried by the incident wave is thus converted into heat by this viscous absorption, which constitutes the primary mechanism for ultrasound-induced hyperthermia (ter Haar G. and Coussios 2007).

As the pressure amplitude of the propagating sound wave increases, nonlinear propagation converts part of the spectrum of the single-frequency pressure waveform into higher harmonics, as demonstrated in Figure 2-6 (bottom). These higher frequencies are absorbed at a higher rate than the fundamental frequency. The higher rate of absorption of these higher frequencies causes increased heating compared to what would be expected under linear conditions, where only the excitation frequency would be present.

After initial propagation, the heat diffuses slowly into the tissue. The cooling effects of blood perfusion *in vivo* must also be included in an estimation of temperature elevation. Once a uniform temperature distribution is established and the heat source is turned off, temperature decays exponentially as

$$T = T_0 \exp[-t/\tau] \qquad \text{Equation 2-11}$$

where T_0 is the initial temperature and τ is the perfusion time constant. For heart τ is 1.15 min whereas for fat, τ has a relatively large value of 66.7 min which contributes to its high thermal insulation properties. It is thus expected that ultrasonically heated fat will cool down rather slowly (Szabo 2004).

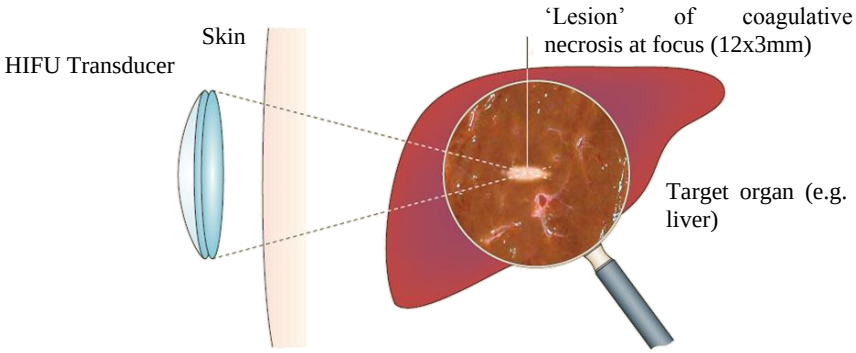

Figure 2-8: Schematic showing an extra-corporeal HIFU transducer generating an ultrasound beam, which forms a cigar-shaped focus deep within the target organ (liver). The volume of the 'lesion' following a HIFU exposure is very well confined and localised and will vary according to transducer characteristics. Figure adapted from (Kennedy J.E. 2005).

Cellular activity greatly depends on ambient temperature. Different tissues require different maximum temperatures in order for thermal necrosis to be induced, also known as a thermal lesion, the shape of which is depending primarily on the spatial distribution of the acoustic field. Most of the heating is confined to the focal region, which, for a typical focused cylindrical HIFU transducer operating at 1MHz, is an oblate ellipsoid with a major diameter of approximately 2mm and a length of approximately 1cm. Ultrasound is highly absorbed within the focal volume inducing high temperatures locally at the focus, while temperatures outside the focus are kept at non-cytotoxic levels (ter Haar G. and Coussios 2007). A schematic representation of an extra-corporeal HIFU

transducer generating an ultrasound beam and the typical cigar-shaped lesion that forms following a HIFU exposure is shown in Figure 2-8 (Kennedy J.E. 2005).

2.4.2 Mechanical effects - Acoustic Cavitation

When a large amplitude sound wave propagates through a medium, then the peak rarefaction pressure (p-) of it may be large enough for small cavities to form, which rapidly fill with vapour or gas. Bubble nucleation may occur in a medium when the pressure is reduced to a value less than the pressure of the vapour or the partial pressures of the dissolved gases (Mellen 1954). The pressure amplitude required for these cavities to form depends on the physical properties of the propagating medium (Apfel 1984;Church C.C. 2002). The way these cavities oscillate volumetrically in the presence of a sound field is described as acoustic cavitation activity (Neppiras 1980).

In a biological tissue there are attractive forces that determine its molecular cohesion. Therefore, for a cavity to form, a high negative pressure together with an expansion cycle is needed in order to overcome this molecular cohesion. The negative pressure required depends on the type and density of the tissue. In low density tissues such as adipose tissue, molecular cohesion is weaker, thus lower negative pressures are sufficient. In addition, the presence of interstices in the tissue facilitates the creation of bubbles during the expansion cycle of a propagating wave. In many aqueous media, cavitation nuclei are typically pre-existing gas bodies or imperfectly wetted solids and are plentiful (Apfel 1981;Atchley and Prosperetti 1989). For the purpose of this research, it is assumed that nucleating agents pre-exist in subcutaneous fat tissue and that their number don’t greatly increase after the tissue has been excised due to the absence of any large vessel that would allow the insertion of air. If this hypothesis is correct, it should be possible to initiate and

sustain cavitation activity at relatively modest HIFU pressure amplitudes, as investigated further in Chapter 4.

A bubble exposed to a low-amplitude sound field will exhibit small radial oscillations that are symmetric about its equilibrium radius. In this linear regime, its behaviour is analogous to that of a mass-spring-damper system, where the spring represents the compressibility of the gas, the mass the inertia of the surrounding liquid and the damper any viscous, thermal or radiation losses (Prosperetti 1977;Prosperetti 1984). As for any second-order linear system, the acoustic bubble will resonate for a particular excitation frequency, known as the resonance frequency f_o around an equilibrium size R_0 known as the resonance size. For air bubbles in water possessing radii greater than 5μm, when the effects of surface tension can be neglected, the resonance frequency is given by

$$f_0 = \frac{1}{2\pi}\sqrt{\frac{3\gamma P_0}{\rho R_0}} \qquad \text{Equation 2-12}$$

where P_0 is the ambient pressure, ρ the density of the liquid, R_0 the equilibrium radius in the absence of sound and γ the polytropic exponent for the gas (an adiabatic process is often assumed).

Under the effect of ultrasonic waves, which cause alternating cycles of increased and reduced pressure, the nuclei will expand and contract during the negative and positive pressure respectively. A schematic representation is given in Figure 2-9. The size to which a nucleus will expand under a certain hydrostatic pressure depends on the time available for expansion and thus on the frequency of the sound field. The effects of ultrasonic cavitation will cease above a certain frequency range as a consequence of the limitations in the expansion of the nucleus (Gaertner 1954).

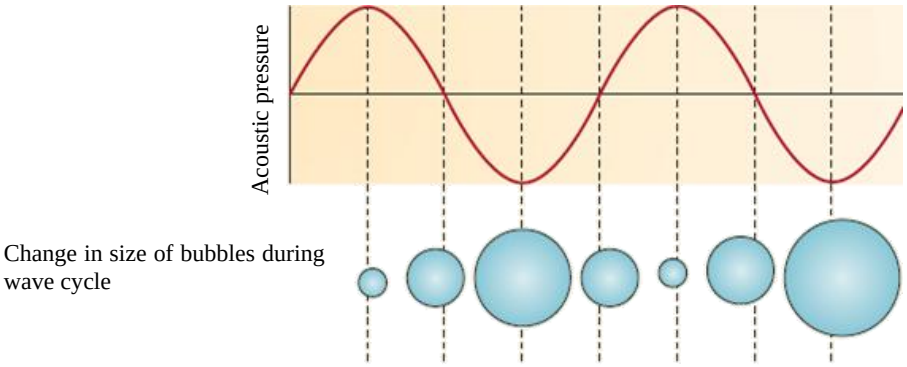

Figure 2-9: A schematic representation of the effect of an ultrasonic wave, which causes alternating cycles of increased and reduced pressure, compression and rarefaction respectively. Gas is drawn out of solution during rarefaction, thus causing the bubbles to expand and *vice versa* during the positive pressure cycle, resulting in the contraction of the bubble. Figure adapted from (Kennedy J.E. 2005).

Ultrasonic waves have been reported to cause potentially beneficial bioeffects, *e.g.* cell disruption and sterilization and acoustic cavitation is acknowledged as the most likely common mechanism underlying these phenomena (Nyborg 1978;Nyborg 2001). In fat cavitation results in strong intracellular destruction and the increased diffusion of fatty acids (Zocchi 1992).

In order to localise and enhance cavitation-mediated bioeffects further, micro-sized bubbles stabilised by a lipid or protein shell, which are most commonly referred to as ultrasound contrast agents (UCA) are widely used. These have been shown to lower the pressure needed for acoustic cavitation to occur (Tran et al. 2003) and to increase ultrasonic absorption (Fujishiro et al. 1998;Umemura et al. 2001), thus making it a more predictable and therefore practical and efficient mechanism for non-invasive ultrasound treatment. However, they have been associated with unwanted shifting of the lesion closer to the HIFU transducer (Tung et al. 2006).

Acoustic cavitation falls into two broad categories, described in detail hereafter: stable and inertial.

2.4.2.1 Stable Cavitation

Stable cavitation is a sustainable, periodic, nonlinear expansion or contraction of a gas body or bubble. In the presence of a sound field, a pulsating bubble can grow over several acoustic cycles by a process known as rectified diffusion. The net inflow of gas into the bubble is greater than the net outflow, thus resulting in the bubble growing until it reaches equilibrium. The stiffness of the entrapped gas controls the response of the bubble and results in a resonant frequency. Stable cavities have sizes that are closer to or greater than the resonant size for the transmitted frequency and continuously oscillate about an equilibrium radius. In the presence of bubbles near the resonance size for the frequency used, the value of *B/A* for this medium is many times greater than the value of *B/A* of the same medium in the absence of these bubbles (Coussios and Roy 2008;Eller and Flynn 1965;Hamilton and Blackstock 1998;Neppiras 1980). Stably oscillating bubbles can undergo asymmetric ‘shape oscillations’ which results in the production of harmonic and subharmonic acoustic emissions (Phelps and Leighton 1997).

2.4.2.2 Inertial Cavitation

Inertial cavitation on the other hand is the rapid expansion of small gas and vapour cavities of size about 1/3 of resonant size, and violent collapse under the effect of the inertia of the surrounding medium. After a few number of cycles these cavities collapse violently, often disintegrating into smaller bubbles. It is in the final stages of the collapse of inertial cavitation that disruptive effects such as: erosion, emulsification, molecular

degradation and biological effects occur. These are the results of the high concentration of energy and consequent high liquid pressures and velocities (Neppiras 1980).

In order for a bubble to cavitate inertially, the pressure amplitude must exceed the so-called Blake pressure, that describes the pressure at which a cavity of a certain size will grow if the surface tension is the limiting factor. This threshold scales as the inverse of the bubble equilibrium size, thus establishing a minimum for bubble sizes that can respond inertially at a given acoustic pressure amplitude at a given frequency. On the other hand, this threshold can be significant for very small bubbles (Leighton TG 1994). Figure 2-10 demonstrates the thresholds in pure water as found by (Apfel and Holland 1991) for numerical models of single cycle excitation at three different insonation frequencies across a range of bubble sizes. The criterion for inertial collapse used was that the gas within the bubble should be heated to temperatures in excess of 5000K from an initial temperature of 300K, though other criteria such as the collapse velocity or energy criterion are also commonly used (Apfel 1982).

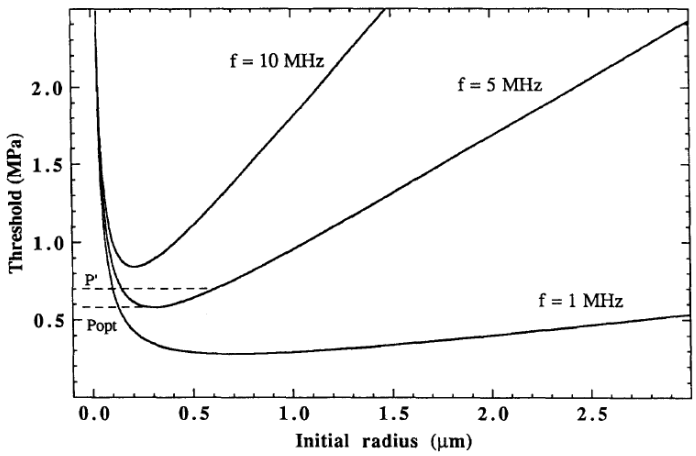

Figure 2-10: Cavitation thresholds as found by (Apfel and Holland 1991) for numerical models of single cycle excitation at three different insonation frequencies across a range of bubble sizes. The criterion for inertial collapse used was that the gas within the bubble should be heated to temperatures in excess of 5000K from an initial temperature of 300K.

In the present study, the cavitation threshold is defined as the minimum acoustic pressure necessary to initiate bubble growth and subsequent inertial bubble collapse in the medium. The cavitation threshold is affected by the initial nucleus size, the pulse characteristics, *e.g.* pulse repetition frequency and pulse duration, the excitation frequency and the characteristics of the propagating medium (Holland and Apfel 1990).

The peak pressure and the frequency of the propagating ultrasound wave are the primary parameters governing the onset of cavitation activity. Lower frequencies are capable of instigating cavitation at lower focal pressure amplitudes than those needed by higher frequencies, due to the greater time available for expansion, as already explained in Section 2-4-2. On the other hand, given the frequency dependence of the attenuation as already expressed in Equation 2-8, higher frequencies get more readily attenuated than the lower ones, thus resulting in greater heat deposition.

When an inertially cavitating bubble collapses, the bubble wall velocity approaches supersonic speed driven by the inertia of the surrounding medium resulting in broadband noise emissions (Hilgenfeldt and Lohse 2000;Holt and Roy 2005).

2.4.3 Cavitation detection

Cavitating bubbles act as secondary sources of sound, emitting spherical waves. Isolating, detecting, monitoring and analysing these acoustic emissions can be used as a means of distinguishing between stable and inertial cavitation, which is believed to be the only source of broadband noise emissions (Brennen 1995;Leighton TG 1994;Mellen 1954;Neppiras 1980) and therefore gain insight into the effect of the ultrasound treatment in real-time.

There are a number of acoustic cavitation detection techniques; with the two most commonly used ones being the active and passive cavitation detection, usually referred to as ACD and PCD respectively, which have been used both independently and in combination (McLaughlan et al. 2010).

Active cavitation detection (ACD) uses focused transducers that transmit a short low-amplitude pulse in the transmit mode and pick up the return echo signal in the receive mode should it encounter any suitable target (Holland et al. 1996;Roy et al. 1990;ter Haar G.R. and Daniels 1981). For the active detector to detect cavitation a pulse must be sent while cavitation is occurring, ACD thus relies on the received echo from the region of interest. However studies have shown that ACD affects the cavitation process and it is therefore a mildly invasive technique for measurement (Madanshetty et al. 1991).

The transducers used for passive cavitation detection are usually focused to maximise signal sensitivity and spatial specificity, although unfocused transducers have also been used (Madanshetty et al. 1991). These data can be processed and displayed providing the user with a real-time useful information about the efficacy of the targeting as recent studies have shown (Leighton T.G. et al. 2008). Passive cavitation detection relies on the strength of the sound source and is a truly passive technique (Madanshetty et al. 1991). In addition, the onset of inertial cavitation on the PCD was shown to happen earlier than the appearance of the hyperechoic region in B-mode (a two-dimensional image) ultrasound imaging (Coussios et al. 2007;Rabkin et al. 2005) which yields two conclusions: firstly that the analysis of the broadband noise is a very reliable and robust way of real-time monitoring of the inertial cavitation activity and secondly that the appearance of a hyperechogenic region on B-mode images is most likely related to the presence of large boiling bubbles.

Figure 2-11 shows the peak output voltage received by a confocally aligned transducer acting as a passive cavitation detector, alongside the frequency spectra of the received signal at three different time instances within a ramped HIFU exposure (amplitude increased every 5 seconds) and suggests that once inertial cavitation activity is initiated, a clear jump in broadband emissions is also depicted, whereas a hyperechogenic region only becomes visible on the B-mode image much later.

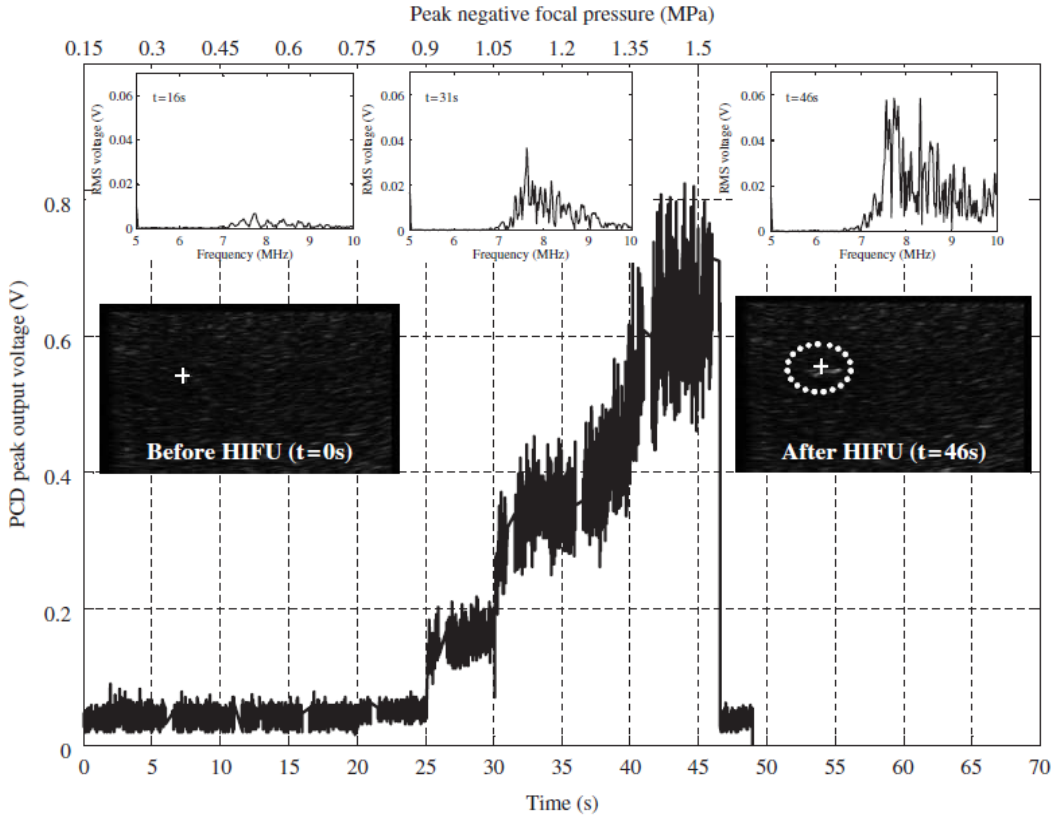

Figure 2-11: Comparison between the peak PCD output voltage, the frequency spectra of the PCD-received traces at three different time instances within the exposure and the pre- and post- HIFU B-mode. The confocal position of the HIFU, PCD and imaging transducers is indicated by the white cross on the B-mode images, with the HIFU transducer being to the left of the image, the PCD transducer pointing out of the image and the imaging transducer lying above the image. A sudden increase in peak PCD voltage is coincident with a clear jump in broadband noise emissions, whereas a hyperechogenic region only becomes visible on the B-mode image much later. Figure adapted from (Coussios et al. 2007).

Experimental results *in vitro* have also shown a tendency of the inertially cavitating region to move towards the ultrasound generating device (Watkin et al. 1996), which signifies even more the adequate real-time monitoring of the inertial cavitation during HIFU exposure, if clinical acceptance is desirable.

2.4.4 Cavitation-enhanced heating

The local rate of HIFU-induced heating is determined by the local, frequency-dependent absorption coefficient. Therefore any mechanism that either increases the high-frequency content of the sound field or extends the distances over which viscous absorption can occur will result in enhanced heating. When a single frequency wave is propagating through a cavitating region, then this sound wave is strongly scattered by these bubbles, which trap the energy within this region thus extending the sonic propagation path and causing greater heat deposition due to viscous absorption of this energy. In addition, the presence of multiple cavities oscillating in the sound field increases the opportunity for viscous absorption in the boundary layers at the bubble surface.

Studies have demonstrated that the presence of small gas bubbles at the ultrasound focus can lead to substantially greater rates of heating compared to the absence of bubbles. This enhanced rate of heating has been observed both *ex vivo* and *in vivo* and is generally attributed to the acoustic cavitation activity. (Holt and Roy 2001;Hynynen 1991;Khokhlova et al. 2006;Sokka et al. 2005).

In the case of inertial cavitation, energy delivered at the fundamental HIFU frequency is redistributed by the collapse of the bubbles into broadband noise, as shown in Figure 2-6 (bottom), with higher frequencies that are highly attenuated and absorbed, causing a great temperature rise close to the inertially cavitating region (ter Haar G. and Coussios

2007). It has been shown that the enhanced heating is mostly due to the re-distribution of the fundamental frequency as broadband noise emissions by inertially cavitating bubbles whilst the scattering and the viscous absorption in the bubble boundary layer contribute very little (Coussios et al. 2007).

Figure 2-12 presents simultaneous cavitation and temperature measurements carried out in a tissue mimicking material demonstrating the enhanced focal temperature rise achieved when inertial cavitation activity is induced at the focus.

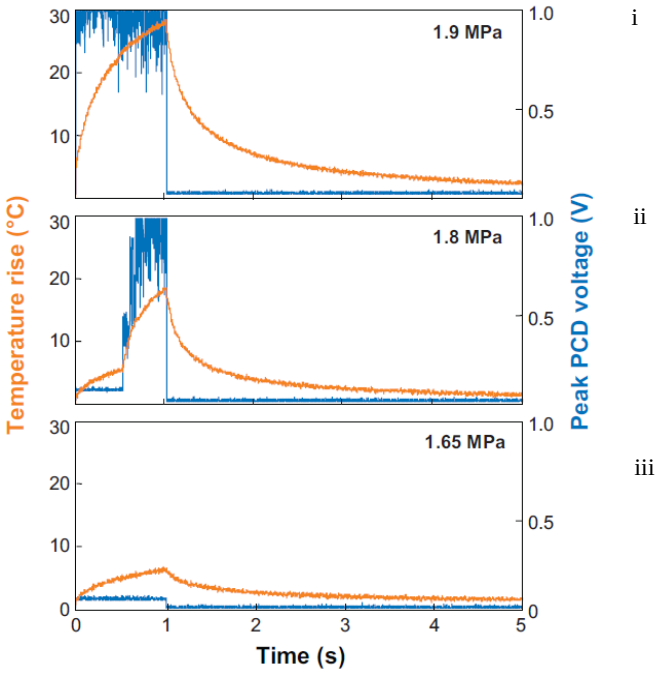

Figure 2-12: Measured temperature rise - labelled 'Temperature Rise' and shown in orange- and PCD output -labelled 'Peak PCD voltage' and shown in blue- as a function of time for a 1-s 1.1-MHz HIFU insonation of an agar-graphite tissue phantom at three different pressure amplitudes. No inertial cavitation occurs in (iii), whilst cavitation onsets halfway through the exposure in (ii) and at the start of exposure in (i). In (ii) and (iii), there is a dramatic increase in the observed rate of heating that is coincident with the onset of inertial cavitation activity. Figure adapted from (Coussios et al. 2007).

Figure 2-13 shows the peak temperature elevation (left) and associated temperature profiles (right) in a tissue-mimicking material over a range of pressure amplitudes. In the absence of inertial cavitation, the peak temperature rise is propoprtional to acoustic intensity, and therefore varies quadratically with pressure amplitude. However, once the inertial cavitation threshold is reached, the peak focal temperature greatly exceeds that predicted by the parabolic profile.

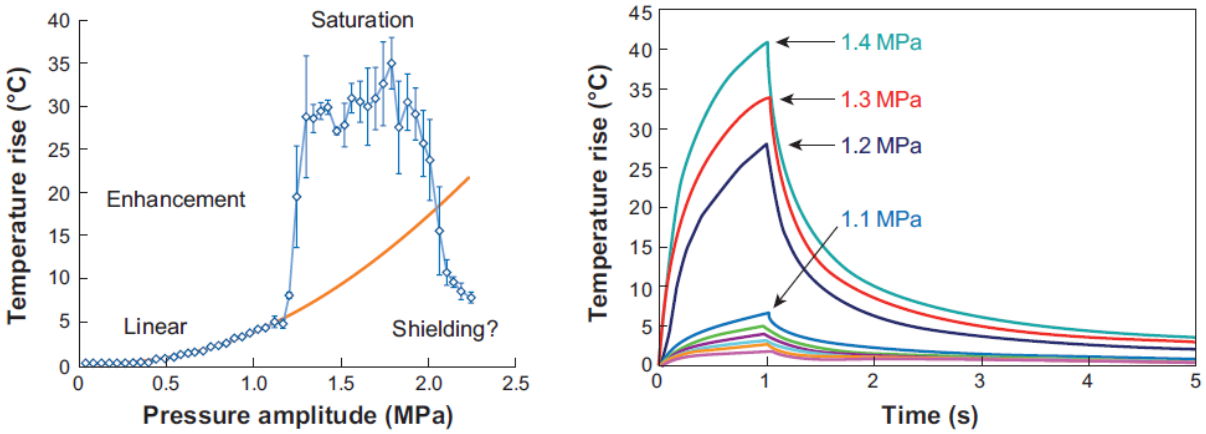

Figure 2-13: Measured (blue) and predicted (orange) peak temperature rises versus the acoustic peak-rarefaction pressure amplitude. The error bars depict the standard deviation of five measurements (left). Measured temperature versus time for increasing peak-rarefaction amplitudes; each curve corresponds to an increment of approximately 0.1MPa. Figure adapted from (Coussios et al. 2007).

The instigation of cavitation activity at the focus therefore has the potential to not only enhance the rate of heating but to also improve the spatial localisation of heat deposition during HIFU treatment. At the same time the desired therapeutic effect can be achieved at intensities much lower than those needed if absorption of the sound wave was the only thermal mechanism (Coussios et al. 2007).

2.5 Monitoring ultrasound therapy

In the context of therapy, a HIFU treatment usually consists of three equally important stages. The first is target identification and treatment planning, which is usually made using computed tomography (CT) or magnetic resonance (MR) scans. Once the target volume is accurately identified and spatially localized, the required acoustic energy is delivered to cause the desirable result. In order to assess tissue destruction, monitoring of the treatment during the delivery phase is performed. It is of great importance to be able to assess the destruction caused within the target volume non-invasively in real-time and crucial if extensive clinical acceptance is to be achieved. This not only provides feedback to the clinician about the change of the tissue, the progress and the effectiveness of the treatment but also provides early alert as to the onset of adverse effects and allows adjustment of the exposure parameters while treating (Rivens et al. 2007).

The next section will focus on the clinically available guidance and monitoring techniques and those used during experimental procedures in the laboratory.

2.5.1 Imaging

HIFU treatment delivery is usually performed under magnetic resonance imaging (MRI) or diagnostic ultrasound guidance, each having its own advantages and limitations. Both are safe, do not have any cumulative biological effect and are reliable clinical tools (Rivens et al. 2007;Szabo 2004;Ziskin and Petitti 1988).

Magnetic resonance has been applied successfully to medical imaging of the human body because of its high water content. In simple terms, MRI detects the net magnetic field of hydrogen atoms in water which is in great abundance in the human body

(Hashemi et al.). However, its very poor portability, the need to use special HIFU equipment that does not interfere with the magnetic field, the slow rate of image presentation and most importantly its very high cost are the main reasons why alternative means of HIFU treatment monitoring are being sought.

Ultrasound imaging on the other hand is very cheap to implement, very efficient and portable. The appearance of very bright regions on B-mode diagnostic ultrasound images, called hyperechoic regions, in a conventional B-mode image has been demonstrated in both *ex vivo* (ter Haar G. et al. 1989) and *in vivo* (Vaezy et al. 2001) tissue and shown to provide a means of determining that lesion formation has taken place. However, studies have shown that diagnostic ultrasound images of hyperechoic regions appear later than the onset of inertial cavitation activity and have no direct correlation with the histological results (Rabkin et al. 2006;ter Haar G. et al. 1989). Furthermore, its use is also limited by its frequency dependent penetration depth. Additionally, during HIFU exposures, the diagnostic ultrasound systems become saturated by the signal from the therapy transducer. This problem though can be overcome to some degree by operating the HIFU transducer in pulse mode, thus allowing the imaging transducer to operate during the HIFU off time (Owen et al. 2006).

2.5.2 Thermometry

In situations where heating is a significant therapeutic mechanism, identifying suitable means of temperature quantification is essential for treatment optimization. In this section, we describe means of monitoring temperature (i) non-invasively for the purpose of clinical treatment guidance and (ii) invasively for the purpose of laboratory studies.

According to previously reported results (Bohris et al. 2001), MRI can be used to plan, monitor and control HIFU treatment and is used to measure temperature rise non-invasively(Wu et al. 2004). However, MR-thermometry presently involves major compromises between spatial and temporal resolution, with sub-millimetric and sub-second temperature measurements remaining a challenge. Furthermore, the presence of vapour bubbles produced at high temperatures can introduce artefacts in the image (McDannold et al. 2006). Widespread adoption of MRI is prevented partly by its cost and lack of portability, as well as compatibility issues regarding the material employed in the hardware. In addition, there is always an artefact due to patient respiration and movement.

For experimental purposes, thermocouples can be employed for measuring temperature elevation during HIFU exposure. A diameter equal to or less than 1/20 of the wavelength of the excitation frequency is sufficiently small for the effect of scattering from the wire on the temperature distribution to be neglected (Fry and Fry 1954a;Fry and Fry 1954b;Rivens et al. 2007). The temperature measurements presented in this report were obtained by using thermocouples and some important considerations in thermocouple-based thermometry are described hereafter.

When HIFU is turned on, there is an artificial rapid temperature rise during the first few milliseconds due to the effect of shear viscosity caused by the relative movement of the thermocouple probe and the tissue. This initial phase, shown as phase A in Figure 2-14, depends on the orientation of the thermocouple with respect to the axis of sound propagation and reaches equilibrium rapidly. It has been shown that placing the thermocouple probe at a 90°, with respect to the sound beam, minimizes viscous artefact. This is followed by a quite linear temperature rise due to the absorption of ultrasound in

the tissue, demonstrated by Phase B in Figure 2-14. This rate of temperature rise is proportional to the ultrasound intensity and independent of the orientation of the thermocouple probe. Eventually, after a longer period of sonication the rate of the temperature rise falls due to energy transportation by thermal conduction and blood flow, Phase B+ in Figure 2-14. Once the sound field is turned off, there is a rapid decrease of the temperature, Phase C in Figure 2-14 due to the removal of the viscous force mechanism, which contributed a heat source confined to the immediate neighbourhood of the wire. Finally, the temperature continues to fall exponentially as a consequence of the cooling of the imbedding medium previously heated by absorption in the body of the medium as shown in Phase D of the Figure 2-14 (Fry and Fry 1954a;Fry and Fry 1954b;Hynynen et al. 1983).

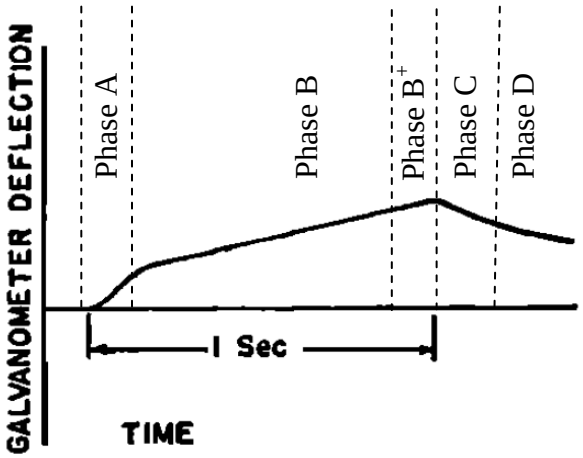

Figure 2-14: Temperature change at a thermocouple probe in response to a pulse of ultrasound with a rectangular envelope. Figure adapted from (Fry and Fry 1954a).

To conclude, temperature distributions within a target region will therefore be determined by two factors: i) instantaneous spatial distribution of energy deposition set by the acoustic beam profiles and ii) time dependent redistribution of heat consequent on thermal diffusion and vascular perfusion.

Thermocouples are widely used to provide the user with information about the heating curves during and after the HIFU exposure. However, they interfere with the ultrasound beam, might cause an error in any measurement of tissue temperature, while they also disrupt the tissue. In addition, the wire of the thermocouple might result in scattering of the ultrasound beam or even introduce cavitation nuclei along its track. In addition, their applicability is limited in experimental work only because they give a invasive real-time measurement of the focal temperature (Hill et al. 1986).

2.5.3 Cavitation-based treatment monitoring

The absence of a universally accepted real-time monitoring technique during HIFU exposures is one of the main barriers to its widespread clinical uptake. All techniques discussed so far are difficult to use in a clinical environment, each possessing its own limitations and disadvantages.

Given that acoustic cavitation is a very well localised source of sound emissions, its potential use as a tool for real-time non-invasive monitoring will be exploited in the following chapters. Furthermore, inertial cavitation has the potential to enhance tissue heating by redistributing the single frequency sent into broadband noise, which is readily attenuated within the cavitating region and thus provides a tool for increased heat deposition efficiency at the focus. If this enhanced heating can be directly correlated with inertial cavitation activity, monitoring the broadband noise emissions produced by collapsing bubbles could provide a means of non-invasive thermometry and therefore treatment efficiency (Coussios et al. 2006;Coussios et al. 2007).

Limitations in the sensitivity of cavitation detectors can be a significant drawback in systems employing very short pulses and low duty cycles in very lossy media (Roy et al.

1990) or when the treatment focus is lying very deep within the body. Additionally, the limited sensing volume of the tightly focused detector transducers, is a major barrier that needs to be overcome before this technique is widely accepted (Farny 2006). A more advanced method for mapping inertial cavitation activity during HIFU exposures has been recently developed (Gyö ngy and Coussios C.C. 2010), whereby signals are passively received by each of 64 elements on a standard diagnostic array and are combined using time exposure acoustics to generate maps of inertially cavitating regions during HIFU exposures. This technique has shown to provide very good mapping not only of a single but also of two disjoint cavitation regions, as shown in Figure 2-15 and to also have several advantages over MRI-based or B-mode imaging techniques.

For the current research long pulses together with long duty cycles have been used while the treatment depth is very shallow given the nature of the application, as it will be further explained in the following chapters. For this reason, a co-axially aligned passive cavitation detector would provide the desired accuracy of localisation of the cavitation activity within the tissue and was therefore used at all times.

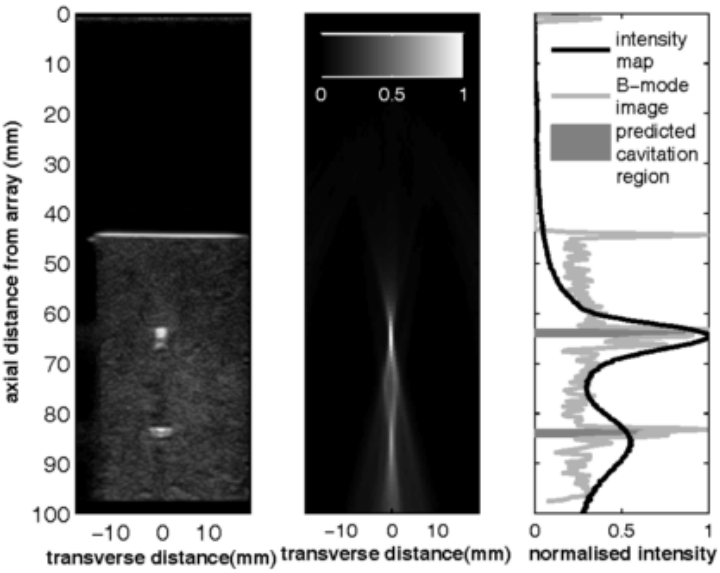

Figure 2-15: B-mode ultrasound image showing two bright spots where cavitation is expected to occur (left). Passive source intensity map from inertial cavitation recorded during HIFU exposure (middle). Comparison of axial cross section of passive source intensity map with M-mode image cross section. Figure adapted from (Gyö ngy and Coussios C.C. 2010).

2.6 Summary and implications for the present work

This chapter provided the reader with the basic understanding of the available literature review, while it also outlined current gaps in knowledge, which the following chapters aim to address.

Given the scarcity of the attenuation coefficients for adipose tissue available in the literature, as shown in Section 2.2.4, a first set of measurements of ultrasound attenuation in subcutaneous fat acquired at four different frequencies under consistent experimental conditions is presented in Chapter 4.

The lack of any published studies of cavitation thresholds and ultrasound-induced heating in adipose tissue motivated a number of *ex vivo* experiments at four different frequencies, with methods and results presented in Chapters 3 and 4 respectively.

The absence of a standardised histological technique for adipose tissue pointed out the need to test numerous histological procedures before identifying the technique best suited for the lipolysis application. These techniques are indentified in Chapter 5 and used extensively in Chapters 6 and 8. *In vivo* experiments, presented in Chapter 6, verified the *ex vivo* acquired cavitation and histology results and confirmed the applicability of the laboratory-based technique in an *in vivo* environment, while pointing out some fundamental limitations.

There is currently no reliable technique for monitoring successful deposition of ultrasound energy in adipose tissue in real-time. Given the great promise of the passive cavitation detector as a monitoring technique, already presented in Sections 2.4.3 and 2.5.3, work presented in Chapter 7aims at developing a real-time monitoring technique

that would provide the user with valuable information about the onset, maintenance and localisation of focal cavitation activity.

Based on limitations and shortcomings confronted during experimentation, an application specific HIFU transducer is lastly developed and tested in Chapter 8, alongside the cavitation-based real-time treatment monitoring technique, thus providing an optimal ultrasound based system for the non-invasive destruction of subcutaneous adipose tissue.

3 Materials and Methods

In order to identify the optimal parameters required for the non-invasive destruction of subcutaneous adipose tissue using HIFU, a new experimental setup was initially developed in the laboratory to enable experimentation *ex vivo*. This setup was intended to resemble the real treatment performed by a physician, with porcine tissue *in lieu* of a patient.

An experimental run includes preparing the experimental setup and tissue, applying ultrasound to the target, measuring the resulting temperature rise, capturing the backscattered signal, analysing the acoustic and temperature data and processing the tissue histologically to conclude about the resulting cellular damage.

This chapter provides the reader with a detailed overview of the main constituents of the experimental setup used *ex vivo*, the experimental procedures followed and the post-processing involved, including all software and hardware used or developed. Modifications performed to this experimental setup for *in vivo* experimentation are discussed in Chapter 6.

3.1 An experimental model for subcutaneous adipose tissue

Tissue Mimicking Materials (TMM) with acoustic properties close to those of tissue and water are very often used during experimentation, in order to simulate the propagation of ultrasound through tissue. These TMM are usually transparent, may have optical properties that change with temperature, thus allowing good localisation and quantification of the damage caused. Unfortunately, no such TMM resembles the acoustic properties of adipose tissue and given that human subcutaneous fat was not

available for the experimentation carried out in this project, a suitable experimental model had to be identified.

Important considerations in selecting such a model included thickness and acoustic properties of the overlying skin layers as well as the thickness and morphology of the adipose tissue layer itself. The English white pig was chosen because of its availability and its many similarities to human fat (Goss et al. 1978). Porcine fat exhibits a coefficient of non-linearity, absorption coefficient and speed of sound that are very similar to those of human fat. Finally, pigs and humans have a similar body mass ensuring that the distances for ultrasound propagation are comparable.

3.2 General *ex vivo* acoustical experimental setup

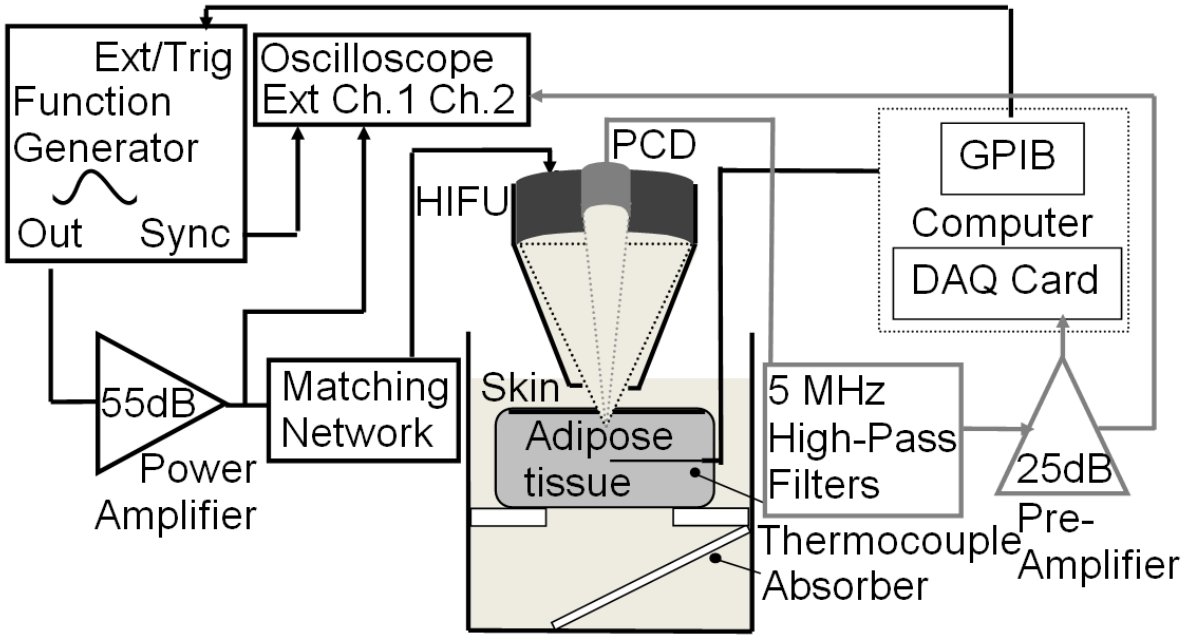

Figure 3-1: Schematic block diagram of the four main constituents of the experimental setup: the HIFU generation loop (in black), the PCD loop (in grey), the thermocouple, the tissue target, and the data acquisition hardware.

Figure 3-1 shows a schematic representation of the general experimental setup used for all *ex vivo* experiments. This can be divided into distinctive groups: the hardware especially constructed for this project, the HIFU generation loop (in black), the coaxial passive cavitation detector (PCD) (in grey), the thermocouples used for thermometry, the tissue target and the data acquisition hardware.

3.2.1 Applicator, tank, histological plate & tubes

For the purpose of this project a tank (20x15x10 cm^3), an applicator, a histological plate and tubes were constructed. The tank and the applicator are made of perspex, a light, transparent and non-corrosive material. The applicator is liquid-tight so that it can be filled with an aqueous fluid to ensure optimal ultrasound transmission from the transducer to the tissue while making it possible to expose subcutaneous fat to HIFU vertically through the skin both in a wet and in a dry environment. An acoustically transparent window, *i.e.* latex condom, is available at the bottom of the applicator to ensure maximum transmission of the ultrasound energy into the tissue whilst the shooting depth (*i.e.* the location of maximum pressure amplitude in the HIFU field) within the tissue is adjustable.

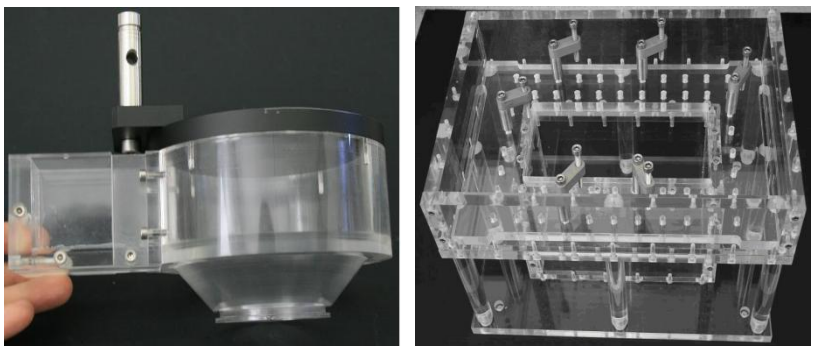

Figure 3-2: The custom built applicator (left) and experimental tank (right).

Given the geometry and the dimensions of the applicator, a tank was constructed to enable sturdy mounting of the adipose tissue for the HIFU exposures. The structure enabled shallow immersion of the skin surface in water and prevented the existence of air between the bottom of the applicator and the skin surface, which would greatly interfere with ultrasound energy transmission. Both constructions are shown in Figure 3-2.

In order to be able to process the treated areas histologically, the volume of the exposed tissue had to be very accurately defined. This was addressed by constructing a series of stainless steel target tubes that accommodated small blocks of tissue. Stainless steel is a strong ultrasound reflector and a strong material that can be hammered through the adipose tissue and the skin. The tube length and inner diameter (25mm x 13mm) were very carefully chosen, so as to be big enough not to interfere with the ultrasonic beam and at the same time small enough to produce blocks of tissue that could be sliced and histologically processed. All constructions are readily cleanable to avoid contamination.

3.2.2 HIFU exposure

Three spherically focussed single-element high intensity ultrasound (HIFU) transducers with an active diameter of 64mm but of different centre frequencies were used for all experiments. Each transducer has a narrowband response at both its fundamental frequency and its third harmonic, and could be driven at either frequency by making the appropriate connections to a custom-built matching network. Each transducer also has a 20mm central hole through which a passive cavitation detector (PCD) transducer could be mounted. Table 3-1 summarizes the properties of the three transducers and Figure 3-3

shows one of the three identical-looking spherical transducers used during experimentation.

Table 3-1: Properties of the HIFU transducers.

Transducer Model	Sonic Concepts H107 S/N-96	Sonic Concepts H102 S/N-020	Sonic Concepts H-107B S/N-10
Operating Frequencies	0.483 & 1.641MHz	1.150 & 3.355MHz	0.508 & 1.680MHz
Focal Length	62.64mm	62.64mm	62.64mm

Figure 3-3: One of the spherical HIFU transducers used for experimentation.

3.2.3 Acoustic data acquisition

Acoustic signals emanating from the focus were captured by spherically focused single element wideband (5-20MHz) tightly focused transducers (V319-SU Panametrics, f_0=15MHz, focal length (f.l.)=75mm, -6dB focal beam-width at 15MHz=800μm, active diameter=12.5mm) used as passive cavitation detectors (PCD). These transducers were chosen because their centre frequency makes it possible to detect broadband emissions associated with inertial cavitation, while suppressing emissions at the fundamental frequency and lower harmonics. A picture of one of the two identical-looking transducers used during experimentation together with its frequency response is shown in

Figure 3-4. One PCD was always mounted in the centre of the HIFU transducer, ensuring that the two transducers were always confocally and coaxially aligned with the objective to isolate, detect and monitor acoustic emissions originating from the acoustic focus. During particular experiments, a second PCD, identical to the coaxial one was also used. This was transversely aligned with the HIFU focus. A detailed explanation of the alignment procedure is presented in Section 7.2.

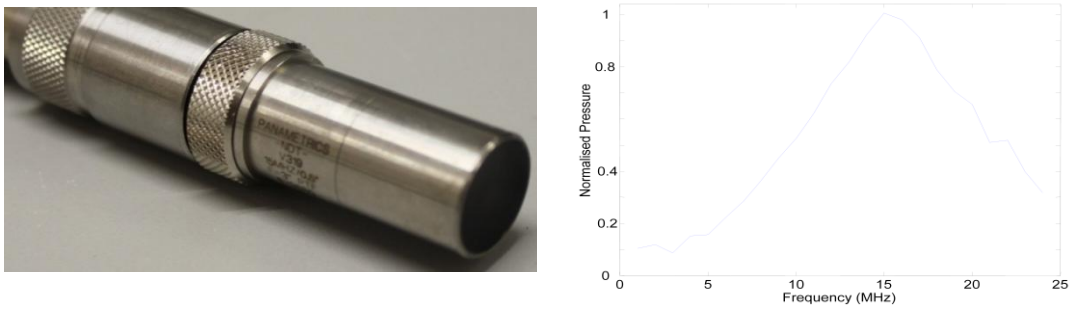

Figure 3-4: The passive cavitation detector (PCD) (left) and its frequency response (right). Graph reproduced from the accompanied documentation report, Panametrics-NDT, Olympus.

Figure 3-5: The Labview interface used for experimentation.

The signal received by the PCD was high-pass filtered above 5MHz (F5081-5PO-B, Allen Avionics, Inc.) and amplified 25 times or at a gain of 28dB (SR445A, DC to 350MHz Amplifier, Stanford Research Systems, Inc.). The high-pass filter was employed to increase the sensitivity of the system to the high-frequency emissions unique to inertial cavitation by filtering out the acoustic energy of the fundamental frequency and its harmonics.

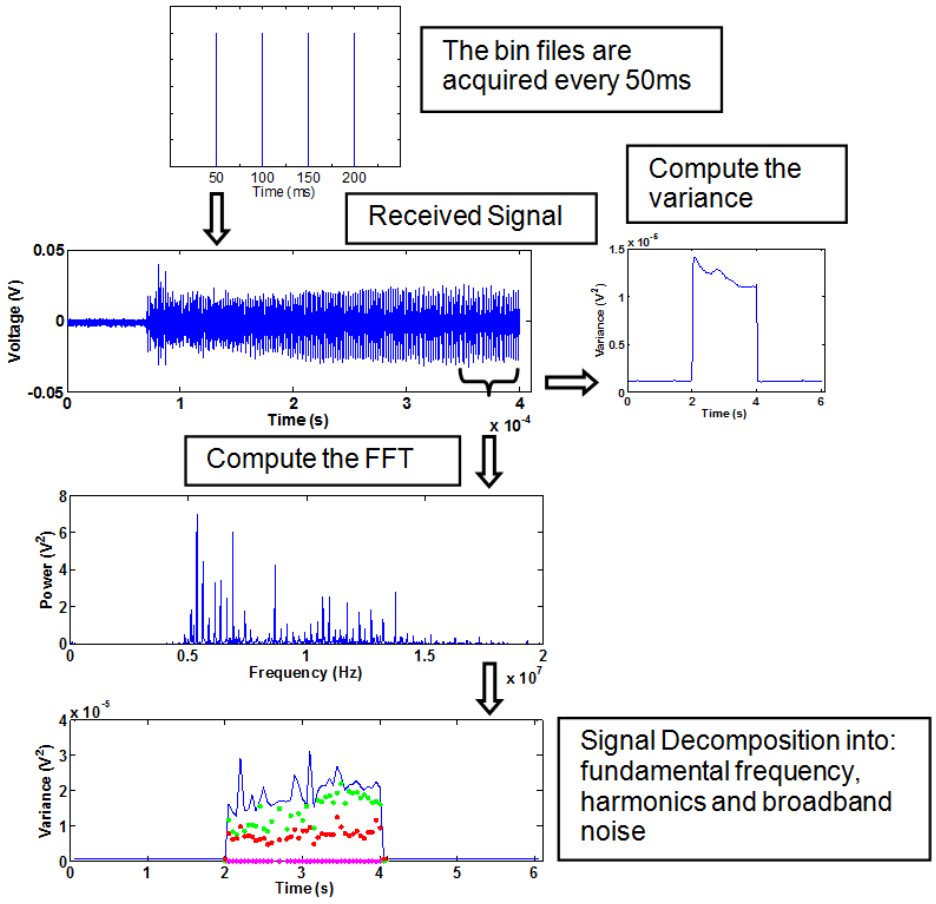

Figure 3-6: A representation of the acoustic analysis followed.

The hardware was remotely controlled *via* Labview (National Instruments Corporation). The interface is shown in Figure 3-5. The computer triggered the signal generator externally *via* GPIB and sent a 95% duty cycle sinusoid, while at the same time the 2-

channel, 14-bit, data acquisition card (DAQ) (PCI-5122) operating at a 100MHz sampling frequency, started acquiring data. This sampling frequency ensured reliable representation and avoidance of aliasing for all signals received over the bandwidth of the PCD (5-20MHz). The DAQ card was acquiring data for 2s before and after the HIFU was on, in order to establish the baseline noise level. Figure 3-6 shows a representation of the analysis followed.

In order to calibrate the HIFU transducers, a membrane and a wide array of needle hydrophones were used. Two factors were taken into consideration when selecting a particular hydrophone for use with a particular HIFU transducer: the size of the sensitive polyvinylidene difluoride (PVDF) element should be smaller than the HIFU wavelength; and the fact that larger hydrophones become saturated at lower pressures, implying that high pressure amplitudes must be measured with smaller hydrophones. Additionally, multiple measurements were also obtained for all frequencies using an implantable needle hydrophone (ONDA HNA-0400, 0.4mm), shown in Figure 3-7. Even though some spatial averaging would be expected for this hydrophone size at the highest HIFU frequency, the decision was made to nonetheless use the implantable hydrophone as it allowed direct comparison of *in situ* measurements with those in the free field.

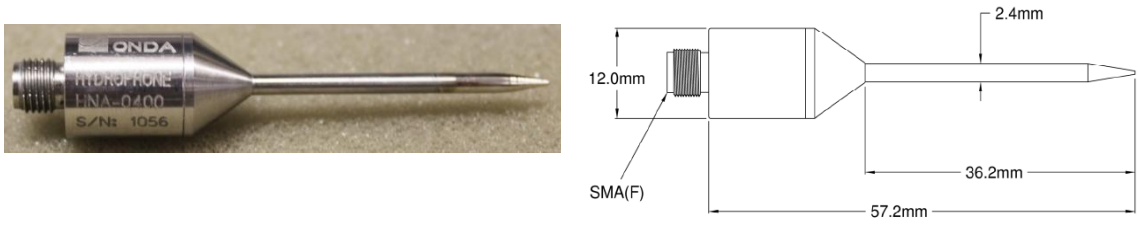

Figure 3-7: The implantable needle hydrophone (ONDA, 0.4mm), which allowed comparison of *in-situ* pressures with those in the free field (left) and its schematic diagram (right)

3.2.4 Temperature data acquisition

During temperature measurements a hypodermic needle thermocouple was embedded inside the tissue with its sensitive tip at the acoustic focus and its axis perpendicular to the axis of wave propagation. Thermocouples that are small with respect to the wavelength of the excitation frequency avoid excessive damage to tissue, but are fragile and hard to use, since they penetrate the tissue with difficulty. Initial experimentation was carried out with sheathed needle thermocouples of diameter 0.2mm (Mini-Hypodermic Thermocouple Probe HYP-0, Omega Engineering). In order to place their tip at focus, the PCD transducer was driven in pulse-echo mode by a pulser receiver (DPR300, JSR Ultrasonic) and the ultrasound reflection of the thermocouple was displayed on the oscilloscope, an alignment procedure that will be described in detail later. The main limitation during experimentation was the non-detectable reflection of the thin shaft, when this was placed inside the tissue. To overcome this problem, thicker thermocouples of shaft diameter 0.8mm (Thermocouple Probe Model HYP-2, Omega Engineering) were used instead.

According to a series of experiments carried out in the laboratory, these thicker thermocouples have shown to detect similar temperature rises and have the same temperature response as the thinner ones. Their edge was better detected on the oscilloscope and they could be positioned inside the tissue with great accuracy since they are robust and strong. It was therefore concluded that for our temperature measurements a hypodermic needle thermocouple (HYP-2, OMEGA Engineering) would be used to measure the induced focal temperature rise. Figure 3-8 (left) shows a picture of the HYP-2 thermocouple used next to a HYP-0 thermocouple for comparison and gives detailed information about its dimensions (right). Though the tip of the thermocouple was large compared to the wavelength at 3.4MHz, the higher frequency investigated during

experiments, (Fry and Fry 1954b), the ratio of viscous artefact to absorptive heating was sufficiently small for any associated errors to be deemed negligible (Morris et al. 2008). The insertion of a foreign object inside the treated tissue might alter the tissue volume of interest in a way that is very hard to quantify, by introducing nuclei or a rough hydrophobic surface that facilitates nucleation. However, measurements of acoustic cavitation with and without the thermocouple at the focus resulted in similar signals being received by the coaxially aligned PCD. It is concluded that insertion of a smooth needle thermocouple in the present work has negligible impact on the observed cavitation threshold.

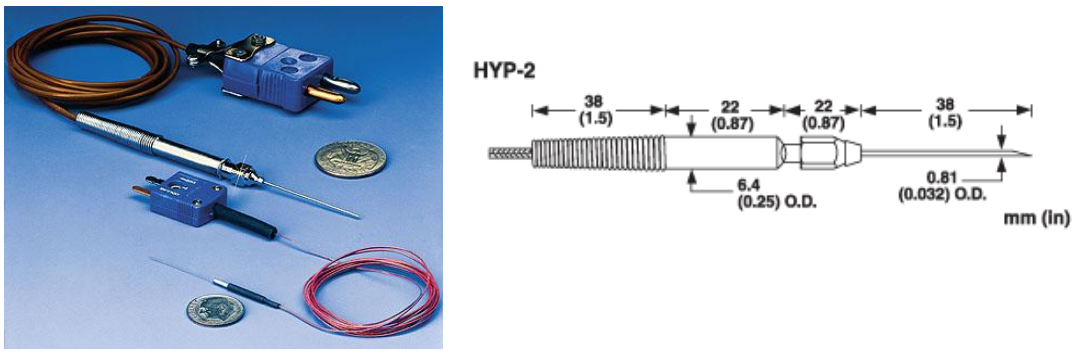

Figure 3-8: The thick hypodermic needle thermocouple (HYP-2) used positioned next to a thinner one (HYP-0) for comparison (left), and its dimensions (right). Figure reproduced from Omega, Engineering.

3.3 Experimental procedure

3.3.1 Transducer alignment

Before every experiment the HIFU and PCD transducers were confocally aligned using a pulser receiver (DPR300, JSR Ultrasonics) and a brass spherical target (r=3.18mm). The HIFU transducer was connected directly to the pulser-receiver and the spherical target

was mounted onto a 3D manual positioning system. Given the water temperature, the speed of sound and the time delay corresponding to the focal length was calculated. The pulse-echo output was displayed on the oscilloscope. The sphere was positioned along the ultrasound propagation axis using the appropriate time delay and moved transversely until the reflection from the brass sphere was maximised. The coaxially positioned PCD was then driven in pulse-echo mode and moved so as to maximise reflection from the brass target, ensuring confocal alignment between the two transducers.

To check that the signal received on the coaxially aligned PCD originated from the HIFU focus a second PCD - identical to the coaxially aligned one - was used: this was positioned at 90° to the HIFU transducer so that its focus overlapped with the HIFU focus. The exact same procedure was repeated to align this PCD transducer transversely and confocally with the HIFU. An illustration of the experimental setup is shown in Figure 3-9. Following successful alignment of the HIFU and PCD transducers, the target ball was removed and replaced by the tissue sample.

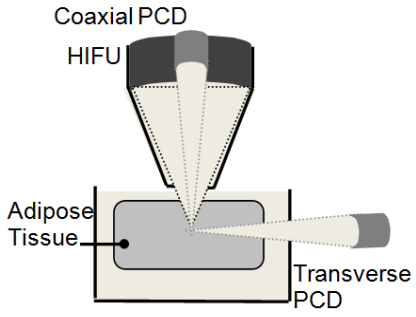

Figure 3-9: Illustration of the operating setup

3.3.2 Thermal alignment

The thermocouple had to be aligned with the acoustic foci of the HIFU and PCD transducers before every exposure in order to provide a measure of the focal temperature

rise induced, which is another way of guiding and monitoring the treatment in real-time and indirectly assessing the tissue damage caused.

The thermocouple was firstly positioned by hand inside the tissue and fixed into position. The coaxial PCD transducer was then driven in pulse-echo mode to acoustically detect the edge of the thermocouple shaft lying just outside the tissue. The HIFU/PCD transducer assembly was moved over the skin by a distance equal to the thermocouple shaft, so that the acoustic focus was approximately over the edge of the thermocouple inside the tissue. Because the thermocouple junction is not exactly coincident with the needle tip, acoustic thermocouple alignment could only provide approximate positioning and a thermal technique was used for fine alignment. Multiple short HIFU exposures of very low pressure amplitude were carried out and the temperature rise for each one was measured. The pressure amplitudes used were chosen so as to be below the inertial cavitation threshold or significant heating, but high enough to generate a measurable small temperature rise (on the order of tenths of a degree). After each and every such low pressure amplitude exposure the transducer assembly was moved in small steps in one of the three orthogonal directions until the greatest temperature rise was detected, which was an indicator that the HIFU/PCD acoustic foci were exactly on the sensitive area of the thermocouple junction.

3.3.3 Preparation of the adipose tissue and sample alignment

Slabs of subcutaneous adipose tissue obtained from a local surgical research facility were used for all *ex vivo* experiments performed in the lab. The tissue was preserved in saline solution at 4°C and was used within a few hours of harvest.

The metal tubes described in Section 3.2.1 were fixed inside the slab of skin and fat, accommodating a cylindrical piece of tissue without altering the structure of the fat. The volume of the exposed tissue was therefore very accurately defined, allowing good localisation of the HIFU focus, which is of major importance if histological assessment needs to be carried out. One of these metal tubes already filled with tissue, was placed inside the hole of the histological plate which was firmly screwed inside the tank. The PCD was driven in pulse-echo mode aiming to detect two diametrical edges of the metal tube. Once this was achieved, the HIFU/PCD transducer assembly was then moved and positioned over the centre of the tube. All exposures could then be performed at the exact same spot every time, by replacing the last tube with a new one each time. Since the thickness of the adipose tissue varies, the transducer had to be moved along the axis of sound propagation prior to every exposure so that the shooting depth remained constant. This procedure enabled a very accurate localisation of the exposed porcine tissue volume, which was required for the tissue to be histologically processed.

3.3.4 Experimental exposure

For all experiments, both the applicator and the tank were filled with degassed (dissolved $[O_2]$ =2-3mg/L) water at room temperature (20°C), and the applicator was positioned so as to ensure that the HIFU focus was located at 15mm below the skin surface. In each experiment, one of the HIFU transducers was used to generate therapeutic ultrasound pulses, driven either at its resonance frequency or at its third harmonic. A function generator (Agilent 33250A) was used to send a 95% duty cycle sinusoid to the power amplifier (ENI A-300, Electronics & Innovation Ltd, 55 dB gain for 0.3-35MHz), the output of which was connected to an impedance matching network. The HIFU/ PCD transducers were placed inside the cone-shaped applicator designed to be positioned

perpendicularly to the skin and mounted to the 3D manual positioning system *via* a fixed rod. The front circular opening of the applicator was covered with a latex membrane, an acoustically transparent medium. During *ex vivo* experimentation the tissue was fully immersed in water to prevent the existence of air in between the applicator and skin surface, which would interfere with ultrasound transmission. Using the embedded needle hydrophone, it was ensured that no standing waves or secondary reflected waves were recorded at the HIFU focus for any of the exposure conditions used in the present work.

3.4 Acoustic data analysis

During HIFU exposure, the PCD is continuously sensing acoustic emissions. Due to memory limitations, not all data acquired during an exposure can be stored. 400-μs windows of PCD data were therefore digitized every 50ms at a sampling frequency of 100MHz and stored in binary form. Binary data files are subsequently imported into Matlab (The MathWorks, Inc.), and a 50μs window is subsequently extracted from the time trace to coincide with active HIFU excitation. The 5,000 data points corresponding to each 50μs window are subsequently analyzed in the frequency domain using the Fast Fourier Transform. By implementation of suitable 20kHz bandwidth digital filters, each PCD trace can thus be separated into its fundamental, harmonic and broadband noise components. Figure 3-6 shows a representation of the acoustic analysis followed after every experiment.

3.4.1 Passive cavitation detection

Dimensionally, the variance of the PCD trace will be proportional to the power of the received signal minus any DC offset. Plotting the variance of each PCD trace over the course of a HIFU exposure will therefore provide a direct indicator of changes in the

power of acoustic emissions emanating from the focus. The variance of the broadband component of the PCD trace is chosen as a metric of inertial cavitation, as it will be proportional to the power of broadband noise emissions (Collin 2009;Kennedy P. et al. 2009). The proportion of the overall signal variance that is attributable to fundamental, harmonic or broadband emissions also provides a direct indication of whether a particular PCD trace is dominated by inertial cavitation, as is often the case at 0.5MHz, or by non-linear propagation, as is often the case for the higher frequencies employed in this study.

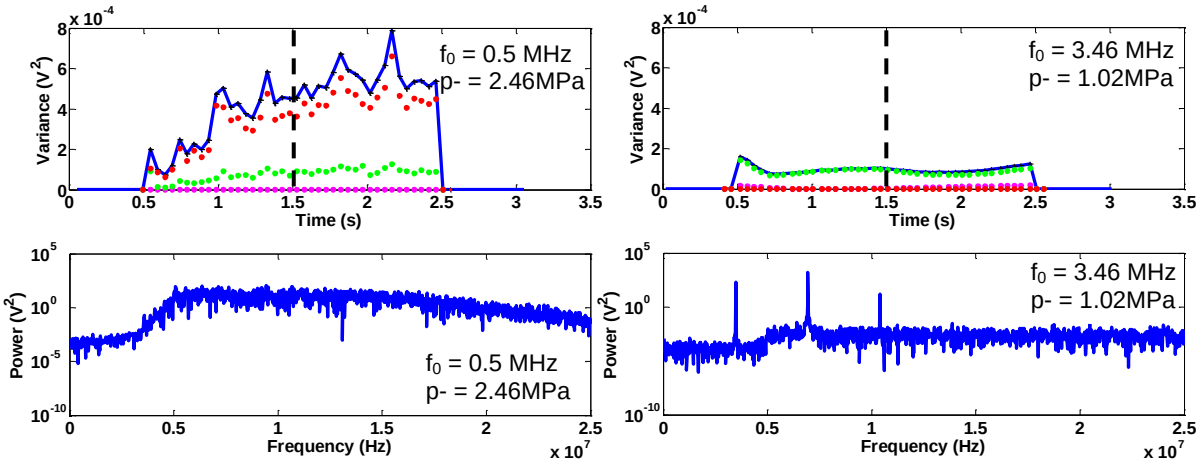

Figure 3-10: (Top) Two representative plots of the variance of the signal received by the PCD during a 2s exposure with 0.5s off time before and after the exposure, at 0.5MHz and at a peak rarefactional pressure (p-) 2.46MPa when inertial cavitation is present at the acoustic focus (left) and at 3.4MHz at 1.02MPa p- when inertial cavitation is not present (right), both shown in continuous line. The energy distribution of the fundamental, harmonics and broadband noise is separately plotted on the same graph in magenta, green and red dots respectively. At 0.5MHz, the increase of the variance of the received signal is due to increased broadband noise emissions, whereas at 3.4MHz harmonics components are dominating. (Bottom) The FFTs of the received PCD signals at t=1.5s further verifying the increased broadband noise emissions (bottom left) and the presence of harmonics (bottom right) and in particular the 2nd and 3rd harmonic.

This is illustrated in Figure 3-10, which shows two representative plots of the variance of the signal received by the coaxially aligned PCD, one for a 0.5MHz 2-second exposure at 2.46MPa p- and one for a 3.4MHz 2-second exposure at 1.02MPa p-. The Fast Fourier

Transforms (FFTs) for each signal are also shown in the lower part of Figure 3-10. In Figure 3-10 (top left), the variance of the PCD signal received during HIFU exposure is dominated by broadband noise, indicating the presence of inertial cavitation at the focus. However in Figure 3-10 (top right), the signal is dominated by harmonic components, which are primarily attributable to non-linear propagation. The FFTs of the received PCD signals further confirms that the signal primarily consists of broadband noise at 0.5MHz (bottom left), confirming the existence of inertial cavitation, whereas at 3.46MHz the PCD signal variance is dominated by harmonics arising from non-linear propagation through the medium (bottom right). It should be noted that the use of the 5MHz high-pass filter resulted in greatly reduced emissions below 5MHz for all exposures.

3.4.2 Passive cavitation localisation

Based on the assumption that cavitation activity is induced instantly and along the axis of sound propagation, the coaxially aligned passive cavitation detector was used to localise the front point, *i.e.* the point closest to the HIFU transducer, of the bubble cloud generated during a cavitation inducing HIFU exposure within the tissue. Given the temperature of the water and the fat, the corresponding speed of sound in the two media and the expected time delay from the HIFU focus was computed. For each one of the 400-μs windows of PCD data a threshold level was defined and was always set to be a multiple of the standard deviation of the signal received during the first μs of each voltage trace, which represented the baseline signal. The time delay of the first point of the received signal to be above this threshold was converted to the corresponding distance from the HIFU transducer and was used as an indicator of the front of the bubble cloud.

In order to confirm that acoustic emissions recorded by the co-axial PCD are representative of focal rather than pre-focal activity, a second PCD, identical to the first, was transversely aligned with the HIFU beam, as shown by the schematic representation in Figure 3-11. The transversely aligned PCD was confocally aligned with the HIFU focus, but was also moved along the axis of sound propagation, in order to confirm the location of the emissions detected by the coaxial PCD.

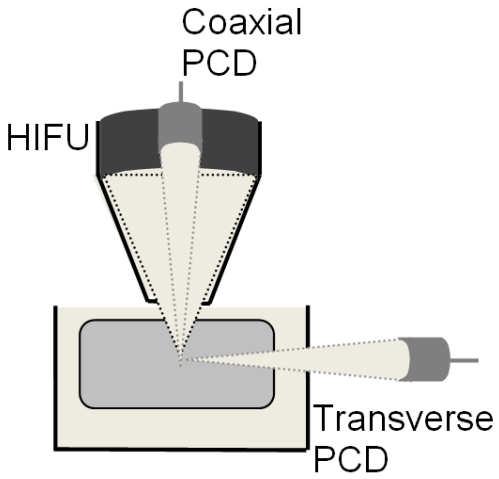

Figure 3-11: Schematic representation of the operating setup. The HIFU transducer was co-axially aligned with one PCD and transversely aligned with a second PCD, identical to the first one. The second PCD was used to confirm the location along the axis of sound propagation of the acoustic emissions received by the coaxial PCD.

3.4.3 Cavitation detection and definition of cavitation threshold

In analyzing the passive emissions recorded during a particular HIFU exposure, inertial cavitation was deemed to have occurred if the variance of the broadband component of the PCD signal increased by more than six standard deviations above noise. The lowest value of peak rarefactional pressure for which such an increase in broadband emissions was detected represents the cavitation threshold for that particular tissue sample. However, cavitation is a highly probabilistic phenomenon and the pressure required to

initiate inertial collapses varies across tissue samples and across locations within a single sample. In order to quantify the likelihood of initiating cavitation activity at a particular pressure amplitude, a Probability of Cavitation (POC) is defined: this is calculated by exposing different regions of the same tissue sample and different tissue samples to the same set of exposure parameters and reporting the percentage of these exposures for which the cavitation threshold, as defined above, was exceeded. Last but not least, it is desirable from a treatment perspective to identify the peak rarefactional pressure for which cavitation will always occur in fat tissue. This is the pressure value for which POC reaches 100% and is hereafter referred to as "the 100% POC threshold".

3.5 Optical imaging assessment of tissue damage

Imaging the blocks of tissue immediately after an exposure provided information on the damage caused to the tissue after HIFU treatment. The aim was to identify any gross changes in the skin and/or the adipose tissue both between the control samples and the sonicated ones, but also among the sonicated ones treated with different exposure parameters, in order to reach a conclusion about the extent of the induced damage. A 10Mpixel digital Canon camera (EOS 400D) with macro photo lenses (MP-E 65mm F2.8 1-5X) was used.

3.5.1 Processing the adipose tissue

In order to identify the structural changes induced to the exposed tissue at a cellular level, the tissue was histologically processed by Dr. Tahera Ansari in the Department of Surgical Research in Northwick Park Research Institute in London. Since no previous histological work had been done on ultrasound effects on adipose tissue, a number of

fixing, cutting and staining techniques had to be developed and tested from scratch in the histology laboratory before making the decision about the optimal one.

Following an ultrasound exposure, the block of tissue was immediately dropped into a 10% Neutral Buffered Formal (NBF) saline solution, which fixes the samples, *i.e.* the cellular structure is permanently maintained for future reference.

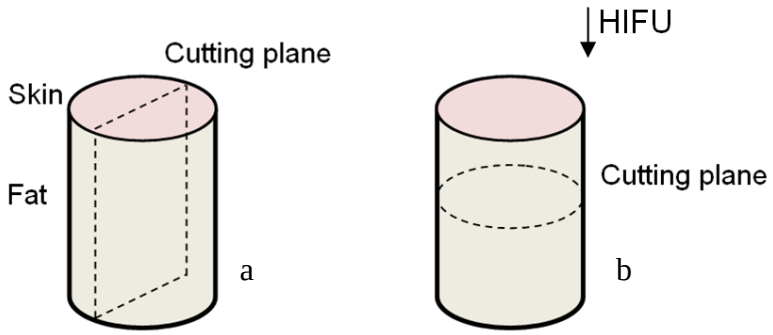

Figure 3-12: A schematic showing the geometry of the metal tubes used for histology while being filled with a block of tissue. Sections were performed transversely, through the skin layer and the subcutaneous fat (left) and parallel to the skin, through the fat layer only (right)

Given the geometry of the metallic tubes, two different ways of sectioning the tissue were tried and are demonstrated in Figure 3-12: a transverse one through the skin layer and the subcutaneous fat resulting in rectangular slides (a) and one parallel to the skin, through the subcutaneous fat tissue only giving circular ones (b), enabling us to see the cellular destruction at two different cutting planes.

3.5.2 Histology of the adipose tissue

The optimal staining technique had to (i) show the cellular structure of the tissue in great detail, (ii) be relatively fast and easy to perform, (iii) show evidence of the ultrasound-induced bioeffects while (iv) avoid artefacts. Figure 3-13 shows representative tissue sections stained with some of the staining techniques tested. After numerous trials with a

variety of stains, summarized in Table 3-2, it was concluded that Haematoxylin and Eosin (H&E) will be used to highlight the cellular structure, while Picro Miller will be used to define the condition of the collagen fibres (Cook 1974).

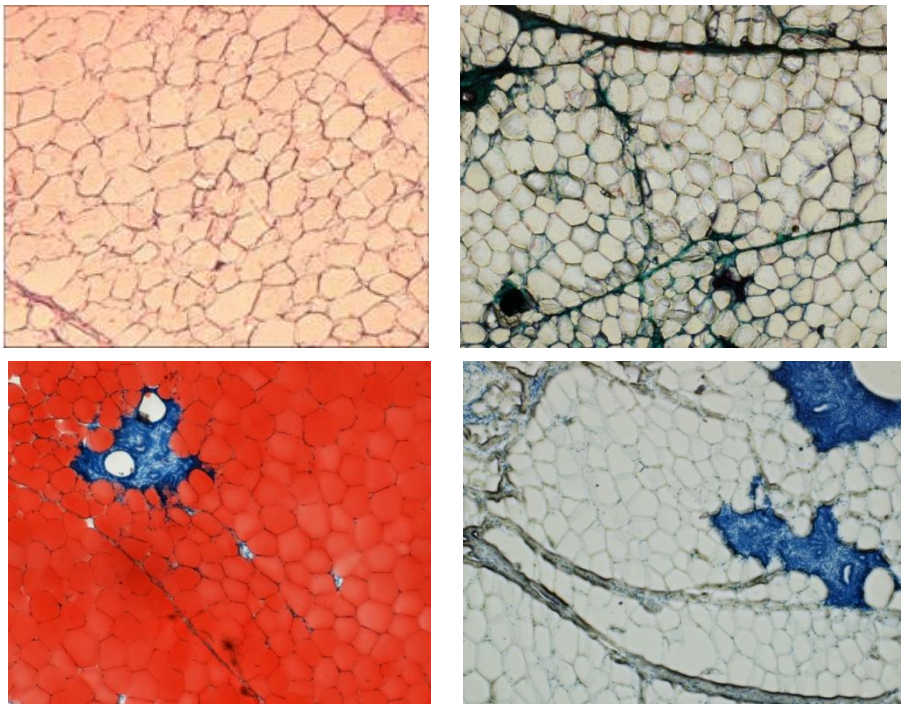

Figure 3-13: Control samples stained with Haematoxylin & Eosin (top left), Masson's Trichrome (top right), Oil – red- O without and with prior de-lipidisation (bottom left and right respectively).

3.6 Summary

Following the detailed description of the hardware and software developed and used during *ex vivo* experimentation, the data analysis and the histological techniques applied to assess the tissue damage, the next chapter focuses on the preliminary experimental results obtained in the laboratory. Cavitation and temperature measurements at four frequencies and at multiple pressure amplitudes were performed *ex vivo*, aiming to identify the optimal set of parameters for this application.

Table 3-2: Staining techniques for lipids

Staining Techniques	*Specific compound it stains*
Haematoxylin & Eosin (H & E)	Nuclei : Blue Cytoplasm : Pink
Masson's Trichrome	Nuclei : Blue-Black Cytoplasm : Orange-Red Collagen : Light Green
Oil – Red - O	Nuclei : Blue Lipid : Red
Picro Miller with Elastin	Elastin : Dark Purple Collagen : Pink-Red

4 Ultrasound-induced cavitation and heating in subcutaneous fat

The preliminary aim is to identify the optimal operating frequency for this application, based on *ex vivo* cavitation and temperature measurements. This chapter starts by presenting the full pressure field characterization of all HIFU transducers used, a procedure performed prior to the start of experimentation in order to measure the pressure amplitudes deployed during experimentation. Preliminary results obtained from *ex vivo* experiments performed in the laboratory using the spherical HIFU transducers are then presented. The level of cavitation activity and the focal temperature rises induced by HIFU at 0.5, 1.1, 1.6 and 3.4MHz in excised subcutaneous porcine fat over a range of pressure amplitudes and exposure durations were measured across several tissue samples from different animal donors.

4.1 Characterization of HIFU source

The characterization of the HIFU transducer is a process of major importance and was performed regularly to check the consistency of the output of our experimental devices. This included absolute calibration, spatial calibration and frequency calibration, when the operating frequency of the transducer was not accurately specified by the manufacturer. Characterization of the fields produced by HIFU transducers at each of the four frequencies investigated was initially performed in the free field using needle hydrophones with known voltage-pressure calibrations.

A signal generator sent a sinusoid wave of the operating frequency to the amplifier and then through the impedance matching network to the HIFU transducer. The number of cycles sent varied for each frequency but always ranged between 10-20 cycles and was chosen so that the output of the hydrophone reached steady state. For each measurement

the input pressure amplitude was gradually increased, while the corresponding voltage detected by the hydrophone was first recorded and then converted to a pressure measurement based on its sensitivity (mV/MPa) at the given frequency. It should be noted that pressure calibrations could only be obtained for focal pressure amplitudes below the safe limit of the hydrophones, therefore pressure values for higher input voltages to the HIFU were linearly extrapolated from the low-amplitude measurements. The increasing effect of non-linearity at these higher amplitudes was not taken into account in reporting these values therefore peak rarefactional pressures (p-) in excess of 4MPa should be treated as indicative.

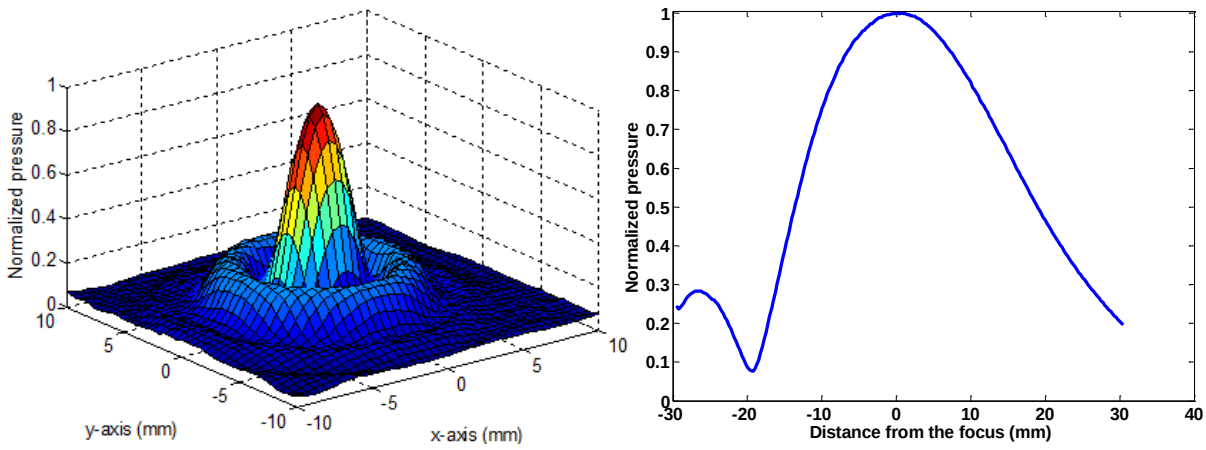

Figure 4-1: Transverse 2D scan at the focus (left) and the axial profile of the HIFU transducer operating at 0.5MHz.

Keeping the input pressure amplitude constant and scanning the hydrophone in front of the transducer across different planes, provides us with information about its acoustic pressure profile. The 2D transverse scan at the focus and the axial profile along the axis of sound propagation of the spherical HIFU transducer operating at 0.5MHz are shown in Figure 4-1. The axial and transverse -6dB beamwidths, i.e. the areas where the pressure is half the maximum pressure, were found to be: 30mm and 3 mm at 0.5MHz;

14mm and 2mm at 1.1MHz; 10mm and 1mm at 1.6MHz; and 5mm and 0.7mm at 3.4MHz.

The resulting relationships between the input peak-to-peak (pkpk) voltage to the HIFU transducer and the output pkpk pressure amplitude, together with the focal dimensions (-6dB beamwidths) at all four frequencies are summarised in Table 4-1, and are the ones all experimental results presented here are based on. Individual measurements carried out at all four frequencies are given in Appendix B.

Table 4-1: Relationships between the input voltage to the HIFU and the resulting focal pressure together with the -6dB beamwidths at each one of the four frequencies. FP_{pkpk} stands for focal pressure peak-to-peak and $V_{mn,pkpk}$ for voltage input to the matching network peak-to-peak.

Frequency (MHz)	*Absolute Calibration*	*Focal Dimensions - Half Pressure (mm x mm)*
0.5	$FP_{pkpk}=0.017V_{mn,\ pkpk}-0.039$	30 x 3
1.1	$FP_{pkpk}=0.034V_{mn,\ pkpk}-0.043$	14 x 2
1.6	$FP_{pkpk}=0.041V_{mn,\ pkpk}-0.052$	10 x 1
3.4	$FP_{pkpk}=0.066V_{mn,\ pkpk}-0.12$	5 x 0.7

4.1.1 Characterization of the acoustic field *in-situ*

During all experiments involving tissue, the operating transducer was mounted inside the applicator with an elastic, acoustically transparent membrane positioned in the front circular opening and the HIFU focus was always placed at 15mm beneath the skin surface within the fat tissue. It was therefore very important to characterise the HIFU pressure field under those experimental conditions. Multiple measurements (N> 20) were obtained at all four frequencies using an implantable needle hydrophone (ONDA 0.4mm). Even though some spatial averaging would be expected for this hydrophone

size at the highest HIFU frequency, the decision was made to nonetheless use the implantable hydrophone as it allowed direct comparison of *in situ* measurements with those in the free field. The *in situ* focal pressures at each operating frequency were measured at 15mm depth -which is where the focus is always placed- and compared to those obtained in the free field.

The resulting correction factors that need to be applied to the pressures measured under free field conditions at each frequency to account for transmission losses due to the propagation of sound through multiple tissue layers are shown in Table 4-2. Given our experimental measurements and the values available in the literature for the speed of sound and density for skin (c_{skin} = 1615m/s, ρ_{skin} = 1090kg/m^3) and fat (c_{fat} = 1450m/s, ρ_{fat} = 950kg/m^3) (Goss et al. 1978;Hill et al. 1986), the attenuation coefficient of fat was also computed. This was done by taking into account the transmission loss at the water-skin and skin-fat interface, but neglecting attenuation through water and the skin layer, which is considerably thinner than the wavelength at any of the four frequencies used. The attenuation coefficient α in subcutaneous fat could therefore be computed as

$$\alpha = \frac{\ln\left(\frac{p_w}{p_f} T_{w-s} T_{s-f}\right)}{d_f} \left[\frac{Np}{cm}\right] \qquad \text{Eq. (1)}$$

where p_f is the *in situ* pressure amplitude in fat, p_w is the pressure amplitude in the free field in water, $T_{w\text{-}s}$ and $T_{s\text{-}f}$ the transmission coefficients at the water-skin and skin-fat interface, and d_f the distance travelled through fat in cm. The results obtained are summarized in Table 4-2, alongside a previously reported value for attenuation in porcine fat at 1MHz provided for comparison. To the best knowledge of the author, this

represents the first set of measurements of ultrasound attenuation in subcutaneous fat acquired at four different frequencies under consistent experimental conditions.

All the focal pressures reported take into account the induced losses at each frequency under the exact experimental protocol followed at all times. Measurements of the pressure field carried out with and without the latex membrane on the front of the applicator showed that the latex membrane does not affect the resulting focal pressures at any of the four operating frequencies.

It is the negative acoustic pressure cycle that is responsible for generating the stresses that result in cavitation inception; therefore all pressure amplitudes cited in this work refer to peak negative acoustic pressures (p-).

Table 4-2: Experimentally determined insertion loss through skin and fat (at 15mm depth beneath the skin), and experimentally deduced attenuation coefficient in porcine fat at 0.5, 1.1, 1.6 and 3.4MHz

Frequency (MHz)	*Intertion loss factor*	*Attenuation coefficient in fat*		*Literature*
		(Np/cm)	*(dB/cm)*	*(dB/cm)*
0.5	0.82	0.076	0.66	1.8 ± 0.1 at 1MHz (Goss et al. 1978)
1.1	0.63	0.25	2.17	
1.6	0.53	0.36	3.19	
3.4	0.34	0.66	5.76	

4.2 Passive cavitation detection during HIFU exposures

Inertial cavitation was hypothesised to be an important mechanism in ultrasound-induced destruction of subcutaneous adipose tissue. The experiments aimed to identify the HIFU parameter range over which inertial cavitation activity can be reliably induced and in particular, the effects of (i) excitation frequency, (ii) pressure amplitude and (iii) exposure duration were investigated. Passive cavitation detection provides a real-time

indicator of the extent of inertial cavitation within its sensing volume, effectively defined by the focal region of the PCD transducer. Its output can be processed and displayed providing the user with a non-invasive monitoring tool. During all exposures of subcutaneous fat, acoustic emissions were captured by the confocally aligned PCD providing both confirmation of successful operation of all electronic devices and a quantifiable measure of cavitation activity.

4.2.1 Cavitation threshold and evolution of cavitation activity

The probability of cavitation (POC) at 0.5MHz and across a range of tissue samples and exposure parameters is shown in Figure 4-2, which suggests that no cavitation was ever observed at 0.41MPa p-, that inertial cavitation was observed in about half of all exposures at 0.82MPa p-, for 80% of all exposures at 1.23MPa p- and could always be initiated (100% POC) for peak rarefaction pressure amplitudes in excess of 1.6MPa, irrespective of pulse duration. On the basis of these results, the cavitation threshold in *ex vivo* porcine subcutaneous adipose tissue under the experimental conditions already described in Chapter 3 was concluded to be 0.82MPa p-, varying from 0.82MPa p- to 1.64MPa p-. The 100% POC threshold was therefore defined to be 1.6MPa p- at 0.5MHz.

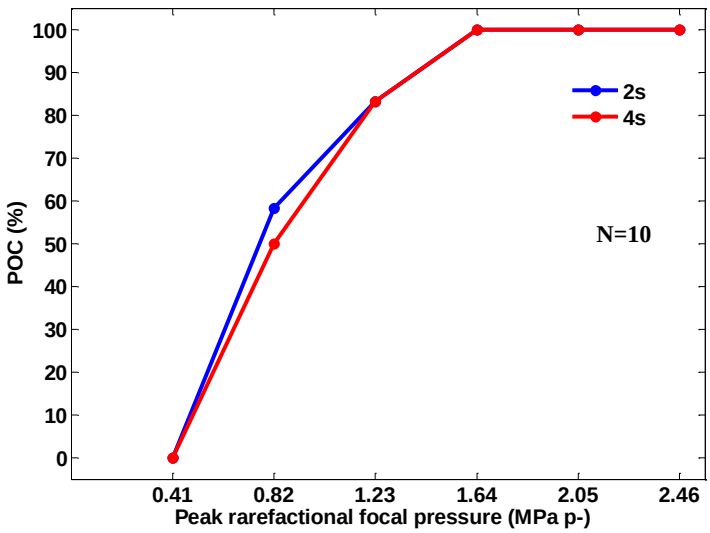

Figure 4-2: Probability of cavitation at 0.5MHz across six *in-situ* pressure amplitudes for 2 and 4s exposures.

It is not merely the presence or absence of inertial cavitation that is likely to be important for treatment. Changes in the variance of the signal received by the PCD over the duration of the exposure can also indicate a change in the level of cavitation activity at the focus. It should be noted that the variance of the broadband component of the PCD can only provide a general indication of the level of cavitation activity at the focus, but cannot distinguish between the number of bubbles and the violence of individual collapses.

A plot of the variances of the signals received by the PCD for 2s exposures at multiple *in situ* pressure amplitudes plotted against time is shown in Figure 4-3. At 0.41MPa p- (lowest continuous blue line, indistinguishable from baseline noise), there is no cavitation present. The signal obtained for the particular exposure shown here at 0.82MPa (green line) exceeds that at 0.41MPa p- by more than an order of magnitude, confirming that cavitation activity occurs. Increasing the excitation amplitude beyond the cavitation threshold to 1.23 MPa p- (red line) and 1.64 MPa p- (black line) results in a significant increase in the power of the PCD signal, with broadband noise always dominating and sustained throughout the HIFU exposure, as verified by the frequency-domain analysis of all received waveforms (not shown). Further increase of the excitation amplitude to 2.05MPa p- (light-blue line) results in saturation as there is no further increase in PCD signal variance. Increasing the exposure duration from 2 to 4s didn’t result in any significant change in the variance of broadband noise emissions over the course of an exposure.

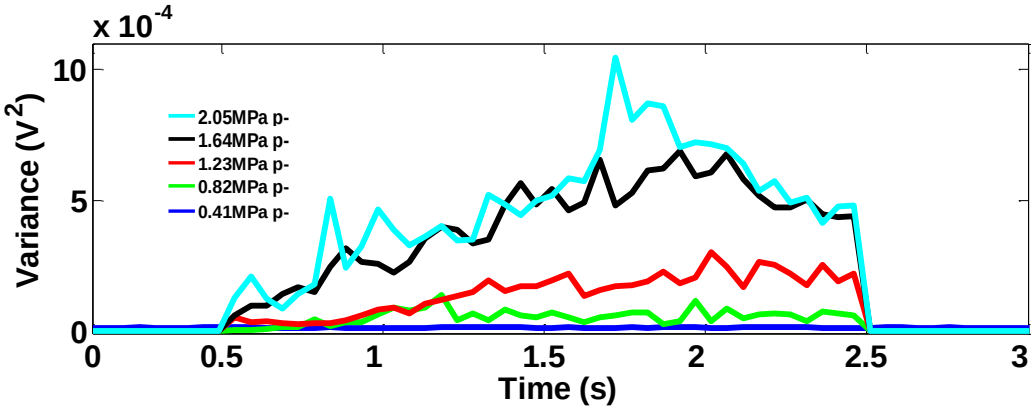

Figure 4-3: Variances of the PCD signals over 2s exposures at 0.5MHz and multiple *in situ* pressure amplitudes. HIFU was on from 0.5-2.5 sec.

A most interesting feature of the above results is that even at pressure amplitudes well above the 100% POC**,** there is a clear increase in broadband emissions immediately upon HIFU exposure but the level of cavitation activity, as quantified by the variance of broadband emissions, continues to increase and cavitation is sustained throughout the HIFU exposure. This behaviour has been observed in other recent studies of cavitation activity in *ex* vivo bovine tissue exposed to HIFU (Mast T. Douglas et al. 2008). It is hypothesized that, in a poorly vascularised and highly viscous medium such as subcutaneous fat, initial nuclei grow slowly by a combination of rectified diffusion and thermal effects (Church C. C. 1988;Webb et al. 2010 - in press), resulting in the observed increase in broadband noise emissions over the course of the exposure.

Frequency domain analysis gives a detailed overview of the spectral characteristics of the received signal. A typical spectrogram of a 2s exposure at 0.5MHz and at a pressure amplitude above the 100% POC threshold, shown in Figure 4-4, further clarifies the dominance of broadband components throughout the whole duration of the exposure. When operating at 0.5MHz, frequencies lower than the 10^{th} harmonic are greatly filtered

out by the 5MHz high-pass filter used. However, the power of the fundamental frequency is great enough, for a part of it to still be present on the received signal.

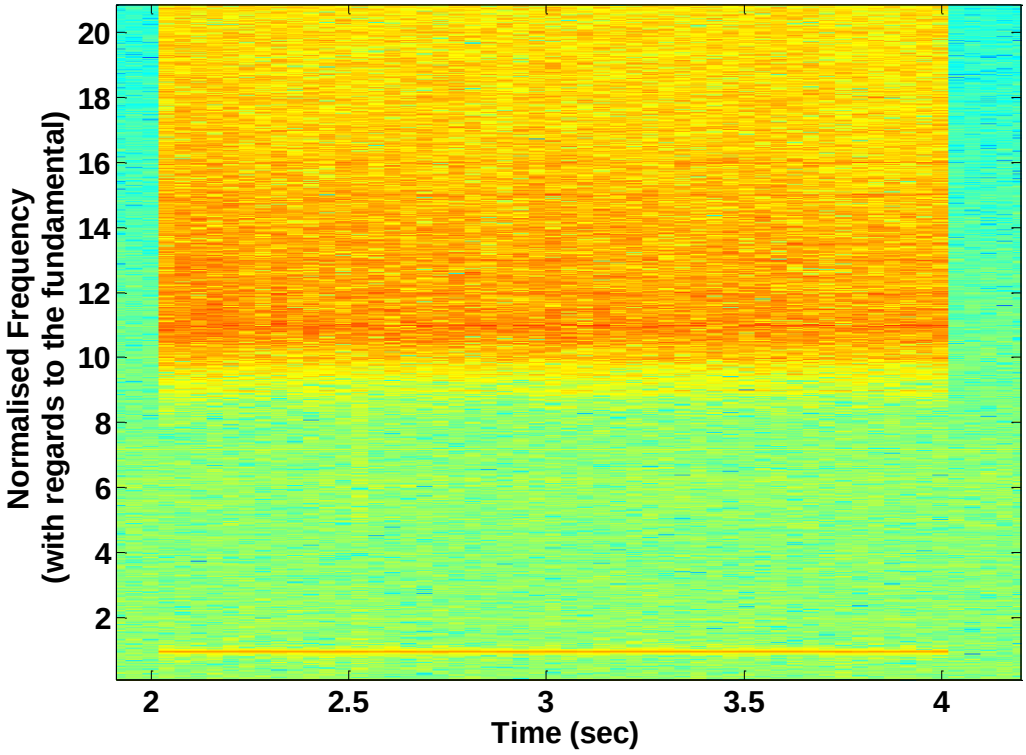

Figure 4-4: A typical spectrogram of the signal received on the PCD during a cavitation inducing regime, at 0.5MHz, at 2.05MPa p- and for 2s.

The POC graph shows whether or not inertial cavitation activity is happening but doesn't include any information as to the magnitude of the variance of broadband noise emissions. Comparing the broadband noise received on the PCD after each and every exposure with the noise floor provides insight on the evolution of cavitation activity at the focus. Figure 4-5 shows the mean broadband noise received over the duration of a HIFU exposure normalised to the noise floor against the corresponding pressure amplitude. Figure 4-5 is intended to provide a measure of the expected value of the variance (which is proportional to the energy) of radiated broadband noise for each set of exposure conditions. In other words, this indicates how mild or strong, the cavitation

activity is likely to be for a given set of exposure conditions. At 0.41MPa p-, only the noise floor is detected. As the pressure amplitude is further increased to 0.82MPa p- (≈50% POC) and 1.23MPa p- (≈80% POC) there is mild cavitation happening at the focus. The relatively large error bars are due to the fact that even mild cavitation is not always instigated at these two pressure amplitudes, which is in strong agreement with the POC graph. Once the 100% POC threshold, 1.6MPa p-, is reached there is a dramatic increase in the received broadband noise indicative of strong cavitation activity happening at the focus.

Further increase of the pressure amplitude to 2.46MPa p- results in a decreased broadband noise being received by the PCD. This can be attributed to cavitation bubbles being formed along the propagation path towards the HIFU transducer that shield the original acoustic focus, as it has been previously reported in tissue-mimicking material (Thomas et al. 2005). The -6dB focal depth of the spherically focussed HIFU transducer at 0.5MHz being 30mm, the pressure amplitude in the region between the skin and the nominal focus is more than half the focal pressure. When the focal pressure is 2.46MPa p-, the pressure in the pre-focal region exceeds 1.23MPa p-, which as demonstrated by Figure 4-2 is amply sufficient to cause cavitation. Pre-focal occurrence of cavitation activity will result in a decrease of the focal cavitation activity due to shielding. These backscatter emissions are therefore not representative of the focal activity and can't be used for further reference.

With the exception of the results obtained at 1.23MPa p-, which can also be attributed to experimental uncertainty, the mean broadband energy received is greater for longer exposures. This strengthens even further the conclusion that in adipose tissue and within the experimental parameter' range tested, cavitation activity isn't instigated instantly but

takes a number of cycles to evolve even under pressure amplitudes greater than the cavitation threshold. However, once it sets it is sustained throughout the exposure.

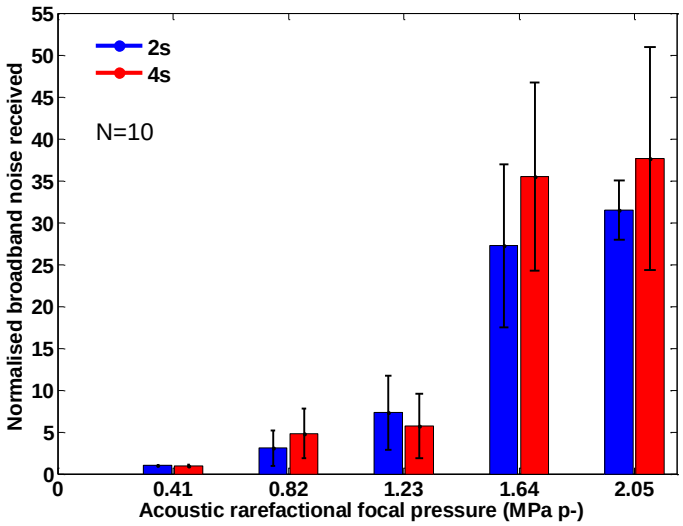

Figure 4-5: Expected value of the broadband noise variance received over HIFU exposure normalized to the noise floor. Error bars indicate the standard deviation of the exposure-averaged broadband noise variance across 10 independent exposures carried out in several tissue samples and at several different locations within each tissue sample. It should be noted that the expected values at 0.82 and 1.23 MPa p- take into account those exposures for which no cavitation was observed. Broadband noise received increases dramatically once the 100% POC threshold is reached. Further increase of the pressure amplitudes to 2.46MPa p- results in a decreased broadband signal received attribute to an unstable growth of the bubble cloud towards the HIFU transducer and shielding of the original focus.

The exact same procedure was repeated at 1.1, 1.6 &3.4MHz to identify the corresponding inertial cavitation thresholds. It was found that inertial cavitation was never instigated at any of the higher frequencies even at the max *in situ* peak rarefactional pressures tested, which were specified by the upper operating limit of the HIFU transducers. It was concluded that the cavitation threshold at these higher frequencies was much higher than at 0.5MHz, as would be expected on the basis of the underlying theory, and thus lower, non-cavitation-inducing pressure amplitudes are used in all subsequent exposures.

4.3 HIFU-induced heating

The peak focal temperature rises induced in adipose tissue during HIFU exposures at each of the four operating frequencies were measured for multiple pressure amplitudes and for two exposure durations, 2s and 4s. Given that inertial cavitation was readily initiated within the range of pressure amplitudes used at 0.5MHz, simultaneous measurements of cavitation activity and temperature rises further enabled investigation of cavitation-enhanced heating in adipose tissue.

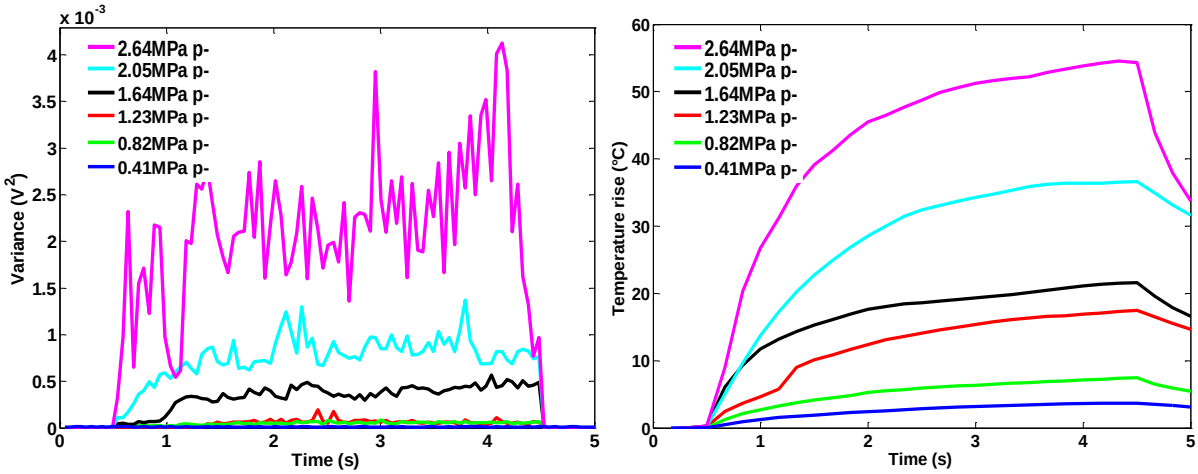

Figure 4-6: Variance of the PCD signal received during exposures at 0.5MHz for 4s at multiple *in situ* pressure amplitudes (left) and the corresponding focal temperature rises detected.

During thermometry at very high pressure amplitudes, unexpected fluctuations in the temperature measurements were sometimes observed. These are believed to be due to artefactual activity on the thermocouple surface, because the rate of temperature change was much faster than the timescales normally associated with tissue heating. Any such measurements were therefore discarded.

Figure 4-6 shows the variance of the received PCD signal (left) and the simultaneously detected focal temperature rises (right) as an illustrative example of the pressure amplitudes they correspond to. At 0.41MPa p-, pressure amplitude below the cavitation threshold, the noise floor was only detected by the PCD and there was a subtle corresponding focal temperature rise of 3.6°C. This particular exposure at 0.82MPa p-, already defined as the cavitation threshold in porcine *ex vivo* adipose tissue, didn't instigate focal cavitation activity as can be concluded by the low variance of the received signal and induced a moderate focal temperature rise of 7.5°C due to gradual and linear heating. The exposure at 1.23MPa p-, which is below the 100% POC threshold, resulted in a received signal of very low amplitude with no strong broadband noise components as the frequency domain analysis revealed. A closer look to the temperature profile obtained during this particular exposure at 1.23MPa p-, suggests that the shape of the curve has a sudden increase after 0.5s within the exposure, which is completely unexpected and results in a peak temperature rise that is much greater than the one that would have resulted given the initial slope -from 0.5 to 1s- of the temperature curve. Such temperature measurements were therefore assumed to be artefactual due to uncharacteristic cavitation activity surrounding the thermocouple tip and the decision was made to discard them.

At pressure amplitudes above the cavitation threshold, 1.64, 2.05, 2.46MPap-, there is a dramatic increase of the variance of the received signal with broadband noise always dominating and sustained throughout the duration of the exposure - as it is verified by the frequency analysis-, indicative of the onset of cavitation activity. The corresponding peak focal temperature rises are great, which suggests that cavitation produces heating at

rates well above those present in the absence of cavitation, when linear heating is the primary cause of the temperature rise.

To further verify this last finding, that cavitation enhances heat deposition, sample cavitation and thermocouple traces obtained during 2s exposures at 0.5MHz and at 0.82MPa p- are shown in Figure 4-7. These results, which show the recorded temperature rise at the same pressure amplitude in the presence (top) and in the absence (bottom) of cavitation activity, suggest that there is a very significant contribution of cavitation to heating.

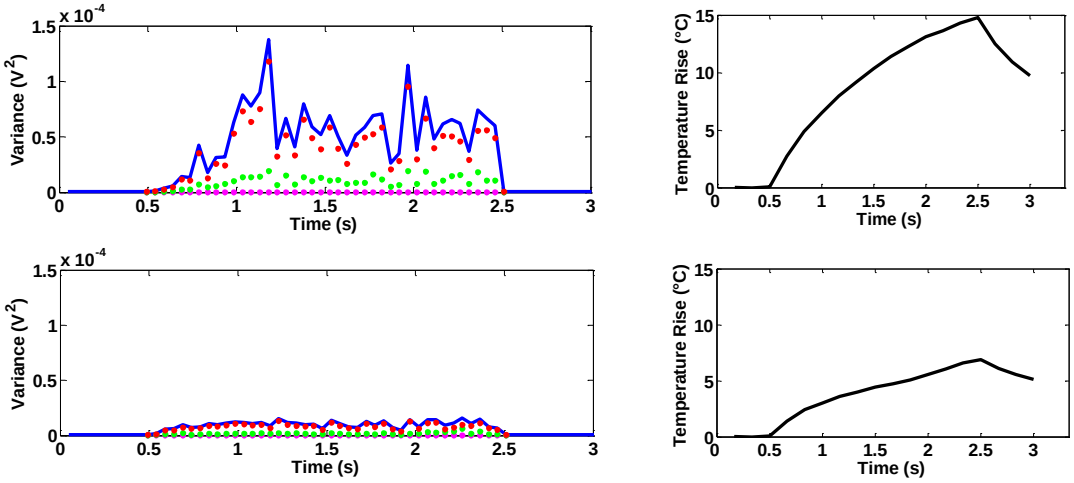

Figure 4-7: Cavitation and thermocouple traces at the same *in-situ* pressure amplitude in the presence (top) and in the absence (bottom) of cavitation activity.

Cavitation activity could not be initiated at any of the three higher frequencies over the range of *in situ* pressure amplitudes investigated in the present work. However, these are expected to favour heat deposition due to the higher attenuation coefficient. A representative set of measurements is shown in Figure 4-8, for exposures at all four operating frequencies, 0.5, 1.1, 1.6 & 3.4 MHz, at multiple *in situ* pressure amplitudes and for two exposure durations.

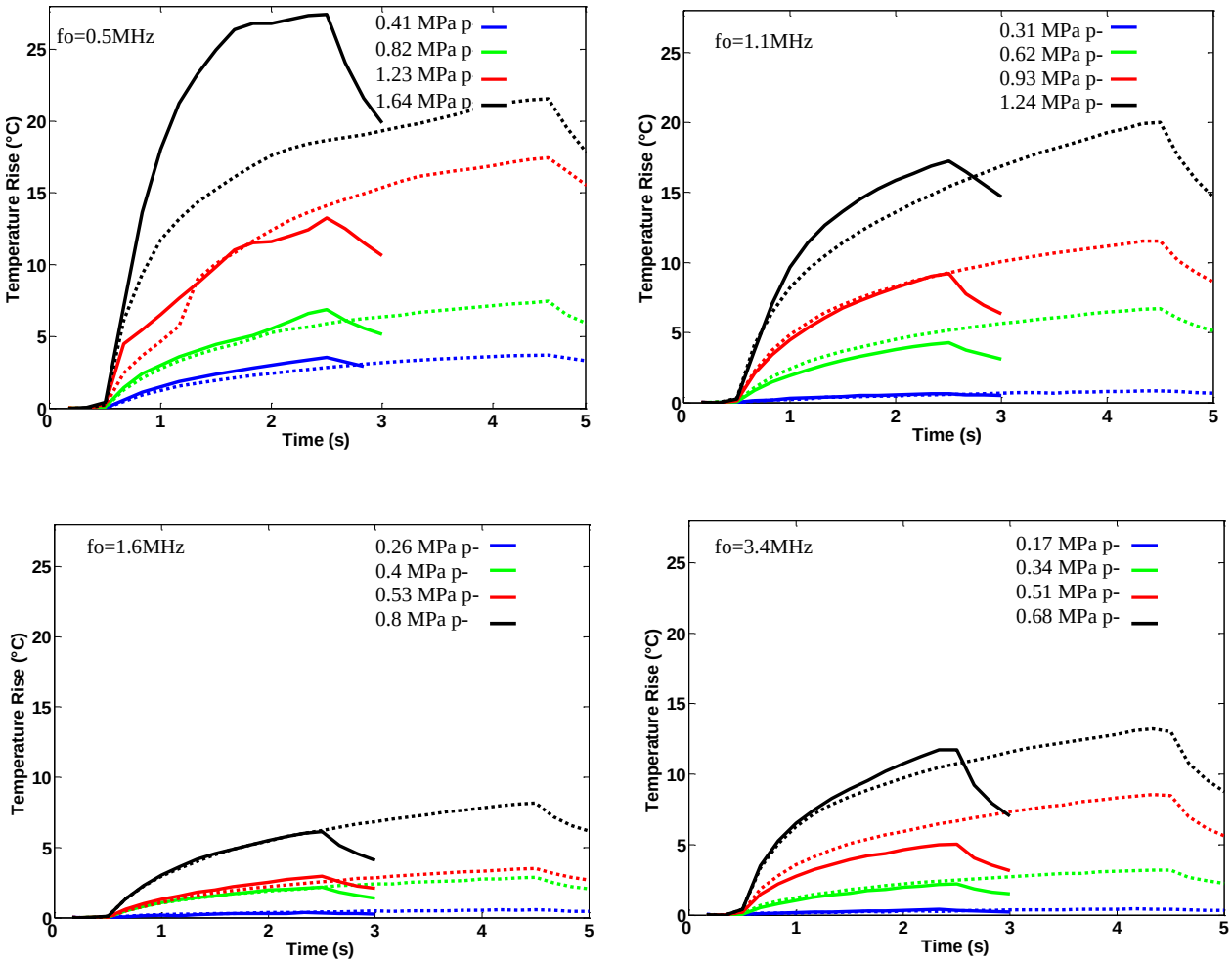

Figure 4-8: Representative temperature profiles obtained at all four frequencies, at multiple *in situ* peak rarefactional pressures and over 2 and 4 s exposures.

After numerous repeats (N>6 for each setting) of the above temperature measurements, the mean peak focal temperature rises and the corresponding standard deviations were computed for exposures carried out under all exposure parameters mentioned earlier, and are summarized in Table 4-3.

Table 4-3: Summary of the mean peak focal temperature rises detected at all frequencies, pressure amplitudes and exposure durations tested (N>6).

Frequency (MHz)	*Exposure Duration (s)*	*In-situ rarefactional pressure (MPa p-)*	*mean dT± standard deviation*
0.5	2	0.41	1.9 ± 1.3
		0.82	10.9 ± 4.1
		1.23	11.2 ± 2.9
		1.64	26 ± 1.9
		2.05	39 ± 9.8
		2.46	54.4 ± 7.9
	4	0.41	3 ± 1.6
		0.82	8.3 ± 6.4
		1.23	17.2 ± 0.2
		1.64	19.4 ± 3
		2.05	44 ± 10.5
		2.46	58 ± 4.9
1.1	2	0.31	0.6 ± 0.04
		0.62	4.3 ± 0.09
		0.93	8 ± 1
		1.24	18 ± 1.5
		1.55	25.6 ± 2.2
		1.86	36.2 ± 4.8
	4	0.31	0.8 ± 0.1
		0.62	6.7 ± 0.07
		0.93	11.6 ± 0.8
		1.24	18.7 ± 5.5
		1.55	28.7 ± 1.7
		1.86	36.6 ± 2.5
1.5	2	0.26	0.3 ± 0
		0.4	1.7 ± 0.45
		0.53	3.1 ± 1.1
		0.8	5.6 ± 1.05
		1	7.1 ± 1.4
		1.32	13.3 ± 3.8
		1.6	15.6 ± 4.2
	4	0.26	0.4 ± 0.1
		0.4	2.4 ± 0.5
		0.53	3.8 ± 2.2

		0.8	7.7 ± 1.5
		1	9.6 ± 1.8
		1.32	17.9 ± 6.8
		1.6	20.7 ± 4.3
3.3	2	0.17	0.4 ± 0.02
		0.34	2 ± 0.3
		0.51	5.1 ± 0.1
		0.68	10.9 ± 0.6
		0.85	13.1 ± 5.6
		1	18.5 ± 9.6
	4	0.17	0.4 ± 0.01
		0.34	2.8 ± 0.5
		0.51	8.4 ± 0.8
		0.68	12.4 ± 2.8
		0.85	17 ± 2.5
		1	18 ± 3.8

These results are also summarized in Figure 4-9, which shows the mean peak focal temperature rise achieved at all four frequencies during 2 and 4s HIFU exposures as a function of the acoustic intensity. At 0.5MHz, it should be noted that for the three intensities that are lower than the 100% POC cavitation threshold, cavitation occurred in some of the exposures but not all, in accordance with Figure 4-2. At the lowest intensity (6W/cm^2 or 0.41MPa p_-), no cavitation occurs, and there is a modest temperature rise of 2°C over 2s. At the second lowest intensity (24W/cm^2, which corresponds to 0.82MPa p_-), the temperature rise is 10.9°C, which is 5.5 times (i.e. more than four times) the temperature rise observed at the lowest intensity, even though at 0.82MPa p_- cavitation only occurred in half the exposures as shown in Figure 4-2. As the pressure amplitude is increased further, cavitation continues to occur but the extent of pre-focal cavitation correspondingly increases, decreasing the apparent contribution of cavitation-enhanced heating to the overall temperature rise.

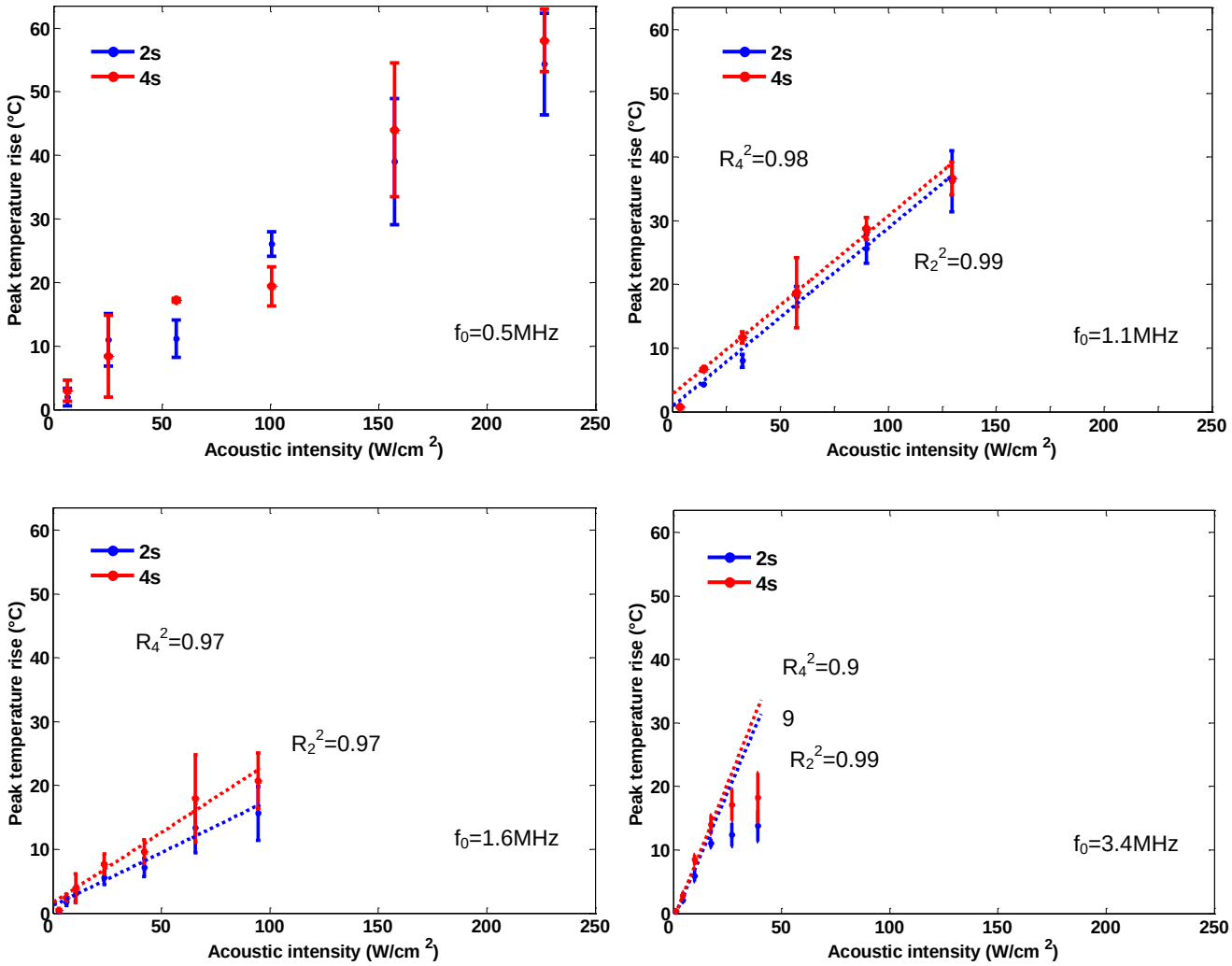

Figure 4-9: Plots showing the mean maximum focal temperature rises achieved at 0.5MHz (top-left), 1.1MHz (top-right), 1.6MHz (bottom-left) and 3.4MHz (bottom-right) during 2 and 4s HIFU exposures as a function of the *in situ* acoustic intensity. Data points are expressed in mean ± standard deviation (N=6). Note that the subscript of R^2 indicates the exposures' duration in seconds.

At the higher frequencies, very repeatable temperature rises, shown in Table 4-3 were induced and a strong linear correlation was found between the acoustic intensity and the mean maximum temperatures achieved, that is well-described by the linear acoustic absorption theory. It is only at the highest operating frequency, 3.4MHz that the highest acoustic intensities resulted in lower maximum focal temperatures than expected. It is hypothesized that this is due to higher levels of non-linear propagation at 3.4MHz in fat,

resulting in increased pre-focal attenuation of the acoustic wave. At all four frequencies, lengthening the exposure duration from 2 to 4s only resulted in a small increase in focal temperature rises.

4.4 Summary of *in vitro* cavitation detection and thermometry

In this chapter, preliminary experimental work carried out in the laboratory using excised porcine subcutaneous adipose tissue was presented. Initial results accurately defined the cavitation threshold in excised porcine subcutaneous fat at 0.5MHz and showed that cavitation activity enhances focal heat deposition. Cavitation activity could not be instigated at any of the higher frequencies within our range of safe operating limits of the HIFU transducers and the resulting temperature profiles exhibited a very good linear correlation with the acoustic intensity. Based on the acoustic and temperature results we concluded that 0.5MHz is the optimal treatment frequency combining instigation of cavitation and therapeutically relevant heating. Additionally, the use of a coaxially aligned PCD proved to be a reliable way of detecting and qualifying the kind of cavitation activity induced in the tissue, thus providing a non-invasive way of checking the successful deposition of HIFU energy to the focus. Given the aim of the final application, which is to non-invasively destroy subcutaneous fat and the results obtained so far, the need to design an application specific HIFU transducer that is capable of delivering more than 2MPa p- over a much larger, therapeutically relevant volume was pointed out.

In the following chapter, we focus on the resulting histological damage caused to the tissue following a cavitation inducing HIFU exposure.

5 Assessment of Ultrasound-Induced Histological Damage in Adipose Tissue *Ex Vivo*

Based on the cavitation and temperature measurements carried out in the laboratory, it was concluded that the use of 0.5MHz, at pressure amplitudes above 1.6MPa p-, the 100% POC threshold, would be optimal for this application. The next step was to check whether HIFU exposures at these input settings result in adipose tissue destruction, which is the desired effect of the treatment.

This chapter presents preliminary histological results obtained in the laboratory using excised porcine subcutaneous fat *ex* vivo. Tissue samples were histologically processed according to the protocol described in Section 3.5. Untreated samples were used as control samples that all treated ones were compared to and treated ones provided information about the presence and the extent of the tissue damage caused following a cavitation inducing HIFU exposure both at a macroscopic and at a cellular level. The experimental setup used for all results shown hereafter is the one described earlier in the Materials and Methods chapter.

5.1 Untreated/ Control samples

The non-sonicated samples served as negative control samples that all treated ones were compared to. Figure 5-1 shows a control sample as seen under the camera and the microscope: top view of the skin (left), side view of one of the two semi-cylinders of subcutaneous adipose tissue resulted after cutting the cylindrical block of tissue trough its centre using a blade (centre) and at a cellular level, a histological slide stained with H&E (right). This last slide reveals normal adipose tissue and collagen. The cellular

structure is very well maintained with no tears present. The adipocytes are the round areas comprising most of the slide and all have healthy round nuclei attached to their membrane (the dark and dense black dots) being attached to the adipocytes membrane. The red long area on the top left of the picture in the form of elongated fibers is the connective tissue, which comprises healthy collagen.

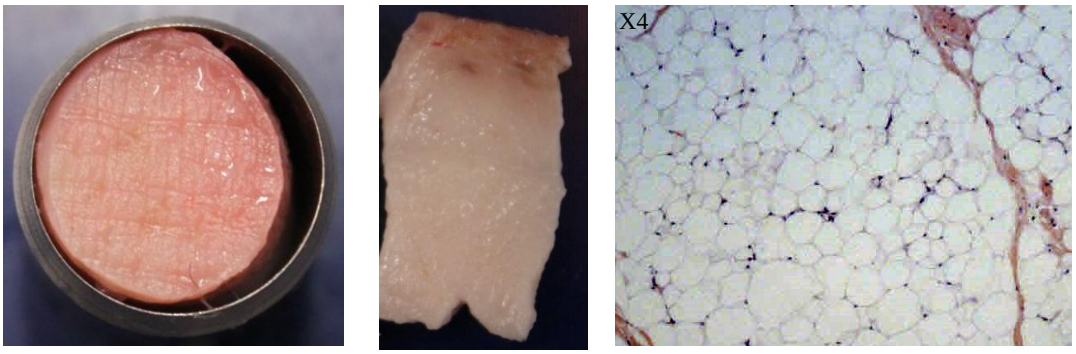

Figure 5-1: Control samples. Top view of the skin (left) and side view of one of the two semi-cylinders that result following slicing of the cylindrical block of adipose tissue through its centre (centre). A histological slide stained with H&E (right), reveals a very well maintained cellular structure with no tears or discontinuities present and with all adipocytes having healthy round nuclei attached to their membrane.

5.2 Macroscopic tissue damage following a cavitation inducing exposure

Preliminary exposures were carried out at 0.5MHz and at 2.5MPa p-*in situ* pressure amplitude, one of the highest pressure amplitudes used and for multiple exposure durations. The 60s exposure is a non-clinically relevant duration but was used as an experimental test and resulted in the macroscopical changes shown in Figure 5-2. The top view of the skin before and after treatment is shown on the left and centre respectively. Signs of skin burns and a subtle change of the colour can be barely seen on the treated sample as indicated by the arrows. The two semi-cylindrical halves of the cylindrical treated block of tissue that resulted after slicing the tissue through its centre

immediately after exposure, are shown next to a control half (right). There is change of the colour of both the treated samples around 15mm, which coincides with the shooting depth, and there was a gradual change of the stiffness, which was only manually tested, with the treated ones being much stiffer than the untreated ones around the focus. The PCD signal suggests that at this frequency and at this pressure amplitude the broadband noise was dominant throughout the exposure, but there was a drop of the total power of the signal after 30s of exposure.

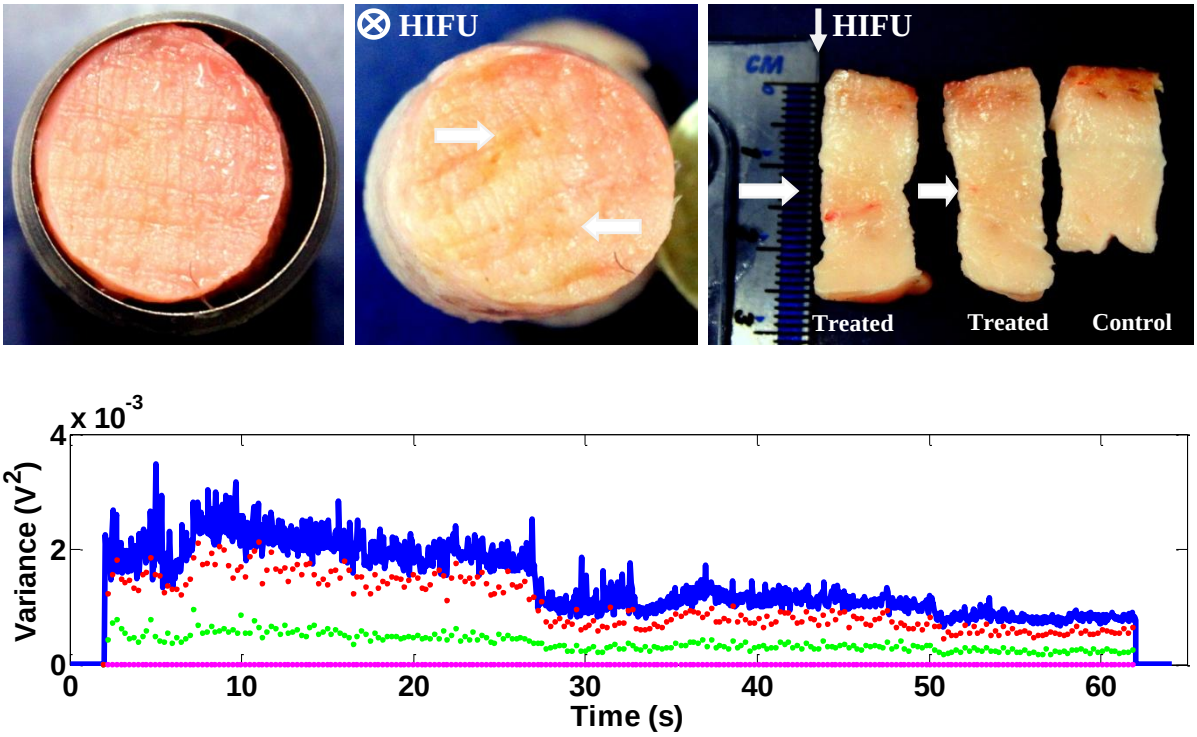

Figure 5-2: (Top) Macroscopic damage following a HIFU exposure at 0.5MHa, at 2.5MPa p- and for 60s. Top view of the skin of the treated sample before (left) and after the cavitation inducing HIFU treatment (centre) and side view of the sliced semi-cylindrical samples (right) as seen under the camera. (Bottom) The variance of the received PCD signal during this particular exposure. Decomposition of the signal to its fundamental (magenta), harmonics (green) and broadband noise (red) verifies the presence of focal inertial cavitation activity.

Following this initial exposure, the effect of the exposure duration to the resulting tissue damage was investigated. The exposure duration was therefore gradually reduced to 5s, while all the other exposure parameters were kept constant. All these exposures invariably

resulted in similar gross macroscopical changes, visualised as faint brown spots on the skin and darkening and stiffening of the adipose tissue at around 15mm below the skin, where the focus was always placed. The corresponding received PCD signals were always very repeatable and verified that inertial cavitation activity was present, dominant and of consistent strength throughout the whole duration of the exposure.

Based on the above results the importance and the extent of the brown spots appearing on the skin following all cavitation-inducing HIFU exposures were assessed. Multiple slices parallel to the skin were cut at 1mm intervals and are shown in Figure 5-3 for a HIFU exposure at 0.5MHz, at 2.5MPa p- for 30s. These brown spots are present until 4mm below the skin, whereas they disappear from this depth onwards.

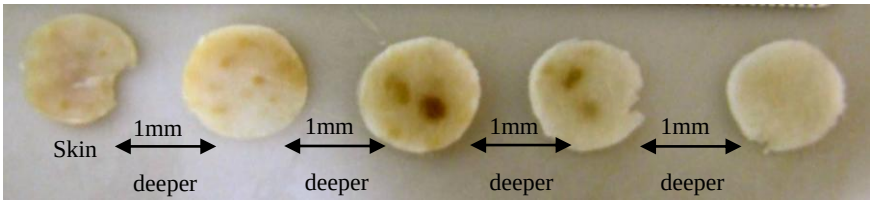

Figure 5-3: Skin damage following a cavitation inducing HIFU exposure at 0.5MHz, 2.5MPa p- for 30s. The top layer of the skin (left) followed by slices cut parallel to the skin at 1mm intervals.

However, these results were not completely unexpected, given the limitations of the existing non-custom built operating HIFU transducer. The spherical HIFU transducer used for all these experiments was positioned inside the cone-shaped applicator, so that the HIFU focus was always placed at 15mm beneath the skin and within the tissue. Given this geometry and the axial pressure profile of this HIFU transducer, for a given *in situ* focal peak pressure amplitude the skin surface is exposed to only slightly smaller pressure amplitude as shown in Figure 5-4.

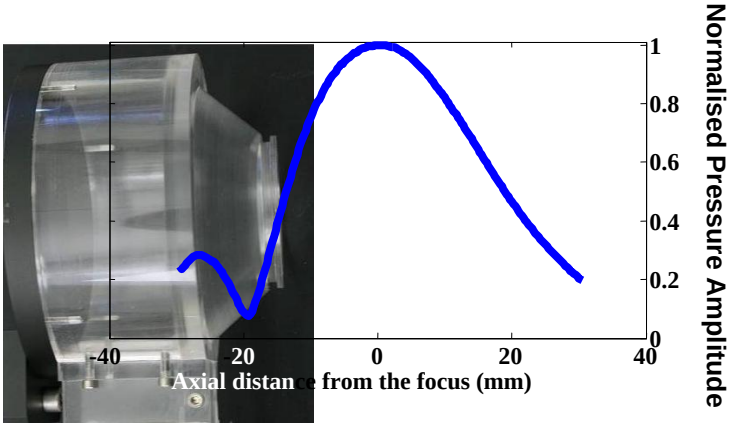

Figure 5-4: Illustration of the operating setup. The front end of the applicator is always placed in contact with the skin, so that the HIFU focus is positioned at 15mm within the tissue.

5.3 Microscopic tissue damage following a cavitation inducing exposure

Given the subtle macroscopic changes observed to the skin and adipose tissue even under extreme exposure conditions, *i.e.* at 2.5MPa p-, a pressure amplitude much greater than the 100% POC threshold and for 60s, where cavitation activity was instigated over long exposure durations, a decision was made to process the treated tissue histologically. The histological study would reveal information about the induced damage at a cellular level.

The histological protocol described earlier in the Materials and Methods chapter was followed at all times and the resulting tissue sections were then analysed under the microscope. The main part of the slide consisted of healthy adipocytes, septa, red blood cells and collagen. All these were histologically intact and maintained a perfect structure. However, there was an obvious loss of integrity and a dramatic change of the cellular structure of the treated tissue around the HIFU focus. Figure 5-5 displays the area around the focus of a tissue section cut through the skin and adipose tissue, taken from a block of tissue that was exposed at 0.5MHz, at 2.5MPa p- for 4s and was stained with H&E. Extensive tears are present at the expected depth within the tissue and the integrity of the

cellular structure is heavily damaged. The adipocytes look ruptured, while their nuclei are no longer round and attached to their membrane. Besides, these nuclei appear elongated and pyknotic, thus verifying that these adipocytes are no longer healthy. In addition, collagen has lost its fibrillar orientation and structure.

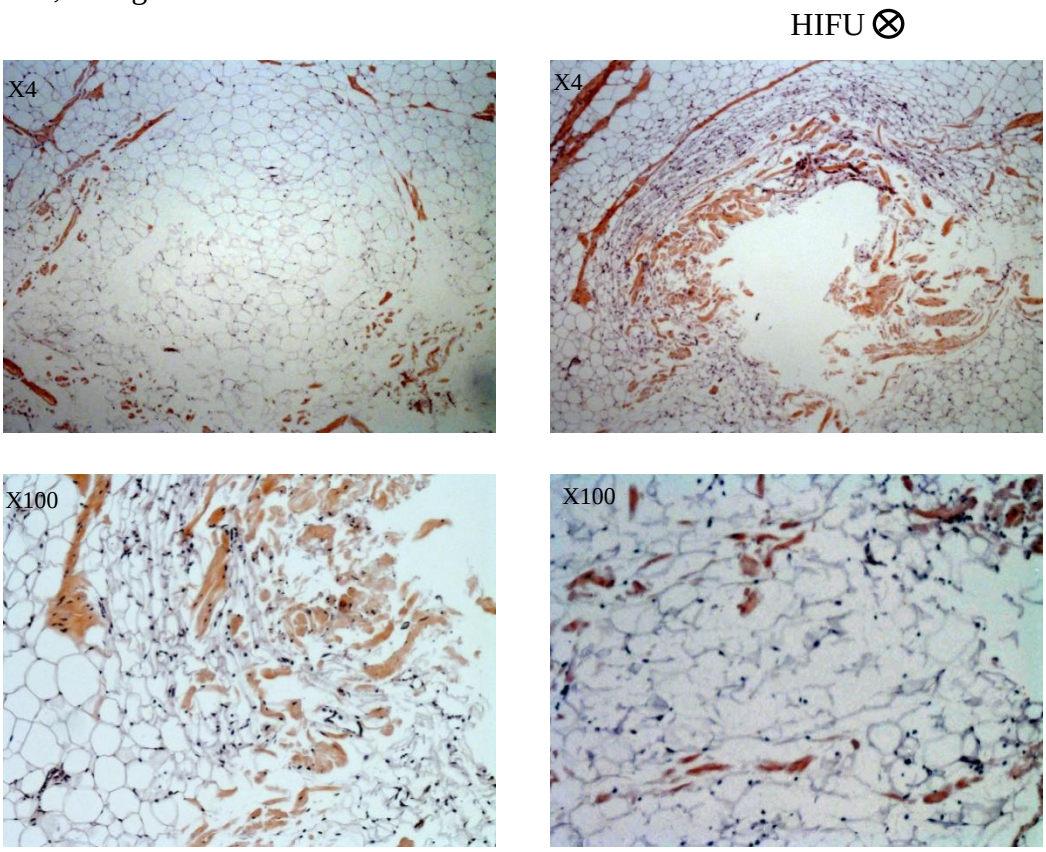

Figure 5-5: Histological slides of the treated area around the HIFU focus following a cavitation inducing regime, at 0.5MHz, 2.5MPa p-, 4s. There is a dramatic loss of the cellular structure, with extensive tears present (up), while the adipocytes are heavily ruptures. The nuclei are no longer attached to the membrane, are elongated and pyknotic. Collagen fibres are also damaged (bottom).

This configuration is recognizable and reproducible among treated areas within the adipose tissue. Furthermore, the absence of any of the above described features in the control samples leads us to the conclusion that these are caused by the HIFU exposure and cannot be attributed to bad handling or cutting of the tissue.

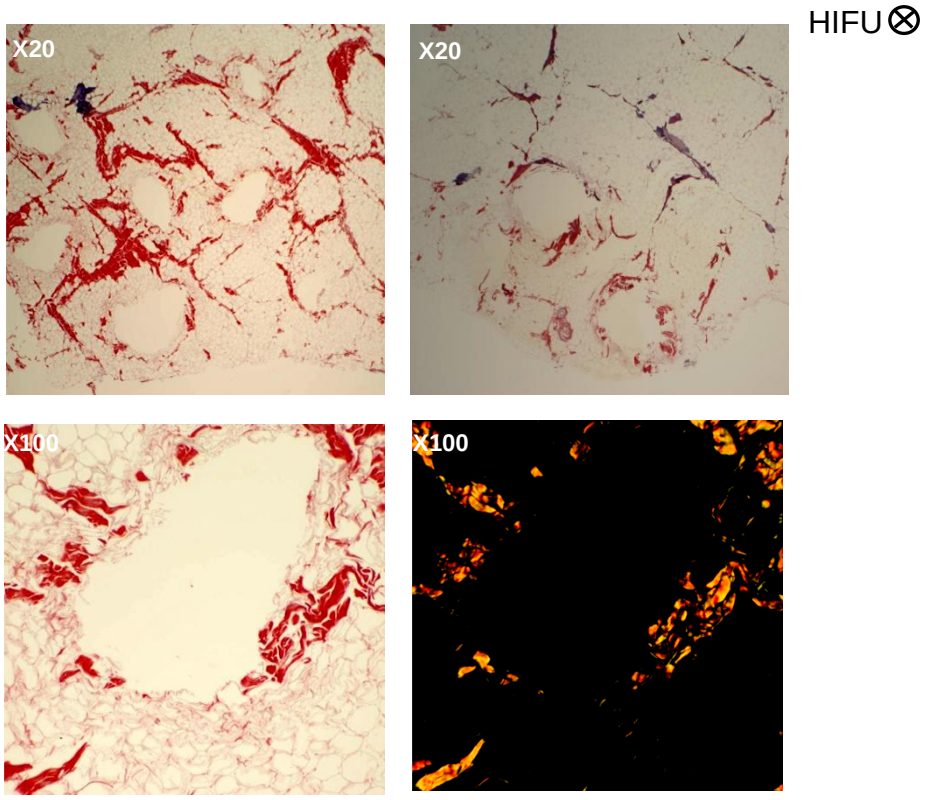

Figure 5-6: Histological slide cut parallel to the skin at 15mm depth of a sample exposed to 0.5MHz, 2.5MPa p- for 30s and stained with Picro Miller. There is extensive cellular damage, loss of cellular structure and connectivity within the tissue, together with tears present over the treated area (top). The de-colouration of the stain, blue, better seen on the top part of the top-right picture denotes heavily damaged collagen. The same lesion as seen under the light microscope (bottom-left) and under polarised lenses (bottom-right) suggests a region of intact collagen.

To further investigate the condition of the various cells within the slides, Picro Millers, a more advanced staining technique used to identify collagen damage was used in addition to H&E. Figure 5-6 shows areas within a section of adipose tissue cut parallel to the skin at 15mm depth, from a block of tissue that was treated at 0.5MHz at 2.5MPa p- for 30s. The treatment resulted in extensive cellular damage, loss of cellular structure and connectivity within the tissue. There are lots of tears present, while the adipocytes membranes are heavily damaged and misshapen (top). The de-colouration of the stain, blue, which is better seen on the top part of the top-right picture, implies that collages is heavily damaged over this region. However, collagen was not totally disrupted over the whole extent of the treated area. Figure 5-6 (bottom) shows the same lesion as seen

under the light microscope (bottom -left) and under polarised lenses (bottom -right). Based on the bright orange colour of the collagen surrounding this lesion, it can be concluded that over this particular damaged area, collagen remained histologically intact, although the adjacent adipocytes are damaged. This is not completely unexpected, since the mechanical properties of collagen are different from those of the very fragile adipose tissue.

5.4 Summary of *ex vivo* histological assessment

In this chapter preliminary histological results obtained in the laboratory using excised porcine subcutaneous adipose tissue were presented. Based on these results, it was concluded that the macroscopical changes induced to adipose tissue following a cavitation inducing HIFU exposure are subtle and thus that a detailed histological procedure needs to be carried. Optimisation of the histological technique allowed the visualisation and localisation of damage caused to the adipose tissue at a cellular level. It was therefore concluded that 0.5MHz exposures at pressure amplitudes above the 100% POC threshold and for exposure durations as short as 5s are capable of causing tissue damage.

A most important conclusion is that the damage was very well confined within the expected cavitating area, given the axial profile of the HIFU transducer. However, there was a noticeable side-effect, a skin burn due to the wide focal depth of the non-custom built spherical HIFU transducer used during all these experiments. Once more, this points out the need for a suitable and application specific HIFU transducer with a very tight and narrow focal depth that could deliver *in situ* pressure amplitudes above the

100% POC threshold over a larger volume within the tissue. Such an application-specific transducer is discussed in Chapter 8.

The next chapter presents the preliminary *in vivo* acoustic and histological results carried out to investigate the validity of the cavitation measurements, temperature measurements and histological observations carried out in *ex vivo* tissue.

6 Ultrasound-induced bioeffects in adipose tissue in vivo

*Ex vivo e*xperimental results provided encouraging initial acoustic, temperature and histological results. Inertial cavitation activity was found to be readily initiated at 0.5MHz, the lowest frequency investigated in the present work, and to result in enhanced focal heating. In addition, cavitation-inducing HIFU exposures resulted in tissue damage, manifesting itself as loss of integrity and cellular structure.

Following this series of *ex vivo* experiments, it was decided to investigate the applicability of the lessons learned in an *in vivo* environment. This chapter presents preliminary acoustic and histological results obtained *in vivo.* Modifications to the original experimental setup for improved portability and to enable *in vivo* use, the animal preparation procedure and the treatment plan are first described in detail. Acoustic results obtained under different exposure conditions are then analysed alongside the histological results.

6.1 Experimental setup

The *in vivo* series of experiments were carried out in an animal facility located in Vic, Spain. All the electronic devices and the equipment needed for experimentation had to be shipped from the Oxford biomedical ultrasonics and biotherapy laboratory in advance. The experimental setup used for the *ex vivo* experiments in the laboratory, as described in Chapter 3, therefore had to be modified in order to become more portable while still being able to deliver the ultrasound energy required and detect the information needed. A schematic representation of the experimental setup specially built for this set of *in vivo* experiments is shown in Figure 6-1.

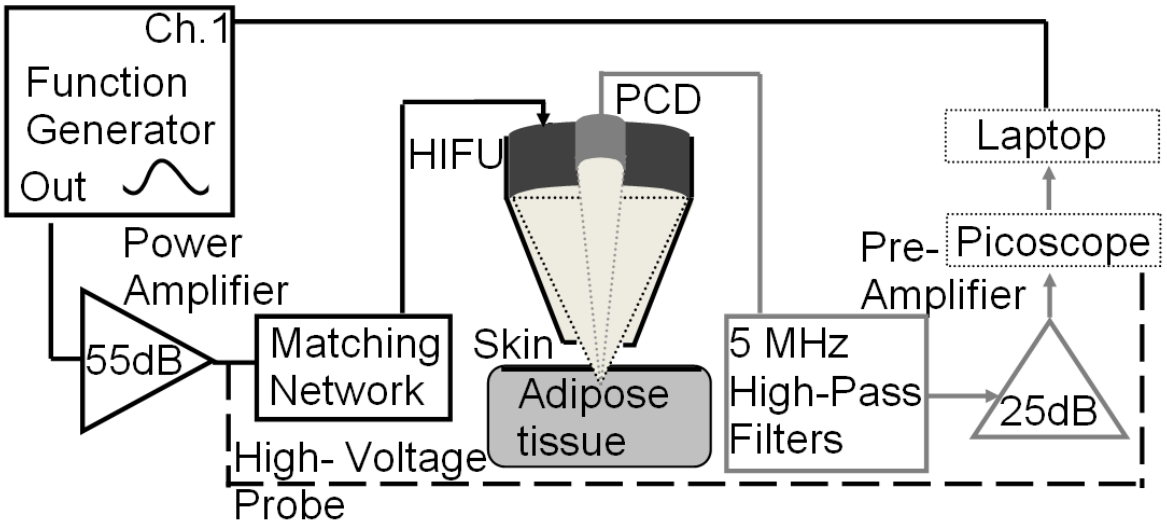

Figure 6-1: Schematic block diagram of the experimental setup used for *in vivo* experimentation: the HIFU generation loop (in black), the PCD loop (in grey), the tissue target, and the data acquisition hardware.

The *in vivo* experimental setup was identical in concept to the *ex vivo* one, but with some significant major differences which are presented hereafter. The power amplifier used (E&I 1040L, Electronics & Innovation Ltd, 55dB gain for 0.01-5MHz) was lighter and smaller than the one operating in the laboratory but of similar power gain within the frequency range of interest. Unlike the previously used amplifier (E&I A300), which was a class A amplifier, this lighter amplifier is class AB, but upon re-calibration of the HIFU transducer it was found that this had no noticeable effect on the output waveforms. The HIFU transducer (Sonic Concepts H-107B S/N-10, f.l.= 62.64mm) sent a continuous wave at 0.5MHz and acoustic signals emanating from the focus were captured by the same spherically focused single element wideband (5-20MHz) tightly focused passive cavitation detection transducer as previously used (Panametrics, f_0=15MHz, f.l.=75mm, focal beam-width at 15MHz=800μm, active diameter=12.5mm). The signal received by the coaxially aligned PCD was high-pass filtered and amplified as already explained in detail in Chapter 3, but was then digitized by a PC based digital oscilloscope (Picoscope

3205, Pico Technology) instead of an on-board DAQ card. The picoscope digitizer differed from the previously used DAQ card in terms of sampling rate (25MHz vs. 100 MHz) and number of bits (8 vs. 14 bits). However, as demonstrated hereafter, the signal-to-noise ratio remained sufficient to detect cavitation reliably in spite of this reduction in dynamic range. 800-μs windows of PCD data were digitised every 25msec at a sampling frequency of 25MHz and stored in binary form.

The HIFU/PCD assembly was positioned inside the applicator and the HIFU focus was always placed at 15mm below the skin. Unfortunately there were no facilities available in the animal centre to de-ionise or de-gas water, therefore water was firstly boiled, allowed to cool to room temperature and then gently poured inside the applicator. The exposed adipose tissue was no longer immersed in water, as was the case for all experiments carried out in the laboratory. An ultrasound coupling gel (Aquasonic 100 Ultrasound transmission gel, Parker Laboratories, Inc.) was at all times applied on the skin of the area to be treated to allow good transmission of ultrasound energy from the water-filled applicator to the tissue.

The acoustic field of the operating HIFU transducer has already been characterised both under free field conditions and *in situ* in adipose tissue, as already described in detail in Section 4.1. Thus *in situ* pressures amplitudes that account for the total transmission losses along the axis of ultrasound propagation in excised porcine subcutaneous adipose tissue are always reported. Given that measurements of the exact focal pressures induced *in vivo* are not possible, those same *in situ* measurements in *ex vivo* tissue, reported in Table 4-2, are also assumed for all *in vivo* experimentation.

6.2 Animal preparation

Two female pigs (Large white breed, 300kg each) were used daily throughout the whole duration of the *in vivo* experimentation. Before every experiment, a vet was delivering a hypodermic injection of a relaxation drug first (Azaperone 40mg/ml, 6ml standard dosage) and anaesthetics (Imalgene 10ml) 10-15min later. The vet was present at all times, checking the health condition of both animals and repeating the tranquilizer injections when needed.

Based on experience from the *ex vivo* experiments, it was known that dorsal subcutaneous fat exhibited the largest adipose tissue thickness and was thus the right area for treatment. An A-mode diagnostic ultrasound device (Lean-Meter Series 12, Renco Corp.) was used to accurately measure the thickness of the subcutaneous fat layer of the whole area of interest. Given the axial pressure profile of the HIFU transducer used, see Section 4.1, the desired area for the treatment had to have a fat thickness of at least 30mm. After shaving the pigs' backs, four large rectangles were drawn on their skin, using waterproof pens (Staedtler permanent), one for each of the four experimental days. Each one of these rectangles was then further divided into six even areas, four to be treated using the four different set of ultrasound parameters investigated and two to be used as controls. One large rectangle was treated on each of the experimental days, and at the end of the fourth day the first animal was terminated, whilst the second animal was kept for a further 30 days prior to termination.

Following animal termination, the entire dorsal fat area was removed as a slab. The aim was to reduce the amount of relative movement between the skin and the adipose tissue attached to it, which could result in a miss-alignment between the grid drawn on the

animal's skin and the actual location of the HIFU focus within the adipose tissue. Individual blocks of tissue (approximately 30 x 30 x 80mm) were then excised from each of the six sub-areas in each of the four large rectangles. These samples were immediately dropped into a 10% NBF and transferred to the Department of Surgical Research in Northwick Park Hospital, in London. Planar sections parallel to the skin's surface were cut at three different depths below the skin, at 10, 15 and 20mm respectively and the histological procedure already described in Section 3.5 was followed. The outcome of these histological investigations is reported in Section 6.6.

6.3 Determination of Cavitation threshold

The *ex vivo* experiments carried out in the laboratory have shown that cavitation activity was always initiated in excised porcine subcutaneous adipose tissue at 0.5MHz at *in situ* pressure amplitudes above 1.64MPa p-, which was then defined as the 100% POC threshold.

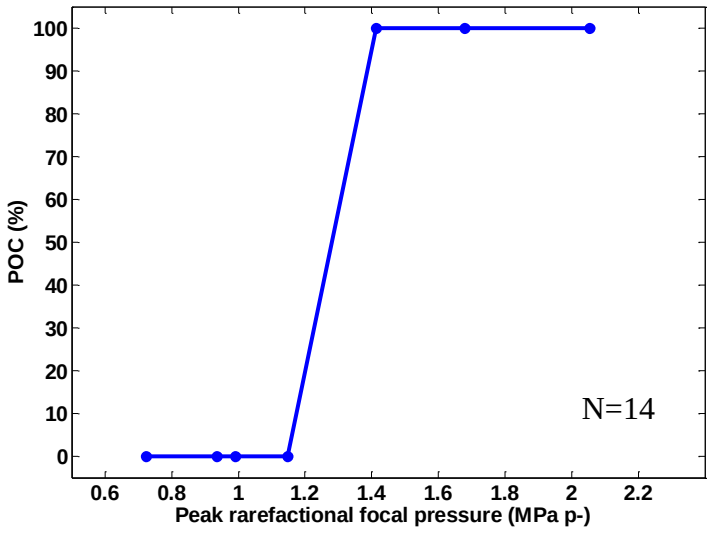

Figure 6-2: Probability of cavitation at 0.5MHz across six *in-situ* pressure amplitudes for 4s exposures.

Similarly, the *in vivo* 100% POC threshold had to be defined prior to the start of this set of experiments. A number (N=14) of short (4s) HIFU exposures at several different *in situ* pressure amplitudes were therefore performed and the results are shown in Figure 6-2. These results suggest that an *in situ* focal peak rarefactional pressure amplitude greater than 1.5MPa always resulted in cavitation activity *in vivo*, which is in very good agreement with the 100% POC threshold of 1.64MPa p- identified during *ex vivo* experimentation.

6.4 Treatment plan

In vivo HIFU exposures were performed for four consecutive days, labelled days 1-4 respectively, and a new area was treated every day. Both animals were exposed to exactly the same HIFU parameters every day throughout the whole duration of this experimentation. The four different sets of ultrasound parameters investigated every day to each animal are summarised in Table 6-1.

After identifying the *in vivo* 100% POC threshold, the *in situ* pressures amplitudes needed to initiate cavitation were known. In order to further investigate whether inertial cavitation activity is the mechanism underlying the resulting histological damage observed in Chapter 5, a long 10s exposure was carried out over Area 1 at 0.5MPa p-, at a peak rarefactional pressure where no cavitation was expected to be induced. The rationale was to then have an area exposed to pressure amplitude just above the cavitation threshold for an exposure duration that is clinically relevant on one hand but not too short for histological damage to occur according to *ex vivo* results on the other hand, so Area 2 was exposed to 1.6MPa p- for 4s. Keeping the pressure constant, a first attempt to perform a continuous scan and treat a large surface was tried over Area 3. The

applicator was scanned over a pre-determined area (3x5cm^2) for a total of 30s, treating each point for approximately 2s. Finally, Area 4 was exposed to 2MPa p-, the greatest pressure amplitude investigated *ex vivo,* for 10s. Strong cavitation activity is expected to be induced at this pressure amplitude both focally and pre-focally throughout the whole duration of the exposure, which was expected to result in definite histological damage. In addition, a fifth un-exposed area was assigned each day to act as a control.

Table 6-1: HIFU exposure parameters investigated during *in vivo* experimentation. Both animals were exposed to all these four different sets of exposure parameters for four consecutive days.

Areas	*HIFU exposure parameters*			
	Frequency (MHz)	*In situ pressure amplitude (MPa p-)*	*Exposure duration (s)*	*Comments*
1	0.5	0.5	10	Point
2	0.5	1.6	4	Point
3	0.5	1.6	30	Scan
4	0.5	2	10	Point
5	-	-	-	Control

Animal donor ‘one’ was put down on the fifth day, the day following the last day of experimentation, in order to check the immediate effects of the different treatment regimes investigated and to identify any differences between blocks of adipose tissue treated on different days, *i.e.* whether there are any histological differences between tissue treated on day 1 and that treated later on. Animal donor ‘two’ was terminated 30 days later in order to check the long-term effects of the treatments. The general health condition of that animal was regularly checked during this period, to check for any potential side-effects following the HIFU treatment.

6.5 Cavitation activity during treatment

Representative plots of the variance of the signal received by the coaxially aligned PCD during the four different HIFU exposure treatment regimes investigated are shown in continuous blue line in Figure 6-3. At sub-threshold pressure amplitude 0.5MPa p-, the received signal was indistinguishable from the baseline, indicating that there was no cavitation activity induced, as expected (top left). The variance of the signal obtained during exposures at 1.6MPa p- (top right and bottom left) was always close to $0.5x10^{-3}V^2$, greater than the baseline noise and consistent throughout the whole duration of the exposure, confirming that cavitation activity was initiated and sustained over the course of the exposures. At the highest operating input pressure setting, 2MPa p-, the variance of the received signal was increased compared to the one received at 1.6MPa p-. The PCD signal received at the three pressure amplitudes investigated *in vivo* was of similar order of magnitude to the one received at the same pressure amplitudes during *ex* vivo experimentation, as presented earlier in Section 4.2.

In order to qualify the type of cavitation activity induced, frequency-domain analysis was performed, as already described in detail in Sections 3.2.3, and the energy distribution of the fundamental, harmonics and broadband noise is separately plotted on all graphs in Figure 6-3 in red, green and magenta dots respectively. This analysis confirms that any increase of the variance of the received signal was always due to increased broadband noise emissions over the course of the exposure, indicative of inertial cavitation, similar to what was observed during *ex vivo* experimentation, presented in Section 4.2.

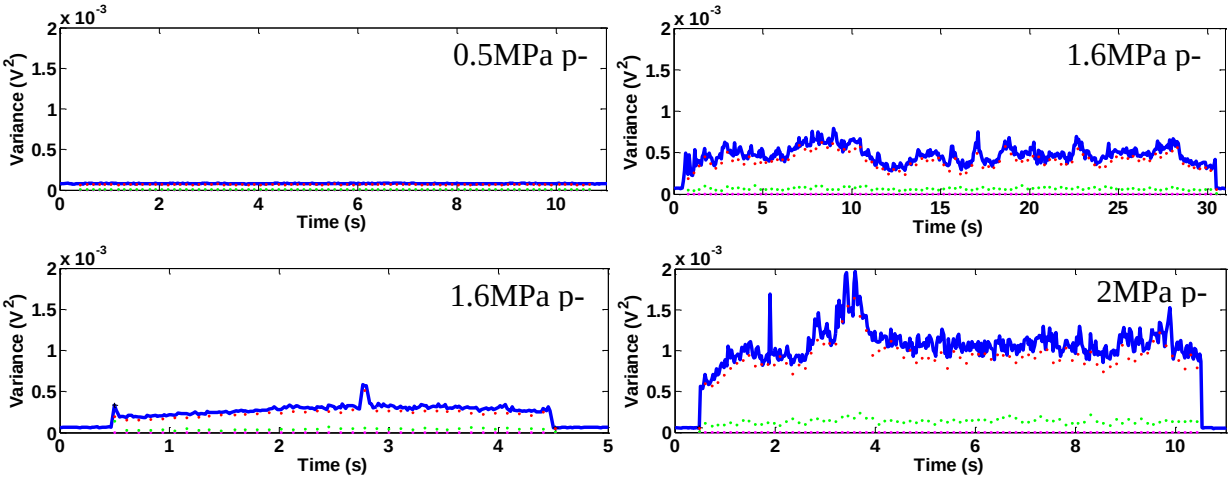

Figure 6-3: Representative acoustic signals received by the coaxially aligned PCD at the four exposure conditions tested during *in vivo* experimentation at 0.5MHz: at 0.5MPa p- for 10s (top left), at 1.6MPa p- for 4 and 30s (top right and bottom left respectively) and at 2MPa p- for 10s (bottom right).

Acoustic emissions recorded during those *in vivo* exposures were both repeatable and consistent. There were not significant variations among signals received during different experimental days, from different treated areas or from one animal or the other.

6.6 Histological results

The condition of the skin of both animal donors was checked daily over the course of the experimentation, and for the second animal donor regularly during the following month. It was concluded that none of the ultrasound treatment regimes investigated resulted in any skin damage or visible skin irritation for either of the two animals neither during nor following the experimental procedure.

Adipose tissue exposed over prolonged periods of time at sub-threshold pressure amplitudes looked invariably healthy when seen under the light microscope. The cellular structure was very well maintained, showing areas of healthy adipose tissue with normal

cell septa and nuclei at all three cutting planes, *i.e.* 10, 15 and 20mm below the skin. Figure 6-4 shows representative pictures capturing a large surface of adipose tissue section that was exposed to 0.5MPa p- and for 10s.

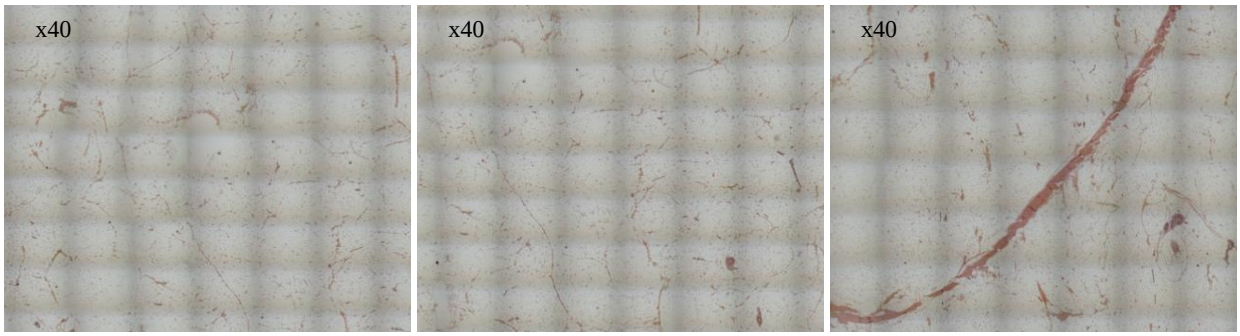

Figure 6-4: Histological slides cut parallel to the skin at 10, 15 and 20mm shown to the left, centre and right respectively and stained with H&E. Each individual scan is magnified by 40. Tissue was exposed at 0.5MHz at 0.5MPa p-, a pressure amplitude below the cavitation threshold and for 10s. Ultrasound exposure resulted in no histological damage at any depth, as can be seen by the intact areas of the slides.

Based on the received PCD signal there was always inertial cavitation activity present at exposures carried out at or above 1.6MPa p-. The histological results revealed that there was a strong indication of extensive tissue damage induced under these input settings. The light microscope enabled the capturing of a very large image by stitching smaller frames together. However, due to a hardware limitation the overlapping edges of two neighbour frames appear slightly darker. For all subsequent figures shown, each frame is acquired at a magnification of 40x. Given the way adipose tissue was sliced, HIFU was always coming into the page for all histological slides shown hereafter.

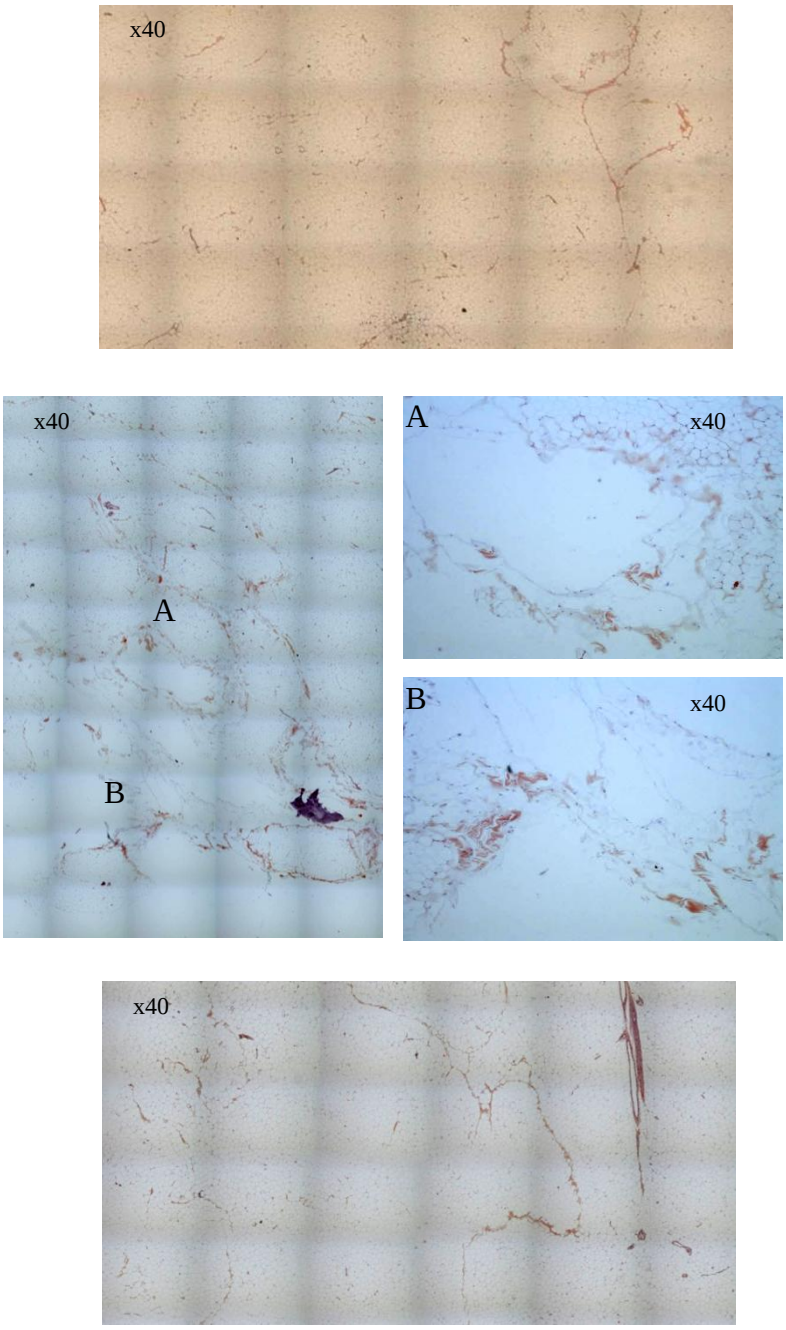

Figure 6-5: Histological slides taken from animal donor 'one' were cut parallel to the skin at three depths below the skin, at 10, 15 and 20mm, shown in the top, centre and bottom figures respectively and stained with H&E following an ultrasound exposure at 0.5MHz, at 1.6MPa p- for 4s on Day 1. At 10mm (top), there is no damage and the whole slide is intact. At 15mm (centre left), there are many tears present throughout the whole surface of the slide. Two of them were chosen, as indicated by the capital letter A & B and are shown in greater detail (centre right). At 20mm (bottom) there is no damage caused to the tissue. Each individual scan is magnified by 40.

Figure 6-5 shows representative planar sections taken from animal donor ‘one’, from three different depths below the skin of a block of tissue that was exposed at 0.5MHz at 1.6MPa p- and for 4s on Day 1. At 10mm there was mostly normal structure present (top), while there was a great loss of integrity seen at 15mm which is where the HIFU focus was placed (centre). A closer look at these damaged areas, labelled A and B, for this particular slide, further verifies the shear damage due to mechanical effects and the extensive loss of integrity. The majority of slides showed an intact cellular structure at 20mm (bottom), which is the greatest skin-depth to be checked.

However, the tissue damage induced was not always that well localised depth-wise and only present at 15mm below the skin. On the contrary it varied a lot among exposures of the same input setting, which could be due to small differences in positioning of the HIFU applicator against the skin. Figure 6-6 presents a heavily damaged slide (left) taken at 10mm below the skin, and individual damaged areas have been chosen and are shown in greater detail (right). The shadow lines present are due to bad stitching of the individual smaller frames. For this particular example, there was no tissue damage present at 15 or 20mm depth, which could be due to pre-focal cavitation activity causing damage at this slightly shorter depth, therefore shielding the original focus.

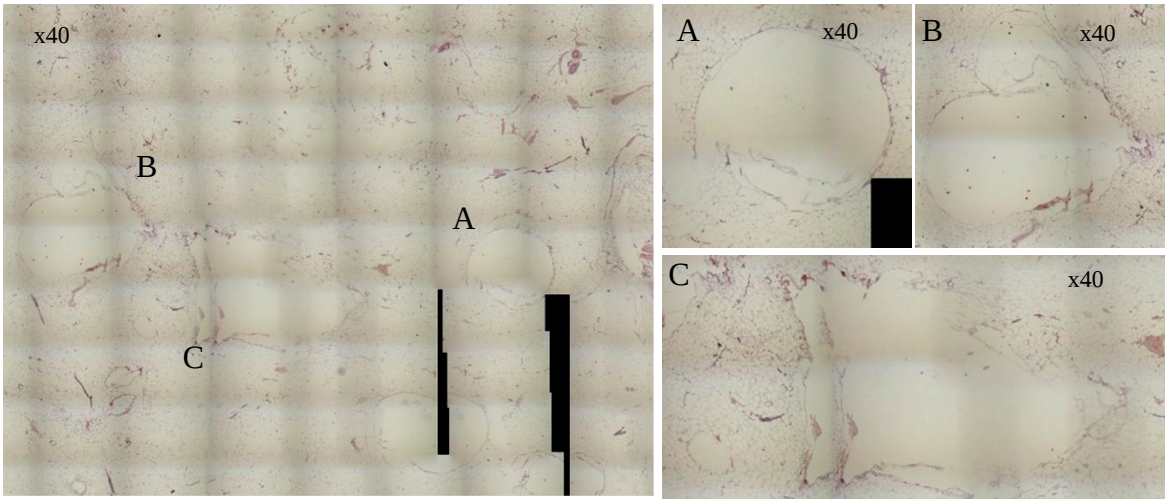

Figure 6-6: The total surface of a histological slide cut parallel to the skin at 10mm and stained with H&E following an ultrasound exposure at 0.5MHz, at 1.6MPa p- and for 4s. There is extensive tissue damage throughout the whole slide (left). Individual damaged areas are selected and are shown in greater detail (right), as indicated by the capital letters A, B and C. Each individual scan is magnified by 40.

Increasing the input pressure amplitude further to 2MPa p- and lengthening the exposure duration to 10s resulted in similar tissue damage as that seen at 1.6MPa p-. The adipocytes looked heavily destroyed, the cellular integrity was lost and the damage was invariably occurring at 10, 15 and 20mm below the skin. Representative histological slides stained with H&E are shown in Figure 6-7, where the majority of the induced damage can be seen at 15 and 20mm below the skin.

The second animal donor was put down 30 days after the last day of treatment and tissue blocks were excised, cut and stained in exactly the same way as the ones from the first donor were. Thorough assessment of the resulting histological damage followed.

These tissue blocks provided histological slides that looked invariably intact. Even the ones treated at 1.6 and 2MPa p-, pressure amplitudes that have been always inducing cavitation activity as it can be concluded from the PCD data received, revealed no sign of

acoustically induced tissue damage. The cellular structure was very well maintained and the adipocytes looked healthy with normal nuclei attached to their membrane.

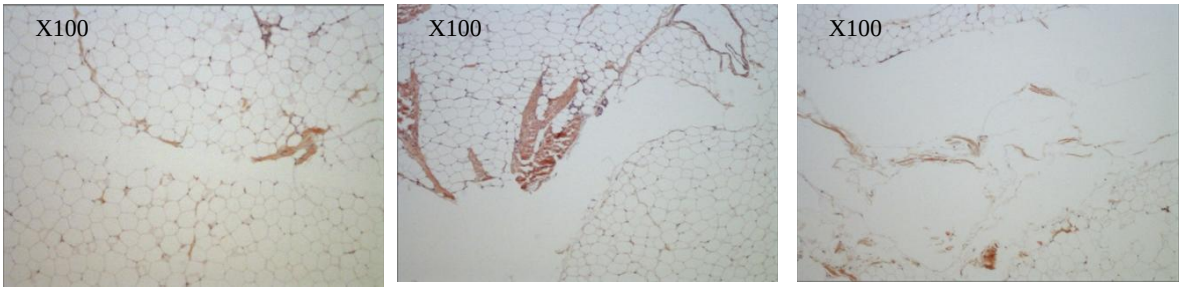

Figure 6-7: Histological slide stained with H&E following a HIFU exposure at 0.5MHz, 2MPa p- for 10s. Hardly any damage was observed at 10mm depth (left), but the adipocytes look completely ruptured and the cellular integrity has been heavily damaged at 15 and 20mm depth (centre and right respectively).

6.7 Limitations of *in vivo* experimentation

However, it should be noted that clearly identifiable histological damage was not identified consistently throughout all treated areas and that Figure 6-5 and Figure 6-6 represented selected results where damage was clearly visible. There are several possible reasons for this.

Manual application of therapeutic ultrasound via the applicator does not necessarily guarantee accurate or consistent positioning of the HIFU focus at the desired position, even if cavitation activity is detected on the PCD. This was particularly problematic for the scanned (rather than single-lesion exposures), where no histological damage was observed, presumably due to intermittent acoustic contact between the applicator and the skin.

A second major challenge was the spatial registration between the position of the HIFU focus and the sectioned tissue samples. This was particularly problematic for the single

lesions, as even a slight misalignment between the cutting plane and the grain-of-rice sized HIFU focus could result in the damaged region being missed.

Last but not least, it should be noted that the axial depth of the HIFU focus is 25mm, implying that a sufficiently strong acoustic field is present both focally and pre-focally to induce damage. This is particularly true at pressures well above the 100%POC, where extensive pre-focal cavitation causing shielding of the intended treatment depth is a distinct possibility.

The issue of cavitation localization and its spatial correlation with histological damage is addressed further in the following chapters. An approach to correcting the limitations induced by the spherical HIFU transducer by design of an application-specific HIFU transducer is presented in Chapter 8.

6.8 Summary of *in vivo* work

This preliminary set of *in vivo* experiments provided valuable acoustic and histological results. As far as the experimental setup used is concerned, this proved to be very robust as it made it possible to both deliver the ultrasound energy required and also detect all information needed. The lack of high quality de-ionised and de-gassed water was overcome by the use of boiled water inside the applicator, which provided a satisfactory solution.

Measurements showed that *in situ* pressure amplitudes above 1.6MPa p- are capable of inducing cavitation activity *in vivo* at all times, which is in very good agreement with similar measurements carried out in the laboratory *ex vivo*. The PCD signals received after every exposure provided a robust technique to check that the contact of the

applicator with the skin was achieved and maintained throughout the duration of the exposures. These were also very consistent with broadband noise always dominating once the *in vivo* 100% POC threshold was reached. The amplitude of the variance of the received signal under similar HIFU exposure conditions was very similar across different areas and different exposure days, for both animals.

In vivo tissue damage was achieved following cavitation inducing HIFU treatment. This extensive damage was present in several treated sites, verifying the successful delivery of ultrasound energy to the adipose tissue. However, it was not possible to come up with a conclusion as to the location of the induced tissue damage under different input pressure settings. A great number of tissue sections had to be discarded, due to areas being torn or physically damaged, which points out the need for a better technique for extracting the tissue from the animal donor.

In addition, the histological results of the second animal donor revealed no damaged tissue. However, due to the very small focal area of the spherical HIFU transducer used during experimentation, the resulting tissue damage was also small. This means that any effort to measure the thickness of the subcutaneous adipose tissue before and after treatment, in order to conclude about possible reduction of it, could not be attempted.

7 Real-time Monitoring of Lipolysis by Ultrasound

The results presented in Chapters 4 and 6 have demonstrated that a passive cavitation detector (PCD) confocally aligned with the HIFU transducer enables robust detection of acoustic emissions emanating from the focus. The 100% Probability of Cavitation (POC) threshold was also found to be reproducible and equal to 1.6MPa p- both *ex vivo* and *in vivo*, whilst *ex vivo* measurements demonstrated that cavitation-enhanced heating occurs for exposures above this threshold. Furthermore, the results of Chapter 5 show that histological damage is readily identifiable at the target depth beneath the skin for those exposures where inertial cavitation activity was clearly present.

Three issues are of particular concern when delivering a therapeutic ultrasound treatment. Are therapeutically significant levels of ultrasound being delivered at all? When has enough ultrasound been delivered to achieve the desired bio-effect? And is the treatment occurring at the right depth, without excessive damage to overlying and underlying tissues?

In order to address the need for real-time treatment monitoring, the present chapter firsts seeks to identify a correlation between the amount of inertial cavitation activity that occurs within the focal volume over the course of a HIFU exposure and the associated temperature rise. If such a correlation exists, it would be possible to identify an optimal range of acoustic emissions, below which insufficient heating to cause tissue damage would have occurred, and above which the tissue would be over-treated, with the risk of skin burns.

Secondly, time-of-flight information from the single-element confocal cavitation detector is used to infer the location of the front of the bubble cloud in real-time during HIFU exposure. A correlation between cavitation location and the extent of histological damage is then sought, by use of a novel method for quantifying the position-dependent volume of destroyed adipocytes. Once again, should such a correlation between the location of cavitation activity and associated histological damage would occur, tracking of bubble cloud position could provide an invaluable tool for real-time spatial monitoring of ultrasound-induced lipolysis.

7.1 Correlation between the inertial cavitation activity and the temperature rise at the focus

Focal temperature measurements are invasive and can therefore not be used in a clinical environment. Inertial cavitation on the other hand, results in broadband noise emissions, which can be captured by a confocally aligned PCD and provide a real-time indicator of both the presence and the evolution of inertial cavitation activity at the focus, as it has been already shown earlier in Chapter 4. *Ex vivo r*esults have shown that at 0.5MHz inertial cavitation can always be instigated at *in situ* pressure amplitudes above 1.6MPa p-, the 100% POC threshold, while also enhancing focal heat deposition. Based on these encouraging results, a thorough analysis followed, in order to investigate the potential use of the signal received by the coaxial PCD as a real-time and non-invasive indicator of the focal temperature rise induced during a cavitation inducing HIFU exposure.

The mean maximum temperatures achieved during HIFU exposures at 0.5MHz are shown in Figure 7-1 as a function of the total energy received as broadband noise by the PCD over 2 and 4s. The total broadband energy is simply the integral of the broadband power

(or variance) integrated over the HIFU exposure. For both exposure durations, broadband noise energy levels equal to the noise floor resulted in a mean temperature rise of 2°C. As the received broadband noise signal increased reaching a value of up to 8 times greater than the noise floor, there was a mean peak focal temperature rise of around 12°C. For a received acoustic energy noise of the order of 30 times greater than the noise floor, which corresponded to *in situ* pressure amplitudes of 1.6 and 2MPa p- that exceeded the 100% POC threshold, mean peak focal temperature rises ranging from 30°C to 50°C and from 20°C to 55°C were achieved for 2 and 4s exposures respectively.

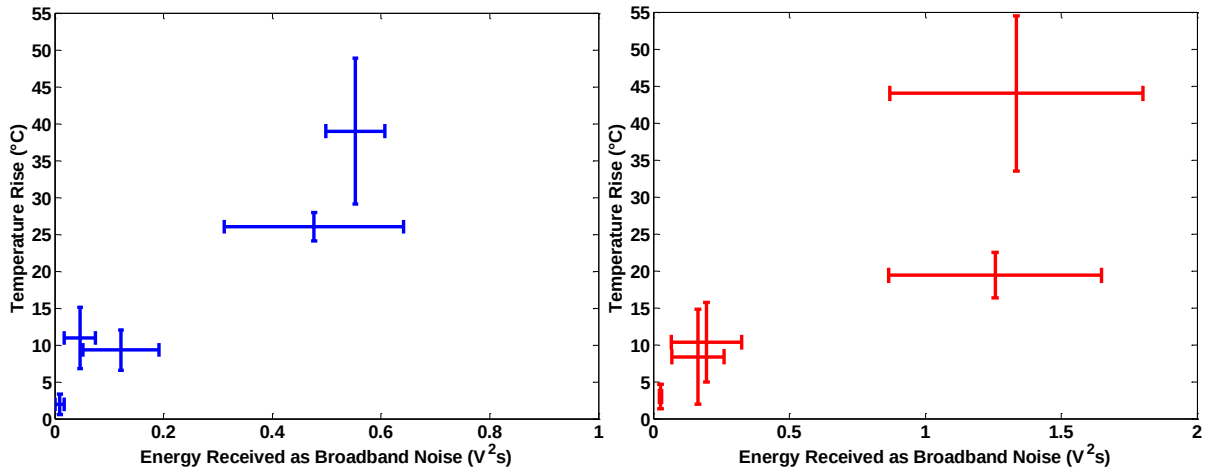

Figure 7-1: Graphs show the temperature rises achieved during HIFU exposures at 0.5MHz as a function of the total energy received as broadband noise by the PCD over 2 (left) and 4s (right). Data is expressed in mean ± standard deviation (N=6).

A good correlation between the energy of broadband noise emissions is found for both exposure durations, the correlation being stronger for the lower exposure duration. This is hardly surprising as the effects of heat conduction will be considerably greater for longer exposures, meaning that the relationship between cavitation-enhanced heating and the observed focal temperature rise will be weakened. Therefore, especially for short exposures, Figure 7-1 shows that the energy of remotely detected broadband acoustic

emissions can provide a strong indicator of successful treatment. In a highly homogenous tissue such as subcutaneous fat, in which the cavitation threshold has already been found to be highly consistent across a large number of *ex vivo* and *in vivo* samples, it is highly possible that this relationship will hold for a given HIFU transducer/PCD combination irrespective of patient-specific features.

7.2 Localisation of cavitation activity

In order to establish a non-invasive method for spatial treatment monitoring, the aim of the analysis presented in this section is to localise the frontal position of the bubble cloud, *i.e.* the one closest to the HIFU transducer, within adipose tissue, given the time-of-flight of the first peak of the signal received by the coaxial PCD, as explained in Section 3.4.2. Two important assumptions are made in order to achieve this; firstly, that cavitation activity is preferentially induced along the axis of sound propagation, which is reasonable since this is where the greatest pressures are being generated; secondly, that cavitation activity is initiated instantly, which has already been shown to occur when operating at low frequencies and pressure amplitudes greater than the cavitation threshold.

In order to be sure that the localisation of the cavitation activity within the tissue using the coaxial PCD was accurate, a second PCD, identical to the first one, was transversely aligned with the HIFU focus. The transversely aligned PCD was focused at different positions along the axis of sound propagation and was used to provide additional information about the exact location of cavitation activity.

7.2.1 Operating setup

Figure 7-2 shows the normalised axial profile of the spherical HIFU transducer at 0.5MHz and an illustration of the operating setup. Based on the axial profile of the HIFU transducer and the 100% POC threshold already defined, when the peak *in situ* rarefactional pressure amplitude is 2MPa p-, greater than the 100% POC threshold, there is a certain area within the tissue exposed to pressure amplitudes greater than the 100% POC threshold. This area is expected to cavitate and is marked with yellow lines in Figure 7-2. The extent of this area was computed and was found to be 20mm long at 2MPa p-, the *in situ* pressure amplitude used for this series of experiments.

The HIFU focus was always placed at 15mm below the skin, illustrated by the dotted black line. One PCD was con-focally and co-axially aligned (CA) with the HIFU focus at all times. In order to confirm that acoustic emissions recorded by the co-axial PCD are representative of focal rather than pre-focal activity, a second PCD, identical to the first, was transversely aligned (TA) with the HIFU beam, as shown in Figure 7-2. Furthermore, this second PCD was also moved along the axis of sound propagation and positioned at multiple locations between the skin's surface and the HIFU focus, as indicated by the red arrow, in order to further verify the extent of the cavitating area experimentally. The tight -6dB focal depth of the PCD (15mm at 15MHz) provides accurate localisation along its axis of sound propagation, which is perpendicular to the HIFU axis.

During experimentation, the HIFU transducer sent a 95% duty cycle sinusoid (47.5ms on, 2.5ms off). A typical 400μs PCD trace received during such an exposure is seen in blue on the top left of Figure 7-3, where *t=0* corresponds to the trigger of the outgoing HIFU pulse. For each one of the PCD data traces, a threshold level was defined and was always

set to be six times the standard deviation of the signal received during the first μs of each voltage trace, where no acoustic activity is expected to be happening thus representing the baseline signal. The time delay of the first peak of the received signal that was greater than this threshold was detected and converted to the corresponding distance from the HIFU transducer. This was then used as an indicator of the front of the bubble cloud.

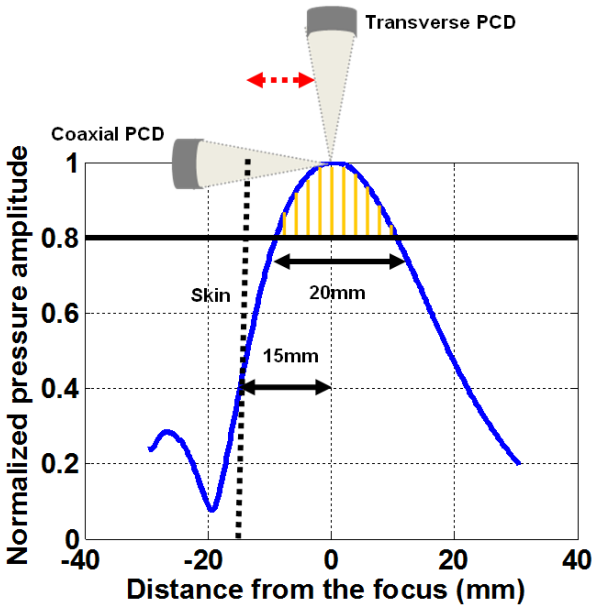

Figure 7-2: The normalised axial profile of the spherical HIFU transducer at 0.5MHz and an illustration of the operating setup, with the coaxial and transverse PCDs being confocally aligned. The area marked in yellow lines, is the region that is exposed to pressures above the 100% cavitation threshold when the *in situ* peak focal pressure is 2MPa p-. The horizontal black dotted line represents the skin and the red arrow shows the range of motion of the transversely aligned PCD.

Given the focal length of the HIFU transducer (62.64mm), if the focus is positioned at 15mm beneath the skin then sound travels through 47.64mm of water and 15mm of skin and fat. The small path length travelled through tissue was found to make little differences to estimates of time of flight, and a constant speed of sound of 1482 m/s in water at 20°C was used for all subsequent calculations.

The time delay corresponding to the HIFU focus on a typical PCD trace was then calculated and was found to be $t=(f.l._{HIFU}+f.l._{PCD})/c_{sound}=92\mu s$. Similarly the time delay from the nearest point to the HIFU transducer that is expected to cavitate at this *in situ* pressure amplitude, which is 10mm away from the focus, is 79μs and finally the reflection from the skin is expected at 72μs.

7.2.2 Real-time localisation of the cavitation activity

Multiple HIFU exposures were carried out at 0.5MHz, at 2MPa p- *in situ* pressure amplitude and for a number of exposure durations using two PCDs. A representative set of acoustic results are shown in Figure 7-3 alongside the normalised axial pressure profile of the HIFU transducer. On this graph, the blue arrow points to the HIFU focus where the co-axially aligned PCD was always focused and the green arrows show the four different locations along the HIFU axis where the transversely aligned PCD was positioned. These locations corresponded to the HIFU focus, 10mm, 5mm and 2mm below the skin respectively.

A typical voltage trace received by the co-axially aligned PCD transducer during the exposure duration is shown in blue on the top left and clearly demonstrates the presence of a well defined first peak having a much greater amplitude than the baseline noise and coming back at 77μs, which corresponds to 10mm away from the focus. At the same time instance during this exact same exposure, the transversely aligned PCD was positioned at the HIFU focus and detected a voltage trace that is shown in green on the top. An important feature to note is the much smaller amplitude of the signals received by the transversely aligned PCD compared to the ones received by the co-axially aligned PCD, due to the much smaller overlapping volume between the transversely aligned PCD and

the HIFU foci. This voltage trace shows a clear increase of the received signal at 90μs indicating the presence of acoustic activity at the focus of the PCD and therefore at this depth below the skin.

When the transversely aligned PCD was moved along the axis of sound propagation and was positioned at 10mm and 5mm below the skin, the voltage traces received looked like the one displayed on the second and third graph of the right column of Figure 7-3, respectively. A clear increase of the signal was present at all times around 90μs, which coincides with the focus of the PCD and therefore indicates acoustic activity originating from a point along the axis of sound propagation. This behaviour is expected, given both the axial profile of the HIFU transducer at this frequency and the time delay of the signal received by the co-axially aligned PCD at these exposure parameters.

Moving the transversely aligned PCD further and positioning it at 2mm below the skin resulted in voltage traces like the one shown in the bottom graph of the right column in Figure 7-3, which suggests that there is only the baseline noise detected back and therefore no cavitation activity occurred at this depth below the skin. This is in agreement with the extent of the area expected to cavitate at this *in situ* pressure amplitude.

Frequency domain analysis -as shown in Figure 3-10- also gave a detailed overview of the spectral characteristics of all received signals and confirmed that broadband noise was dominating, indicating the presence of inertial cavitation.

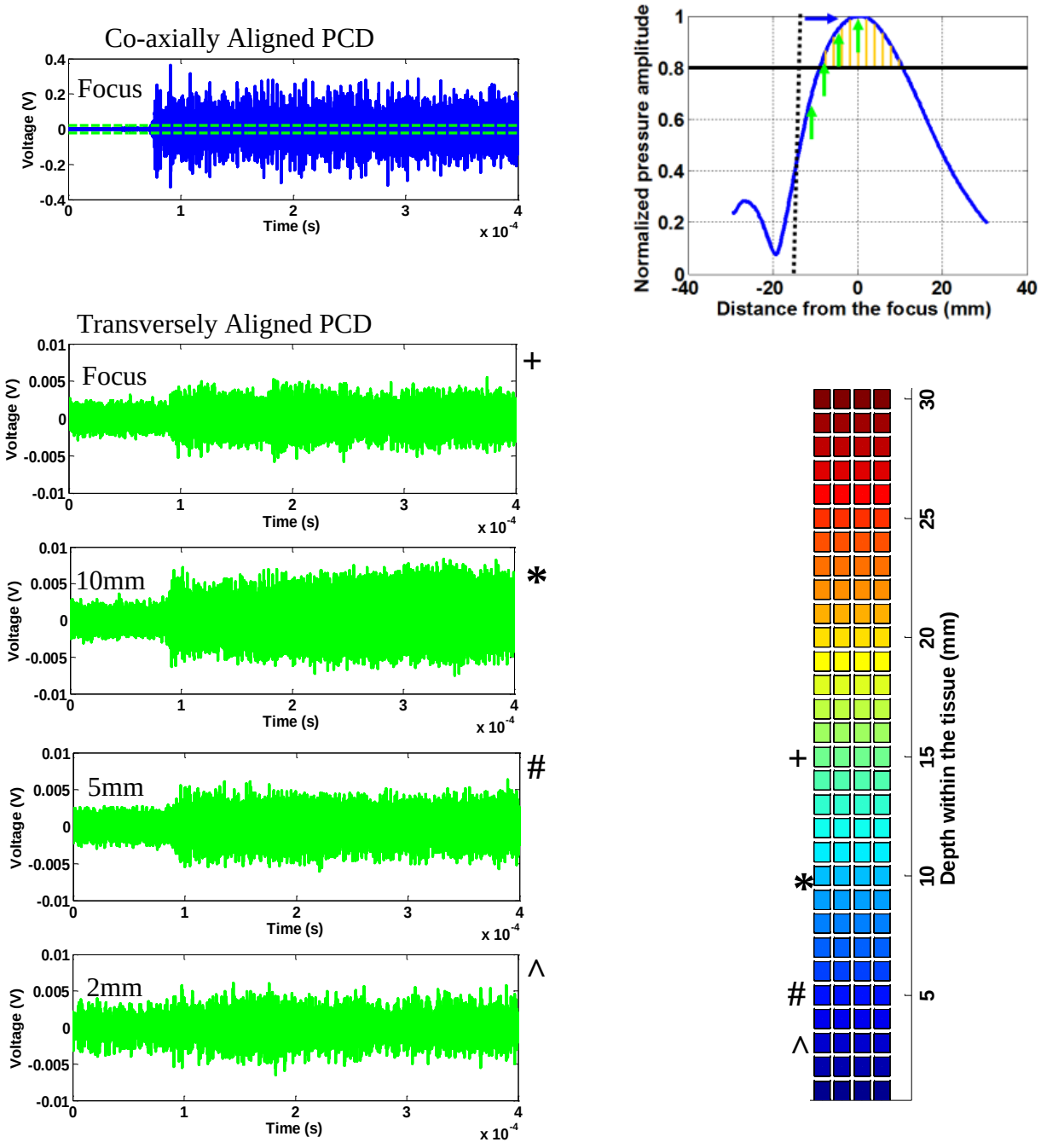

Figure 7-3: Representative voltage traces of the signals received by the coaxial (blue, top left) and transverse PCDs (green, left column) alongside the axial profile of the HIFU transducer (top right). The blue arrow on the this graph indicates the location of the focus of the CA PCD, whereas the four green arrows show the four different locations along the axis of sound propagation the TA PCD was positioned. These were: at the HIFU focus, 10mm, 5mm and 2mm below the skin surface as indicated by the different signs and the colourful graph, which is an illustration of the total damage induced to adipose tissue and is explained in detail Section 7.3.1 (bottom right). The corresponding voltage traces are shown to the right, as indicated by their inner sub-titles as well.

7.3 Correlation of histological damage with the acoustic signal

Preliminary *ex vivo* and *in vivo* histological results have shown tissue damage following a cavitation-inducing HIFU exposure and made it possible to identify and study the resulting destruction at a cellular level. Alongside passive cavitation localisation of the inertial cavitation activity within the tissue based on the acoustic signal received on the PCDs, a histological approach was also carried out aiming to (i) identify the detailed tissue damage induced at multiple locations along the axis of sound propagation under multiple cavitation inducing HIFU exposure parameters, (ii) correlate it with the axial profile of the HIFU transducer used for this particular set of exposures, (iii) correlate it with the acoustic results obtained with the co-axial PCD and finally (iv) estimate the volumetric extent of the tissue damage caused.

7.3.1 Localisation of the tissue damage

In order to identify the tissue damage induced along the axis of sound propagation following a cavitation-inducing HIFU exposure, multiple slides were cut parallel to the skin, 1mm apart from each other, starting from the skin up to 30mm below it, and stained with H&E. The total surface damage was then quantified for each slide.

Figure 7-4 is an illustration of the total damage induced at each tissue section following a cavitation inducing HIFU exposure at 0.5MHz and at 2MPap- *in situ* pressure amplitude as a function of the depth below the skin and the exposure duration. Every sample is represented by one line starting from the blue edge all the way to the red and every column represents a slide with its height being a measurement of the extent of the damage present on this particular slide. This extremely detailed analysis made it possible to reach

several conclusions regarding the resulting tissue damage along the axis of sound propagation.

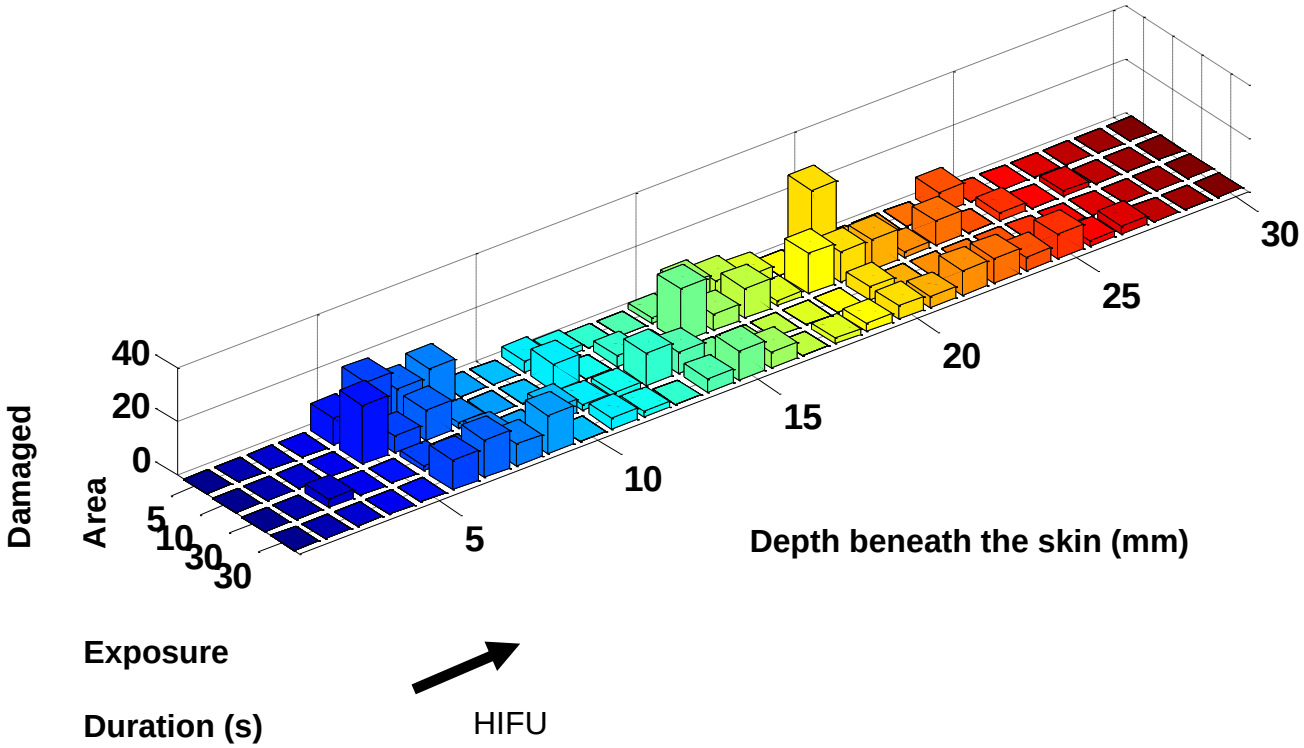

Figure 7-4: Illustration of the total damage induced to four tissue samples following a cavitation inducing HIFU exposure at 0.5MHz and at 2MPa p-, as a function of the depth below the skin and the exposure duration. Every sample is represented by one line starting from the blue edge all the way to the red and every column represents a slide with its height being a measurement of the extent of the damage present on this particular slide. HIFU was coming in the direction of the black arrow.

Firstly, there is a maximum tissue damage occurring at around 15mm below the skin, which is where the HIFU focus is always placed. Secondly, the total damage induced under a cavitation-inducing HIFU exposure didn't vary with varying exposure durations, but was comparable over the exposure durations tested that ranged from 5s to 30s: this

strongly suggests that the bulk of the damage is induced in the first few seconds of exposure.

Another salient feature of Figure 7-4 is how well confined the tissue damage is. There is no damage present over the 5mm adjacent to the skin. It is only expanding over a certain area within the tissue block, starting from around 5mm beneath the skin and going up until approximately 27mm below the skin. The extent of the damage coincides with the extent and location of the expected cavitating region at this pressure amplitude and the signal received by the transverse PCD at multiple locations, as illustrated in the Figure 7-3.

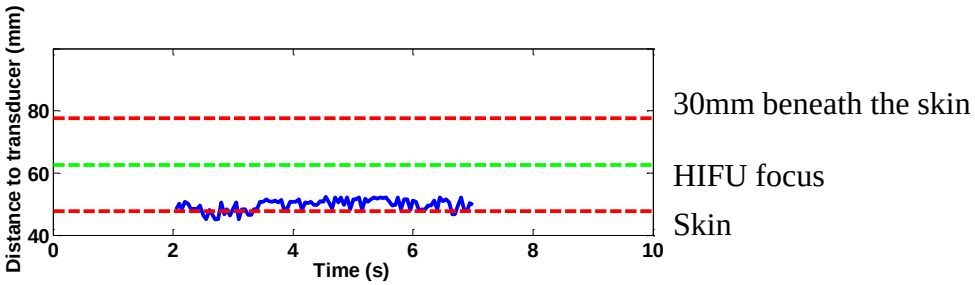

Figure 7-5: Location of the front of the bubble cloud as a function of time for a 5s HIFU exposure at 0.5MHz at 2MPa p- *in situ* pressure amplitude.

The corresponding signal received by the coaxial PCD during all these exposures –not shown here- suggested that inertial cavitation activity was present throughout the whole duration. Additionally, the voltage traces showed a clearly observable first peak corresponding to the front of the bubble cloud. By taking into account the time delay of the first peak corresponding to the bubble activity within the tissue, for the whole duration of the 5s HIFU exposure, Figure 7-5 was constructed. The green dotted line corresponds to the distance of the HIFU focus and the red dotted lines correspond to the skin surface

and to 30mm beneath the skin, respectively. The continuous blue line shows the distance of the front of the bubble cloud from the HIFU transducer as a function of time. This turned out to have a mean of 52mm, which corresponds to 5mm below the skin and is in very good agreement with the histological results presented in Figure 7-4.

7.4 Quantification of the volume of tissue damage

The next step was to try to identify a correlation between the HIFU exposure parameters and the resulting volume of damaged tissue, which is a very important parameter of the efficacy of the treatment. The detailed analysis of the resulting tissue damage at multiple depths below the skin, made it possible to quantify the volume of damaged tissue at each depth. The damaged area was quantified for each slide and was assumed to have a constant value for a depth of 1mm, which is the distance between two consecutive tissue sections. Adding these together provided an approximate value for the total volume of damaged tissue, a method commonly referred to as Cavalieri's principle.

Figure 7-6 summarises the resulting total volumetric damage induced for six tissue samples exposed at 0.5MHz, at 2 and 1.6MPa p- *in situ* pressure amplitudes and for multiple exposure durations. With the exception of one exposure, 30s at 2MPa p-, which resulted in very small damage and might be attributed to experimental error, a first conclusion is that as long as the input pressure amplitude is above the 100% POC threshold, there is a certain amount of tissue damage induced. Increasing the exposure duration from 5s up to 30s didn't result in an increase of the corresponding tissue damage, which once again suggests that the destruction of the tissue is happening during the very first seconds of the exposure. There is therefore no advantage gained from long

exposures. The 60s exposures resulted in increased damage, which could be due to undesirable boiling of the tissue.

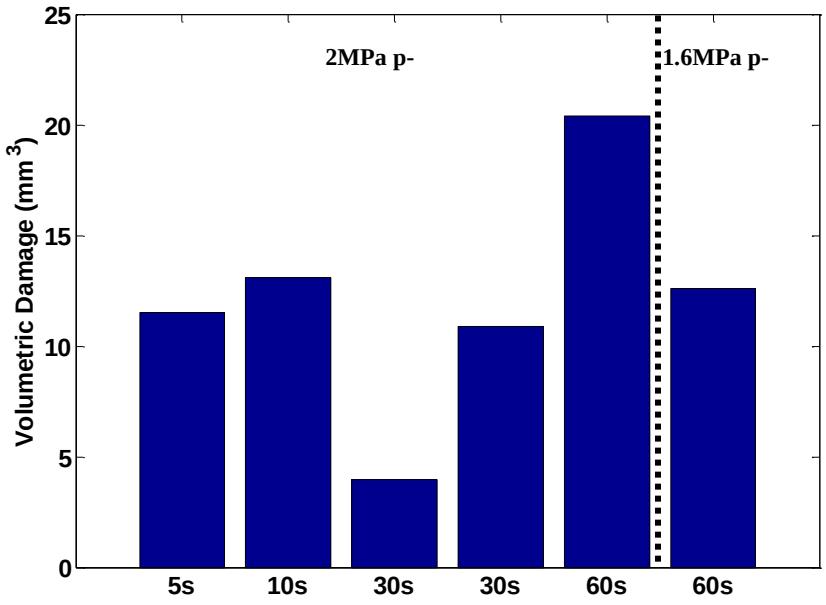

Figure 7-6: Total volumetric damage induced at a number of tissue samples exposed at 0.5MHz, at 2 and 1.6MPa p- *in situ* pressure amplitudes and for 5, 10, 30 & 60s.

7.5 Summary on non-invasive treatment monitoring

Use of a confocal passive cavitation detection (transducer) has been shown to have great promise as an inexpensive method for real-time monitoring of ultrasound-induced lipolysis. The results presented in Figure 7-1 make it possible to conclude that if cavitation activity above a certain value is detected on the PCD, then a certain minimum temperature rise has been achieved at the focus. A minimum value of broadband energy can therefore be taken as a positive indicator of focal temperature rise, but this does not necessarily imply that the temperature rise hasn't occurred if broadband noise isn't detected. Given the fact that, unlike most thermometry methods, cavitation activity can be detected remotely, the results of Figure 7-1, which are particularly useful for 2s

exposures but less so for 4s exposures where heat diffusion damages the correlation, could be used as a positive indicator of successful treatment delivery.

The use of a co-axially aligned PCD proved to be a reliable means of monitoring the location of the front of the bubble cloud within the tissue and thus provide a real-time feedback that treatment is occurring at the expected depth. These acoustic findings were further verified by the use of a second PCD transversely aligned with the axis of sound propagation and by a detailed histological analysis.

Histological results revealed the tissue damage induced at multiple locations along the axis of sound propagation. A most important conclusion is that damage was maximised around the HIFU focus and was very well confined within the expected cavitating area. Damage happens within the first 5s of exposure and lengthening the exposure duration further didn’t result in a greater volume of tissue being damaged

8 Towards an optimized system for cavitation-enhanced lipolysis

Results obtained with the non-custom built spherical HIFU transducer have shown that 0.5MHz is the optimal treatment frequency combining initiation of cavitation activity at modest *in situ* peak rarefactional pressure amplitudes of 1.6Mpa p- and therapeutically relevant heating over the focal volume. In addition, it has been demonstrated both *ex vivo* and *in vivo* that this frequency causes readily identifiable damage to subcutaneous fat at these modest pressure amplitudes, and that non-invasive localization and quantification of cavitation activity can enable treatment guidance and monitoring. However, the spherical HIFU transducer induces tissue damage primarily at the intended treatment depth (15mm) but also pre-focally, increasing the possibility of causing skin burns.

These preliminary experimental results together with the shortcomings of the spherical HIFU transducer motivated the design of an application-specific system, comprising a custom-built HIFU transducer, passive cavitation detector and software to enable real-time treatment monitoring. A full characterization of this new HIFU transducer, acoustic and histological results obtained e*x vivo* are presented hereafter.

8.1 HIFU transducer design

Based on all experimental results presented so far it was agreed that the application specific HIFU transducer would operate at a fundamental frequency of 0.5MHz and at its third harmonic. Additionally, it needed to be capable of delivering more than 2MPa p- over a therapeutically relevant tissue volume without affecting the overlying skin. This *in situ* pressure amplitude of 2MPa p- is greater than the 100% POC threshold in

subcutaneous fat, already defined to be 1.6MPa p-, thus allowing the reliable generation of cavitation activity at the focus. In order to maximise the efficiency of the treatment and minimise its duration, the treated volume had to be maximised, which effectively means maximising the focal volume of the transducer.

One of the main limitations of the spherical HIFU transducer used until now was its long depth of focus along the axis of sound propagation, which resulted in the generation of extensive pre-focal cavitation activity when operating at pressure amplitudes well above the 100% POC threshold. Furthermore this added difficulties with the passive localisation of the front of the bubble cloud and increased the possibility of skin burns. In order to overcome all the above shortcomings, the new custom built HIFU transducer needed to be very tightly focused along the axis of sound propagation and to have very low amplitude pre-focal maxima.

Based on these requirements a new HIFU transducer was designed and built. The intention of this new design was for the focal volume to no longer be a ‘grain of rice’ as was the case with the spherical HIFU transducer used thus far, but rather a long pencil-sized focal region running parallel to the skin at a depth of 15mm, which should enable the treatment of a larger area over a much shorter period of time. Following several interactions with transducer manufacturer Sonic Concepts, who simulated the field produced by a number of possible designs, a new single-element cylindrically focussed HIFU transducer was built (Sonic Concepts, S/N 163-001), of element size 95.25x112mm, centre frequency 0.5MHz and focal length 53.8mm. This focal length was chosen to ensure that the cylindrical focus was formed at a depth of 15mm beneath the skin when the exit plane of the transducer was in contact with the skin. The new HIFU

transducer, which is pictured with its custom-built matching network in Figure 8-1, also had a 20mm hole in the centre to enable mounting of a custom-built PCD.

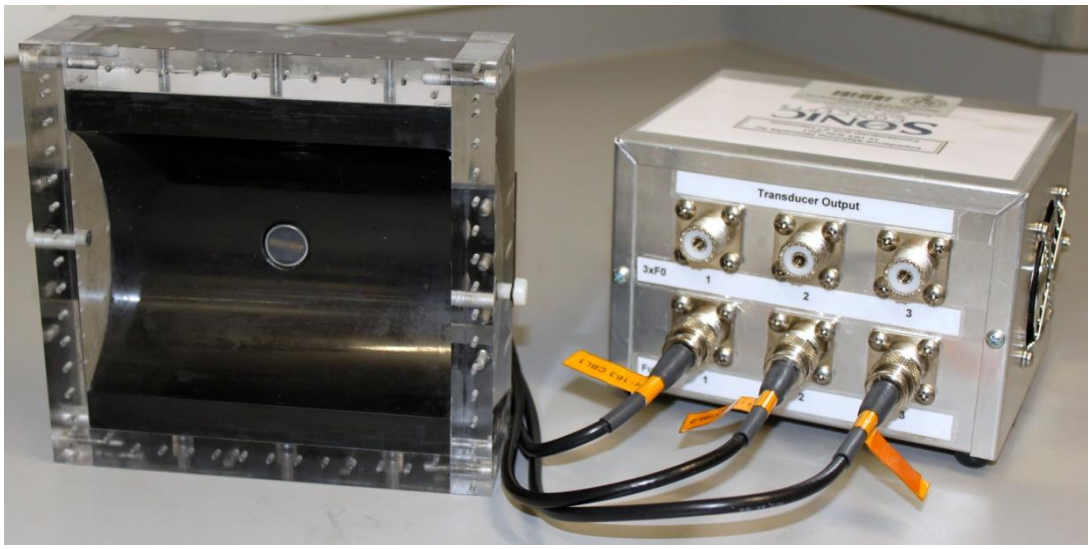

Figure 8-1: A picture of the application specific cylindrically focused HIFU transducer inside the new applicator and next to its matching network. A central 20mm hole was cut through which the new cylindrically focused PCD was mounted.

8.2 HIFU transducer characterization

Initially, a frequency calibration was carried out in order to accurately determine the optimal operating frequencies of the new transducer, which were found to be 0.5MHz (fundamental) and 1.68MHz (third harmonic). Absolute measurements of the focal pressures were obtained in the free field and *in situ* at 15mm inside the fat beneath the skin to resemble the experimental conditions and to have accurate measurements of the pressures induced during experimentation. Figure 8-2 displays the measured values in both cases, which further validate the experimentally determined insertion loss through skin and fat, as shown in Table 4-2.

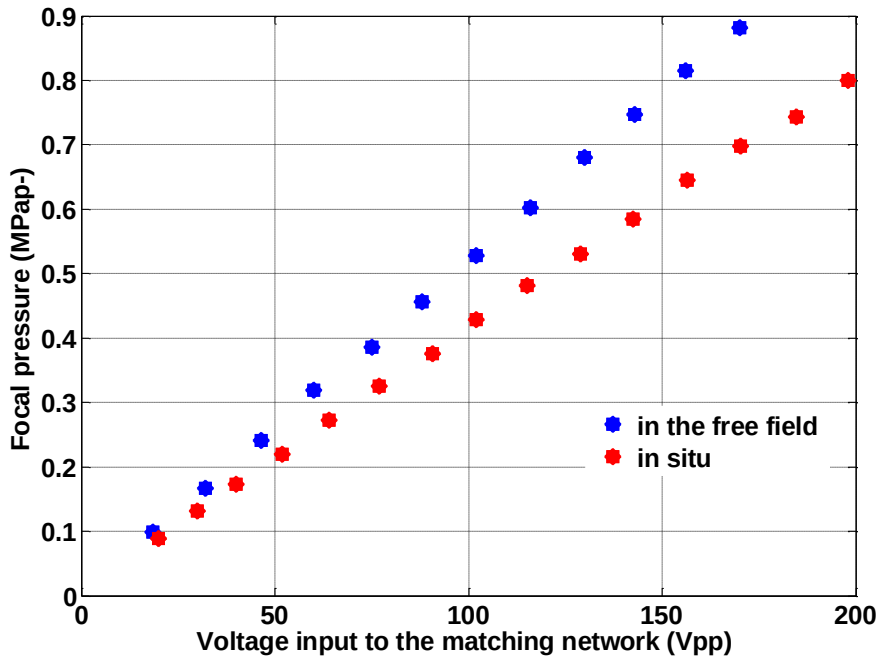

Figure 8-2: Absolute calibration of the cylindrical HIFU transducer.

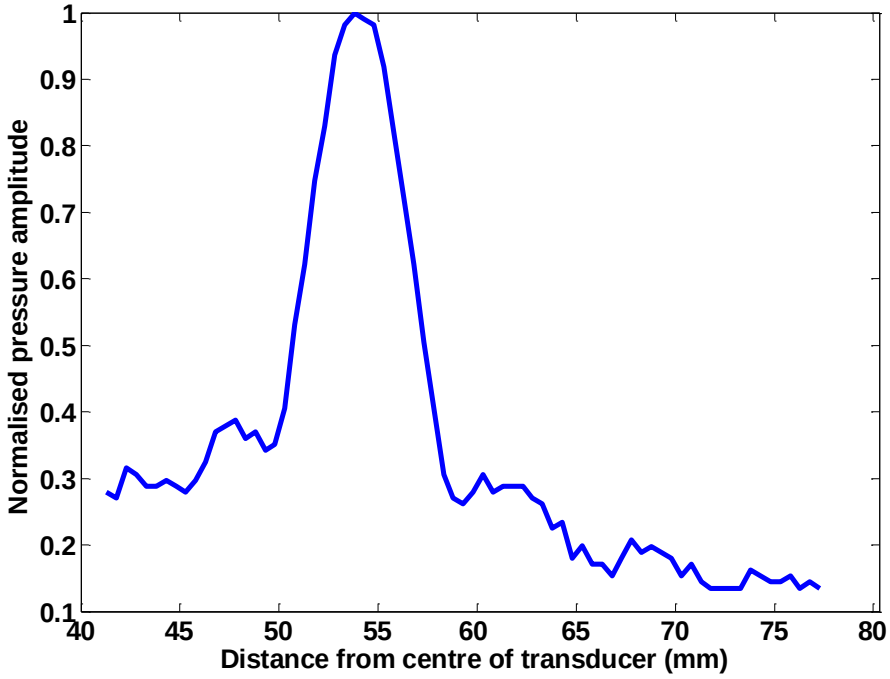

Figure 8-3: Axial profile of the cylindrical HIFU transducer.

The new HIFU transducer is very tightly focused along the axis of sound propagation and has a half-pressure focal width of 6mm at the fundamental frequency, which is optimal for this application, given the proximity of the skin. The axial profile of the cylindrical HIFU transducer is shown in Figure 8-3.

Spatial characterization followed and the resulting plots are shown in Figure 8-4 and Figure 8-5. An important comment is that each one of these acoustic field scans has been normalised to its maximum pressure amplitude, meaning that the color-bars are not directly comparable. The x- and y-axes are parallel to the long and short axes of the transducer, with x=y=0 referring to the central point. The z-axis is along the axis of sound propagation, with z=0 representing the location of the central opening of the HIFU transducer surface and z=53.8mm the HIFU focus. The axial scan (z-x plane at y=0) seen in Figure 8-4 shows a very tight focus for the whole length of the transducer along the axis of sound propagation, as has been already suggested by its axial profile, shown in Figure 8-3.

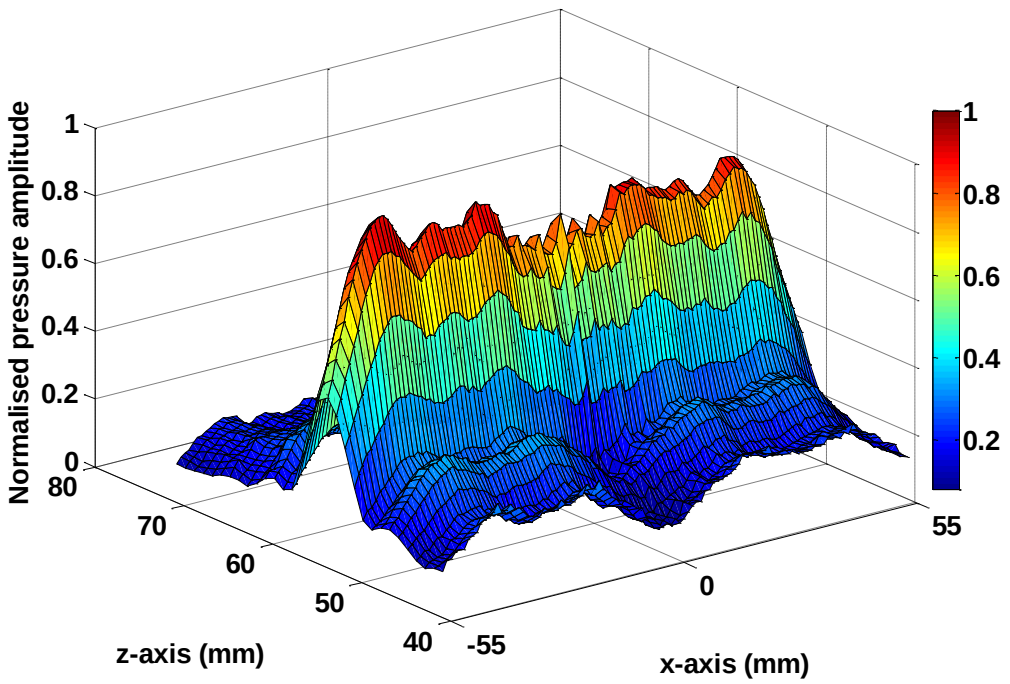

Figure 8-4: Axial scan further verifying the very tight focus of the transducer along the axis of sound propagation.

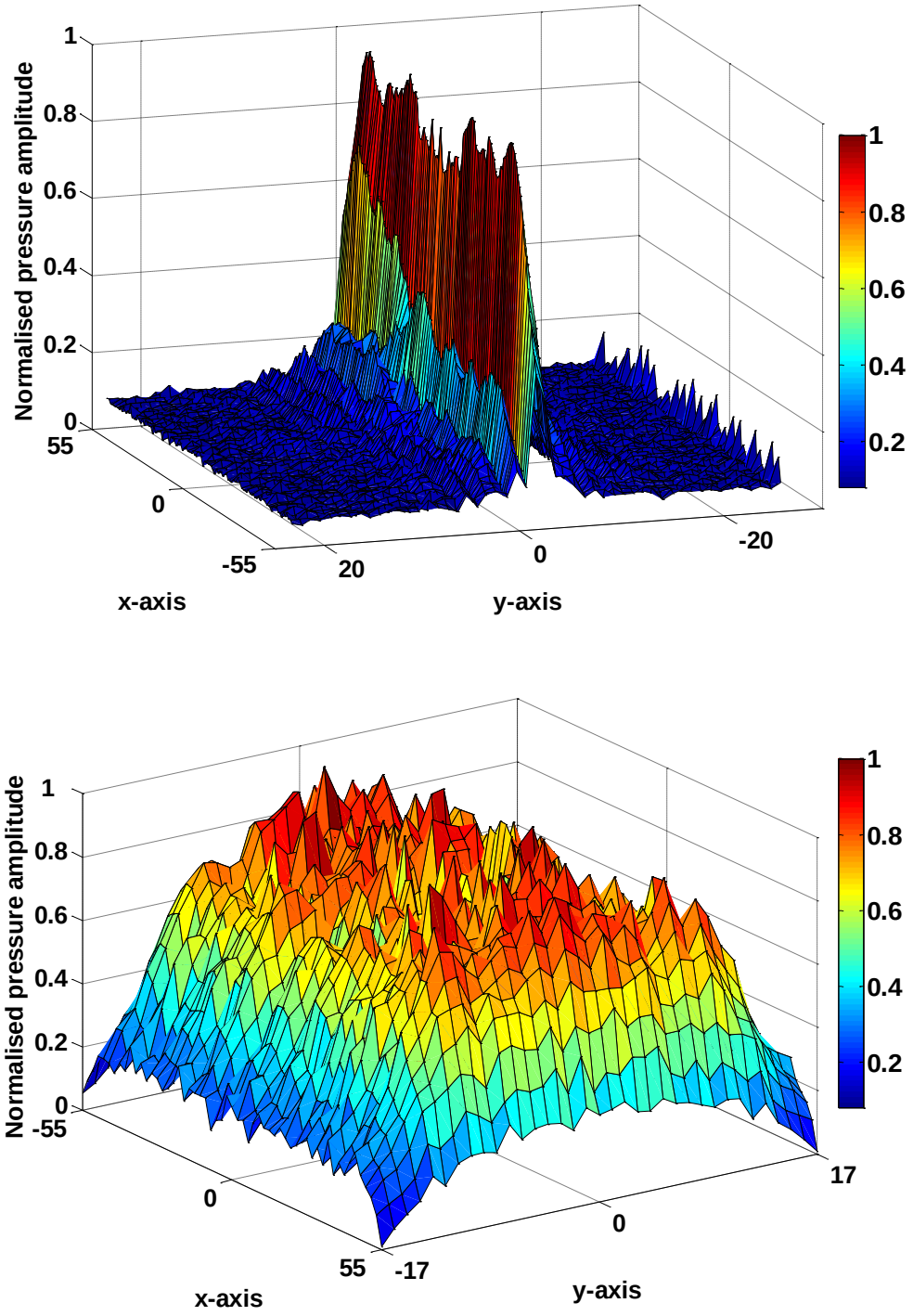

Figure 8-5: Transverse scan at the focus demonstrating a very tight focus (top). Transverse scan at the exit plane of the transducer showing a very steady pressure value throughout, with no unwanted peaks present and a central region of lower pressures due to the present of the central hole through which the PCD was mounted

The transverse scan at the focus (x-y plane at z= 53.8mm), seen in Figure 8-5 (top), shows a very tight focus. Similarly, a transverse scan was also conducted right in front of the exit plane of the transducer (x-y plane at z=40mm), seen in Figure 8-5 (bottom), to check for any unwanted peaks of the pressure amplitude at this plane. The pressure field is quite steady with no unwanted peaks present and with one central area of lower pressure amplitudes which is due to the presence of the central hole accommodating the PCD.

8.3 PCD transducer design and calibration

Given the shape of the new HIFU transducer, a new application specific PCD was also built to account for the new shape of the HIFU focal volume. This was chosen to be a cylindrically focused single element wideband transducer (V319-SU Panametrics, f_0=15MHz, focal length 53mm, active diameter=12.5mm). Figure 8-6 shows a picture of this PCD together with its frequency response.

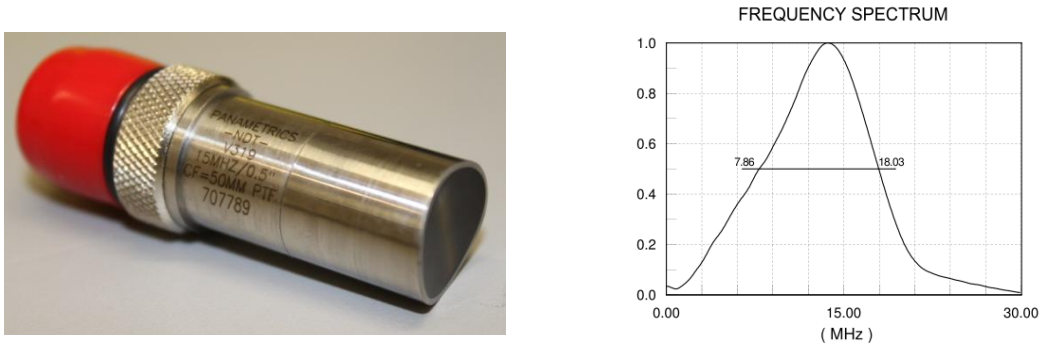

Figure 8-6: Picture of the application specific cylindrical PCD used during all subsequent experiments (left) alongside its frequency response (right). Graph reproduced from the accompanied documentation report, Panametrics-NDT, Olympus.

8.4 Experimental setup and procedure

The experimental setup used for all subsequent experiments is the one described in Section 3.2. The only difference is that a new 1000W amplifier (E&I 1140LA, Electronics & Innovation Ltd, 55dB gain for 0.3-35MHz) was used, as this new transducer requires greater input power due to its considerably larger surface area. In addition, a much larger HIFU tank (30 x 60 x 60cm) was used given the dimensions and the geometry of the new transducer.

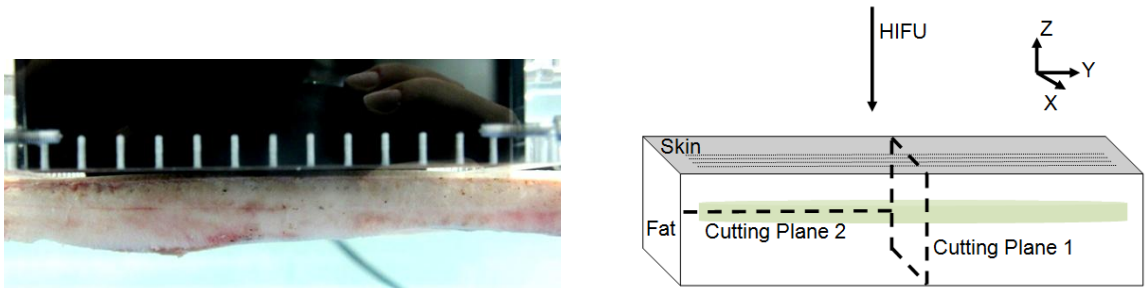

Figure 8-7: A picture showing a close look of the operating setup. The cylindrical HIFU transducer and a block of tissue in water prior to an ultrasound exposure (left). A schematic representation of the experimental setup with information about the different cutting planes the tissue was sectioned through, in order to assess the induced damage following a HIFU exposure.

The cylindrically focused HIFU transducer was at all times immersed in de-gassed and de-ionised water facing downwards and with its exit plane parallel to the water surface. A large block of tissue of adequate thickness (20mm minimum) was needed given the long focal volume of the transducer. This was held firmly, with the skin parallel to and right in front of the exit plane of the transducer as shown in Figure 8-7 (left). The HIFU focus is 15mm away from the exit plane and therefore always aimed to be at 15mm within the fat tissue. However, due to the large and heavy tissue block that was used, some small fluctuations of the skin surface were present. In addition, it was observed that

during HIFU exposures the tissue block translated slightly downwards under the effect of acoustic radiation force. These two effects might add a small uncertainty as to the exact position of the HIFU focus within the tissue depth-wise.

The maximum *in situ* pressure amplitude that could be deployed by the custom-designed HIFU transducer was 2.7MPa p-, but at this pressure a 20% duty cycle had to be used in order to ensure safe transducer operation. The experimental rationale underlying the results described hereafter was as follows. In order to ensure that histological damage would be observed both macroscopically and microscopically, the transducer was first driven at 2.7 MPa p-, 20% duty cycle for 30s to form single lesions, which were always created at least 7mm apart to avoid overlap. Following histological assessment of those single exposures, scanned exposures under the same conditions were then carried out, with adjacent lesions 2mm apart in order to enable treatment of larger areas. Once again, histological assessment of these treated areas was carried out, and the skin was carefully inspected for any evidence of damage which might cause concerns for treatment safety. In the absence of any such indications at these high pressures, the transducer was then driven at 1.8MPa p-, 95% duty cycle, which as previously demonstrated is above the 100% POC and should enable clinically relevant adipose tissue destruction. Scanned areas treated with these more modest pressure amplitudes were also histologically assessed to demonstrate that these clinically applicable treatment parameters can result in successful destruction of subcutaneous fat.

For each of these exposure conditions, PCD data was also acquired using a custom-designed user interface and is presented in the next section. The purpose of these results is to show that PCD data correlates well with histological findings and thus provides a useful tool for treatment monitoring and treatment safety.

8.5 Passive cavitation detection and localisation in real-time

A new Labview interface was developed for this set of experiments that provided the user with real-time information about the variance of the received PCD signal and the location of the front of the bubble cloud throughout the whole duration of the exposure. The analysis of the signal is the one already described in Sections 3.2.3 and 3.4.1 a representation of these real-time graphs is shown in Figure 8-8.

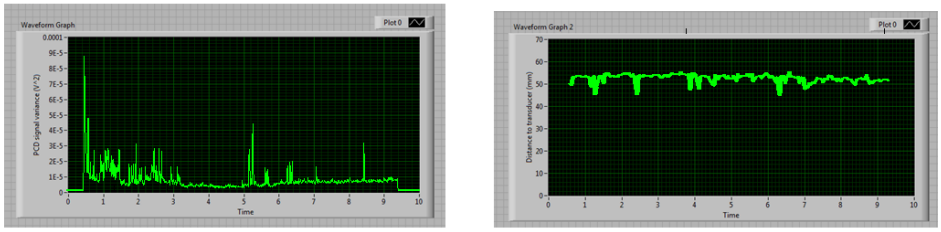

Figure 8-8: Representative graphs of the new Labview interface developed, showing real-time information about the variance of the PCD signal (left) and the location of the front of the bubble cloud (right).

The variance of the signal was used as a real-time indicator of successfull delivery of acoustic energy to the desired treatment depth. Besides, it can also be used to confirm that the contact between the HIFU transducer and the skin is maintained throughout the whole duration of the exposure. Localisation of the front of the bubble cloud acted as a real-time indicator of the safety of the treatment, ensuring that the exposure could be stopped before the cloud reached the skin.

Inertial cavitation activity was initiated and maintained throughout the whole duration of all HIFU exposures carried out during this set of *ex* vivo experimentation. This was expected given the choice of pressure amplitudes investigated.

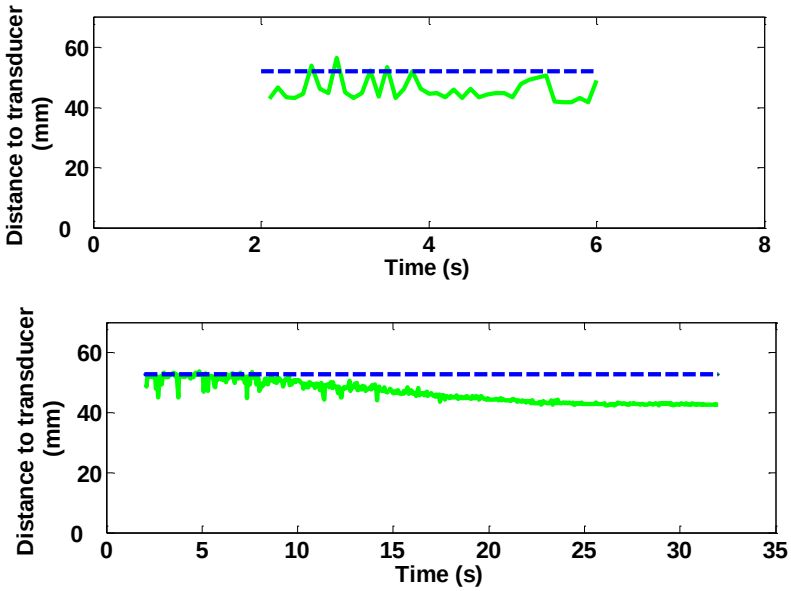

Figure 8-9: Localisation of the front of the bubble cloud during HIFU exposures at 0.5MHz, at 1.8MPa p- for 4s and 95% duty cycle (top) and at 2.7MPa p-, for 30s and 20% duty cycle (bottom).The blue dotted line represents the focal length of the HIFU.

Localisation of the front of the bubble cloud was also achieved at both pressure amplitudes investigated (1.8 and 2.7MPa p-). However, as already mentioned in Section 8.4, there are two uncontrollable sources of uncertainty that might affect the accuracy of the localisation measurements. Figure 8-9 displays the distance to the transducer of the front of the bubble cloud during a 4s and a 30s HIFU exposure at 1.8 and 2.7MPa p- respectively. Data is reproduced and presented in Matlab for clarity.

Inertial cavitation was initiated at the HIFU focus and was maintained at this location during the first seconds of the exposure. For single exposures at the same spot longer than 10s, the distance of the front of the bubble cloud seemed to gradually decrease, as shown in Figure 8-9 (bottom), implying that bubbles are moving toward the HIFU transducer. In any case, this effect was not worrying, as there is little chance that HIFU exposures longer

than 10s will ever be used clinically. In order to be sure though that no overlying tissue was affected, histological assessment of exposures up to 30s long was carried out.

8.6 Assessment of the resulting tissue damage

In order to assess the tissue damage induced following a HIFU exposure, the tissue block was cut through the two cutting planes as shown in Figure 8-7 (right). Given the focal volume of this transducer, sectioning the tissue through cutting plane 1, would enable macroscopic observation of any induced tissue damage as well as study of the condition of the over-lying skin and fat tissue. Furthermore, sectioning through cutting plane 2 would provide information about the whole extent of the macroscopic tissue damage at a particular depth within the tissue.

Following macroscopic observation, and in order to enable detailed histological evaluation of resulting tissue damage, tissue was sectioned in cutting plane 1 and stained with H&E or Picro-Miller as detailed in Section 3.5. H&E was primarily used to assess the viability of the adipocyte nuclei and membrane structure. Picro-Miller primarily enables the study of the state of collagen. Under white light, healthy fibres appear red and unhealthy blue, whereas under polarized lenses healthy collagen appears bright orange and unhealthy collagen appears brown. Figure 8-10 (left) shows a control sample stained with H&E. Control samples had a very good cellular structure, with all adipocytes having a healthy looking round nucleus attached to the membrane. Figure 8-10 (right) shows a control sample stained with Picro-Miller as seen under polarised lenses. Similarly, collagen also maintained its integrity with healthy looking nuclei. The bright orange colour of the septa surrounding the adipocytes and of the cellular

membranes demonstrates the healthy state of the collagen and the well maintained structure of the membranes.

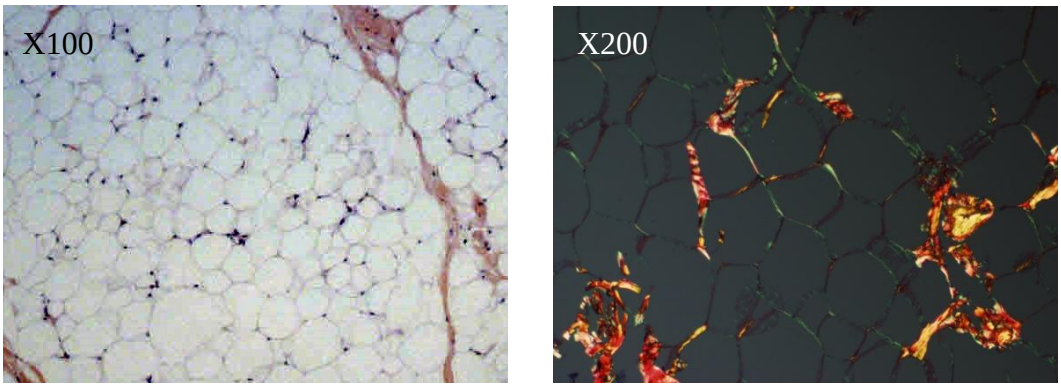

Figure 8-10: A control sample stained with H&E showing healthy adipocytes with their nuclei attached to the membrane (left) and with Picro-Miller as seen under polarised lenses (right). The bright orange colour of the septa surrounding the adipocytes and of the cellular membranes demonstrates the healthy state of the collagen and the well maintained structure of the membranes.

8.7 Histological damage for single exposures at 2.7 MPa p-, 20% duty cycle

A remarkable result was observed during HIFU exposures carried out close to the edge of the tissue. During the exposure a very well distinct line appeared at 15mm within the tissue, which is the depth the HIFU focus was always placed. This looked like blistering of the tissue, was quite uniform along the long axis of the transducer (y-axis, parallel to the skin) and was present after the exposure as well. Figure 8-11 shows a side view of the treated tissue, right after a HIFU exposure at 2.7MPa p- *in situ* pressure amplitude, for 30s and 20% duty cycle, while the tissue was still in water (left) and immediately after taking it out (right).

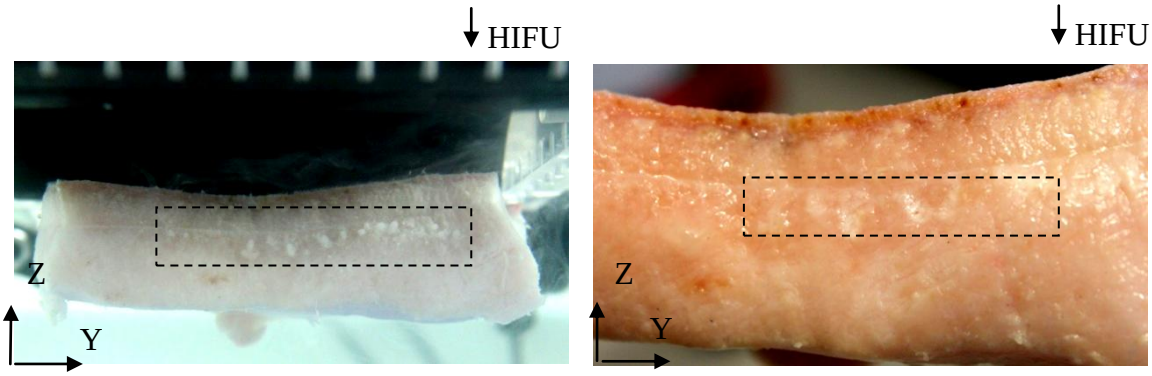

Figure 8-11: A side view of the treated tissue immediately after a HIFU exposure at 0.5MHz, at *in situ* pressure amplitude of 2.7MPa p-, for 30s and 20% duty cycle, while the tissue is still inside the experimental water tank (left) and immediately after it was taken out (right).

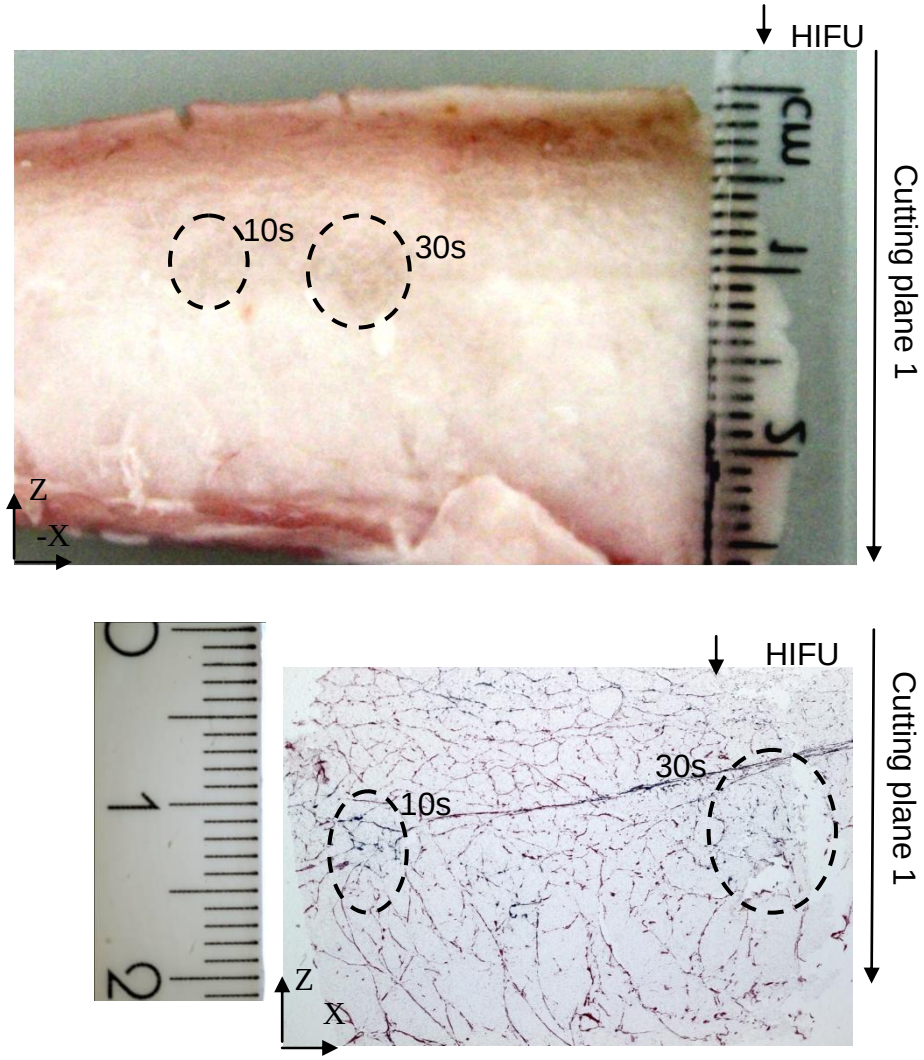

Figure 8-12: Block of treated tissue following single HIFU exposures at 0.5MHz, at *in situ* pressure amplitude of 2.7MPa p-, at 20% duty cycle and for 10s and 30s. Macroscopically observed adipose tissue damage (Top). Tissue section stained with Picro-Miller showing two well defined damaged lesions (Bottom).

Histological assessment of the other half followed and results are shown in Figure 8-12 (bottom). The skin (not shown) is on the top of the picture, but couldn't be captured if the whole area of interest was to be photographed. That's the reason why the ruler is placed slightly higher up to compensate for the missing tissue. The tissue was stained with Picro-Miller and two very well distinguished damaged areas were identified, as indicated by the dotted ovals.

These were in very good agreement with the lesions already seen macroscopically under the camera. Picro-Miller stain gives healthy collagen a red colour, whereas it turns blue when the collagen in question has been damaged. Both exposures resulted in very well localised tissue damage occurring at the right depth within the tissue. The histological examination further verifies that the extent of the tissue damage following the 30s exposure is slightly greater than the one following the 10s exposure and that there was no damage induced to any of the overlying tissue even at this very high pressure amplitude, which was expected given the very tight axial profile of this cylindrical HIFU transducer. These results are also in agreement with the localisation measurements presented in Section 8.5, with the 30s HIFU exposure resulting in tissue damage slightly closer to the skin.

8.7.1 Histological damage for scanned exposures at 2.7 MPa, 20% duty cycle

Following the very encouraging results obtained from single HIFU exposures, a number of scans were carried out in order for larger areas to be treated, for greater clinical relevance. Taking into account the difficulties encountered while continuously scanning a large surface, as described in Section 6.7, a decision was taken to perform all subsequent

scans in steps. Each one of these scans consisted of ten consecutive single HIFU exposures 2mm apart, at the exact same input parameters.

Figure 8-13 is showing a top view of the skin before (left) and after (right) a HIFU scan at 2.7MPa p- *in situ* pressure amplitude, for 30s and 20% duty cycle. Even under these extreme exposure conditions no skin burns were observed following a HIFU scan, which is very well explained by the tight focus of the cylindrical HIFU transducer along the axis of sound propagation. Comparing these results with the ones obtained with the spherical HIFU transducer at a lower pressure amplitude, as described in Section 5.2, clearly points out the advantages of the new HIFU transducer.

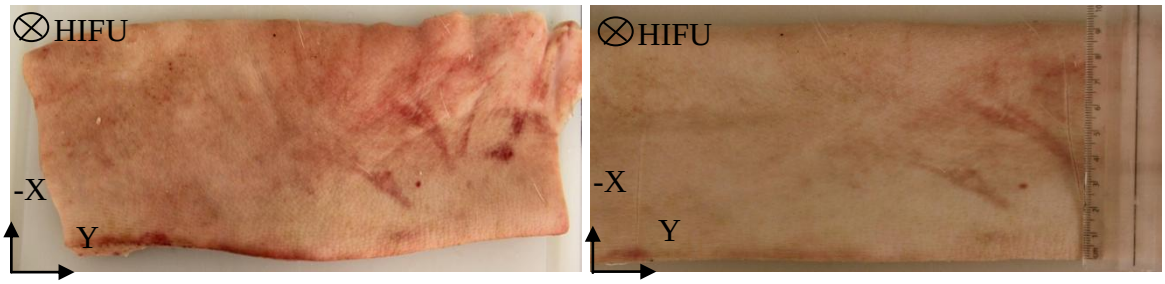

Figure 8-13: A picture showing the top view of the skin before (left) and following a scan, which consisted of 10 lines, each 2mm apart. The HIFU exposure parameters were: 0.5MHz, *in situ* pressure amplitude of 2.7MPa p-, for 30s and 20% duty cycle.

Sectioning this treated block of tissue along cutting plane 1 resulted in two identical blocks. Slicing the first one through cutting plane 2, as this was described in Figure 8-7 (right), at a depth of 15mm provided us with the result shown in Figure 8-14. The tissue was unfolded across the cut, with the two asterisks indicating the parts of the tissue that were originally attached.

There is a dramatic decolouration of the adipose tissue occurring at the expected depth and only over the treated area. Given that the scan consisted of 10 single HIFU exposures carried out at 2mm step (along the x-axis), the total area treated had a width of 20mm, which correlates very well with the extent of the resulting tissue damage, as indicated by Figure 8-14. This decolouration resulted from the disruption of the adipose cells and from fat having leaked out of the cells, which could also very well explain the blistering effect shown in Figure 8-11. Fine capillaries might also have broken due to mechanical damage, thus resulting in the leakage of red blood cells that contain haemoglobin into the extra-cellular matrix, which further explains the de-colouration of the treated adipose tissue. The stiffness of the treated area was also increased compared to the untreated one.

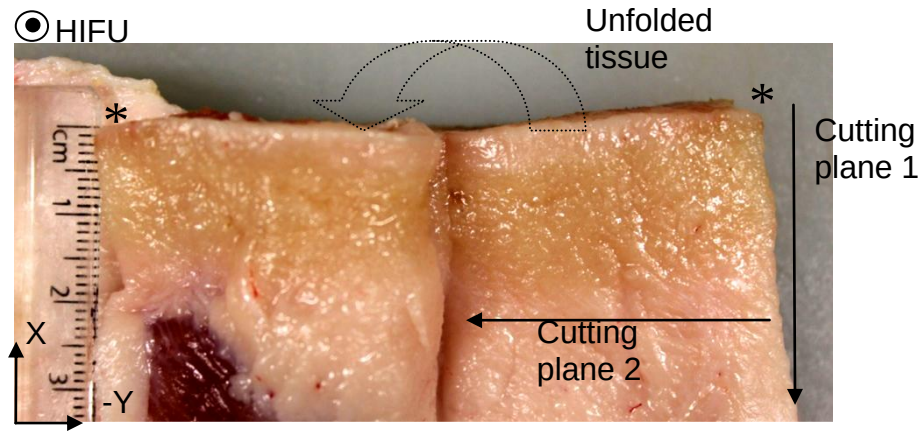

Figure 8-14: A picture showing a treated tissue after having been sectioned through cutting planes 1 and 2, at a depth of 15mm, and having been unfolded as indicated by the dotted arrow, so that the two asterisks correspond to parts of the tissue that were originally attached. The HIFU scan consisted of 10 lines, at *in situ* pressure amplitude of 2.7MPa p-, for 30s and 20% duty cycle, each 2mm apart (along the x-axis).

The second block of treated tissue was histologically processed and stained with H&E and Picro-Miller, following the protocol described in Section 3.5. Slides were cut parallel to cutting plane 1 in order to assess the tissue damage induced at a cellular level.

The resulting slides were very large and couldn't fit in one histological plate they were therefore sectioned through the middle and placed at two individual histological plates. Representative slides are shown in Figure 8-15. Figure 8-15 shows a large block of tissue, stained with Picro-Miller that was sectioned into the two halves shown in left and right respectively.

There is a very well confined area within the tissue where the damage has occurred, as indicated by the dotted rectangle. This is present around the expected treatment depth, 15mm within the tissue. No damage has been observed at any other area outside the treated one. The de-colouration of the stain, suggests that collagen has lost its integrity and is no longer healthy over the treated area. The extent of this damage is in excellent agreement with the extent of the scan, 10 x 2mm.

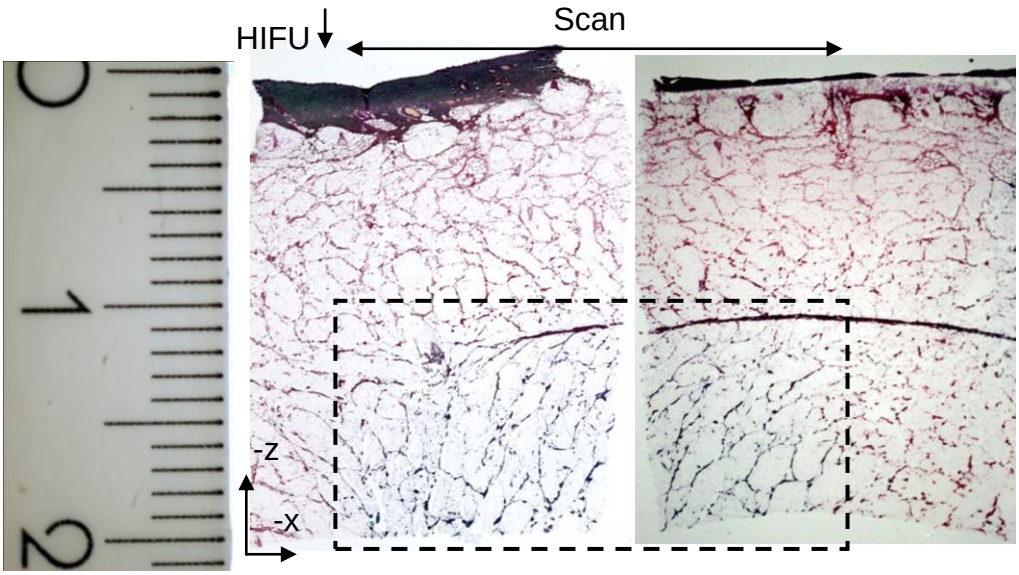

Figure 8-15: Pictures of a tissue section stained with Picro-Miller following an ultrasonic scan, which consisted of 10 lines each 2mm apart. The HIFU exposure parameters were: 0.5MHz, *in situ* pressure amplitude of 2.7MPa p-, for 30s and 20% duty cycle. There is a clear demarcation rectangular area, as indicated by the black dotted rectangular, where the collagen has been damaged.

The extent of the tissue damage depth-wise, is similar to the one obtained during single HIFU exposures at the same input parameter settings as shown in Figure 8-12. In addition, PCD signals used to localise the resulting cavitating area were also in good agreement with the induced tissue damage, as previously shown in Figure 8-8.

A closer look of the area just across the demarcation line is shown in Figure 8-16. The blue colour of the stain defines the area where the collagen has been damaged. At this higher magnification, conclusions about the cellular structure can also be drawn. The dotted line indicates the borders between damaged and healthy collagen. However, the cellular structure of the adipose tissue is mechanically damaged slightly further away than that. The connectivity of the tissue has been heavily damaged and there are many tears present. This can be explained by the fact that collagen is much stronger than adipose tissue. Given its increased strength, it is expected to be able to withstand greater pressures than adipose tissue. Under polarised lenses, shown on the right of Figure 8-16, the two areas are very distinctive, with the healthy left side showing bright orange septa and cellular membranes, whereas the unhealthy on the right appears as completely dark.

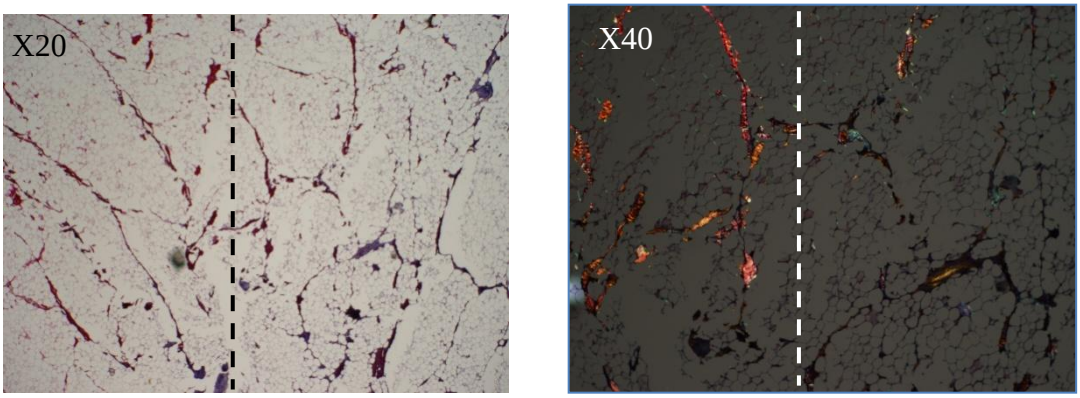

Figure 8-16: A closer look under the microscope reveals more information about the resulting damage. The red colour of the stain indicates a healthy area quite distinct from the blue damaged one, as defined by the dotted black line (left). This is further verified when part of the exact same location is seen under polarised lenses at a higher magnification, demonstrating a bright orange area to the left, next to a quite dark and unhealthy area to the right (right).

8.7.2 Histological damage for scanned exposures at 1.8 MPa, 95% duty cycle

The effects of lower pressure amplitude of 1.8MPa p- *in situ* pressure amplitude, which is above the 100% POC threshold, a shorter and more clinically relevant exposure duration of 4s and a much longer, 95%, duty cycle were also investigated. Very similar exposure conditions have already been shown to cause *in vivo* adipose tissue damage as this was demonstrated in Section 6.6.

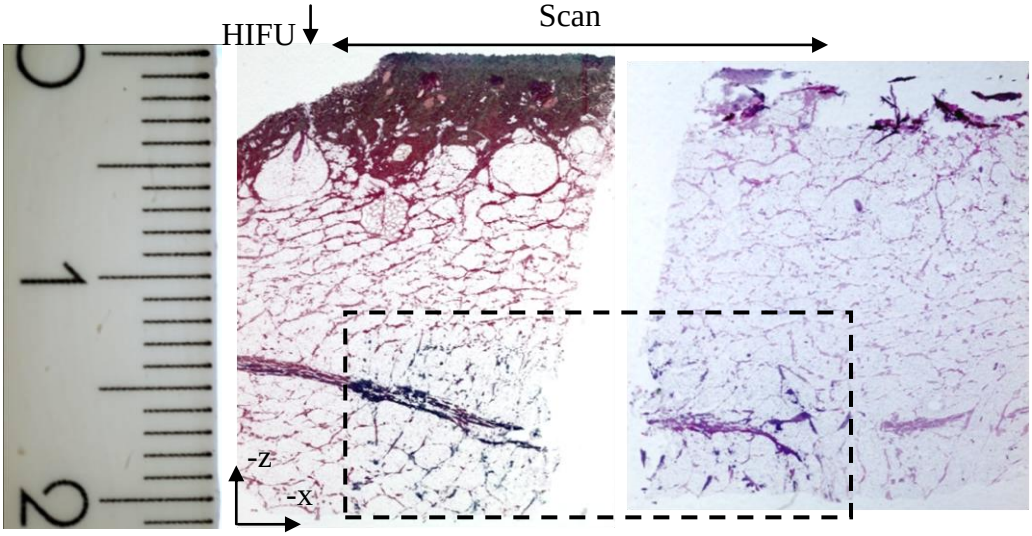

Figure 8-17: Pictures of a tissue section stained with Picro-Miller following an ultrasonic scan, which consisted of 10 lines each 2mm apart. The HIFU exposure parameters were: 0.5MHz, *in situ* pressure amplitude of 1.8MPa p-, for 4s and 95% duty cycle.

Figure 8-17 shows representative histological results obtained following a HIFU scan at these exposure conditions. The scan consisted of 10 single HIFU exposures carried out at 2mm step (along the x-axis) and the total area treated had a width of 20mm. There is a clear distinction between the unhealthy and healthy collagen across the demarcation line. Figure 8-17 shows similar collagen damage to the one previously seen in Figure 8-15, where the *in situ* pressure was 2.7MPa p-. The damaged area is once again very well localised depth-wise and also very well confined only over the area treated during the HIFU scan. The extent of the damaged collagen depth-wise is slightly shorter than the

one observed during HIFU exposures at 2.7MPa p- for 30s with 20%duty cycle shown in Figure 8-15. This is in good agreement with the fact that at 1.8MPa p- a smaller area within the adipose tissue is exposed to pressures above the cavitation threshold and thus expected to cavitate. PCD signals as shown in Figure 8-8, further verified the localisation of the HIFU focus within the adipose tissue and proved to be a reliable real-time monitoring and treatment guidance technique.

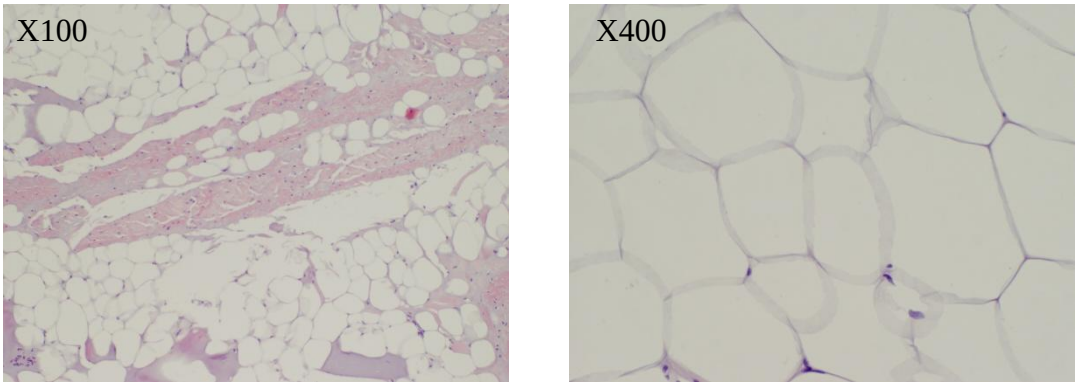

Figure 8-18: Histological slides of a tissue treated at 0.5MHz, at 1.8MPa p-, for 4s and 95% duty cycle and stained with H&E. Great loss of the cellular integrity with many tears present (left). Adipocytes with a well maintained membrane but no nuclei (right).

Figure 8-18 shows the resulting loss of cellular integrity and the many tears present. At a higher magnification, the H&E stain reveals details about the cellular structure of the adipocytes, which has been heavily mechanically damaged. This shear damage is even more obvious along the borders between the thin septa and the adipocytes. Over some regions within the treated area, the grid of the adipocytes membranes looks un-ruptured and well maintained. However, a closer look, Figure 8-18 (right), evidences that these adipocytes are no longer functional. The integrity of the membrane is maintained, however these adipocytes do no longer have a nucleus. They are empty with no cytoplasm. This is in great agreement with the de-colouration observed right after the

HIFU exposure, as shown in Figure 8-14, which is attributed to the leakage of the lipids into the extra-cellular matrix and further explains the blistering of the adipose tissue observed during HIFU exposures carried out close to the edge of the tissue as shown in Figure 8-11.

This loss of tissue connectivity was also observed during experimentation with the spherical HIFU transducer, both *ex vivo* as shown in Section 5.3 and *in vivo* as described in Section 6.6. However, treatment with the spherical HIFU induced many tears over the focal area that were surrounded by healthy tissue. However, exposures with the cylindrical HIFU transducer resulted in extensive damage throughout the focal area. This can most probably be attributed to the very well localised focal volume of the custom-built transducer, and the mitigation of shielding effects by virtue.

8.8 Summary of results obtained with the custom built, application specific HIFU transducer

The custom-designed cylindrically focused HIFU transducer proved to have several advantages over the spherical transducer used in initial experiments. Its larger focal volume enables the treatment of a larger tissue volume minimizing the treatment duration. Its tight axial profile and the very low amplitude pre-focal maxima allow for very good localisation of the acoustic energy only at the intended depth, thus leaving over-lying skin and fat tissue completely unaffected, which is an extremely important safety parameter.

HIFU exposures, even at the highest operating *in situ* focal pressure amplitude for non-clinically relevant exposure durations of 30s, resulted in gross tissue damage that was very well localised and confined only within the treated volume. This effect was also histologically verified and proved to be in excellent agreement with the macroscopically

observed tissue destruction. Most importantly, clinically relevant exposures at 1.8MPa p-, at 95% duty cycle and for 4s, resulted in similar tissue damage that was well and truly confined to the desired treatment depth.

Based on the *ex vivo* results presented in this chapter, we can conclude that the use of this cylindrically focused HIFU transducer in a clinical environment is optimal since it satisfies all the specifications of the project. It ensures very well localised and confined tissue damage, without affecting any of the overlying tissue, while the PCD signal provides the user with real-time information about the extent and the location of cavitation activity throughout the duration of the exposure.

9 Conclusions

The work presented here is an experimental approach carried out *ex vivo* and *in vivo* aiming to investigate the potential use of HIFU for the non-invasive destruction of subcutaneous adipose tissue. The findings of the present study suggest that the use of low-frequency 0.5 MHz HIFU excitation would have multiple advantages both for the treatment of subcutaneous fat but also for the monitoring of the treatment, its efficacy and safety in real-time. All conclusions reached based on experimental results described so far are summarised hereafter.

The first major objective of the present study was to define the optimal operating frequency for this particular application. In order to be able to compare pressure amplitudes across different frequencies a very detailed *in situ* calibration was carried out. Using an implantable needle hydrophone, the transmission losses through skin and fat were measured and the attenuation coefficient of fat at each of the four frequencies investigated was computed. The attenuation coefficients of fat layer were found to be 0.66dB/cm, 2.17dB/cm, 3.19dB/cm and 5.76db/cm at 0.5, 1.1, 1.6 and 3.4MHz respectively.

The level of cavitation activity and focal temperature rises induced by HIFU at 0.5, 1.1, 1.6 and 3.4MHz in excised subcutaneous porcine fat for spatial-peak temporal average intensities in the range 0-250W/cm^2 and exposure durations in the range 2-4s were measured across several tissue samples from different donor animals and were presented in Chapter 4. Based on the signals received by the co-axially aligned PCD, strong cavitation activity was found to be readily initiated at 0.5MHz, for pressure amplitudes in excess of 1.6MPa p-, which was defined as the 100% POC threshold *ex vivo*. Inertial

cavitation activity could not be initiated at 1.1MHz for *in situ* peak rarefactional pressures of up to 2.1Ma p- , at 1.6MHz for up to 1.72 MPa p- and at 3.4MHz for up to 1.22MPa p-.

Taking into account both the cavitation and the simultaneously obtained temperature measurements at 0.5MHz, it was concluded that inertial cavitation is associated with localized heating at rates well above those present in the absence of cavitation, when linear heating is the primary cause of the temperature rise, which is consistent with previous observations of cavitation-enhanced-heating in tissue-mimicking materials (Coussios et al. 2007;Coussios and Roy 2008;Holt and Roy 2001).

At the higher frequencies, the temperature rises achieved exhibit a linear correlation with the acoustic intensity as expected on the basis of linear acoustic absorption theory. At the highest operating frequency, 3.4MHz, the highest acoustic intensities resulted in lower maximum focal temperatures than expected. It was hypothesized that this is due to higher levels of non-linear propagation at 3.4MHz in fat, resulting in increased pre-focal attenuation of the acoustic wave. Comparing the mean maximum temperatures achieved at similar acoustic intensities across the four operating frequencies showed that there is no single frequency that greatly favours heat deposition, as the resulting peak temperature rises are broadly comparable. However, lower frequencies have greater focal volumes and thus result in a bigger treated volume, which consequently means shorter treatment time, a very important parameter that needs to be taken into account if a real clinical application is to be developed.

Given the experimental results described in Chapter 4, it was concluded that 0.5MHz is the optimal frequency for this application since it enables the reliable generation of focal

cavitation activity at moderate pressure amplitudes which is a significant safety consideration given the close proximity of skin. In addition, focal cavitation activity can be readily monitored non-invasively using a passive cavitation detector and therefore provide a means of non-invasive monitoring of the treatment, while it was also found to enhance local heat deposition over the range of pressure amplitudes that did not result in excessive shielding due to pre-focal cavitation.

Preliminary histological results presented in Chapter 5 enabled us to visualise, and localise the resulting tissue damage following a cavitation inducing HIFU exposure. It was shown that HIFU exposures at 0.5MHz, at pressure amplitudes above the 100% POC threshold and for exposure durations as short as 4s are capable of causing observable tissue damage at a cellular level. Unfortunately, skin burns were also present at some of the treated samples, a side-effect that was attributed to the rather long focal depth of the spherical HIFU transducer used for this initial set of experiments.

Based on the findings obtained in the laboratory, a set of *in vivo* experiments was then conducted. The first objective was to define the 100% POC threshold *in* vivo, which was found to be 1.6MPa p- at 0.5MHz, a result that is in very good agreement with the one defined during *ex vivo* measurements. The co-axially aligned PCD proved to be a very reliable means of monitoring the extent and the evolution of inertial cavitation activity during experimentation while it also verified that the contact between the applicator and the skin was achieved and maintained at all times. The PCD signal received at the three pressure amplitudes investigated *in vivo* was of a similar order of magnitude to the one received at the same pressure amplitudes during *ex* vivo experimentation. Histological results revealed extensive tissue damage following cavitation-inducing HIFU exposures up to four days after the treatment. In addition, a histological study performed to adipose

tissue a month after the treatment, revealed no signs of cellular destruction. However, these *in vivo* experiments pointed out some limitations of the existing system that were addressed further in Chapter 8.

The second major objective of the present study was to investigate the potential use of a diagnostic transducer for the real-time monitoring of the treatment, its efficacy and safety. The correlation between broadband noise emissions that can be remotely sensed by a passive cavitation detector (PCD) and focal temperature rise was therefore explored further in Chapter 7. The results obtained make it possible to suggest that if cavitation activity above a certain value is detected, then a certain minimum temperature rise has been achieved at the focus. These results are particularly useful for 2s exposures, where little heat conduction occurs, but less so for 4s exposures where heat diffusion damages the correlation. For shorter exposures, cavitation-based thermometry could therefore be used as a positive indicator of successful treatment delivery.

In addition, the co-axially aligned PCD proved to be a reliable means of monitoring the location of the front bubble cloud within the tissue and thus provides real-time feedback that treatment is occurring at the expected depth. Histological results confirmed that damage is coincident with the location of the front of the bubble cloud as determined by the PCD signal. Furthermore, quantification of the volumetric extent of tissue damage at multiple locations along the axis of sound propagation showed that tissue damage was maximized around the HIFU focus, was very well confined within the expected cavitating area and that it occurred during the first seconds of an exposure. It was concluded that lengthening the exposure duration didn’t offer much added benefit in terms of adipose tissue damage

In order to address the limitations brought about by the original HIFU transducer design, an application-specific treatment system was designed and constructed. This comprised a cylindrically focused HIFU transducer with a very tight axial profile capable of delivering the required focal pressures exclusively at the required treatment depth, and a custom-built cylindrically focused passive detector capable of detecting cavitation activity over the focal volume of the new HIFU transducer. Additionally, a new interface allowed the real-time display of the variance of the received PCD signal and the location of the front of the bubble cloud. Histological results obtained using this system showed highly localized tissue damage occurring at the intended depth and confined to the treated area only, even at pressure amplitudes much greater than the 100% POC threshold. In particular, damaged collagen, loss of cellular integrity and loss of adipocyte nuclei was observed in regions that had been exposed to HIFU-induced cavitation at 0.5 MHz. These results were even more apparent when multiple lesions were juxtaposed, creating a uniform and contiguous area of damaged adipose tissue and demonstrating the clinical relevance of the custom-designed ultrasonic lipolysis system.

9.1 Further work

In order for this technique to be used in a clinical environment, some further work needs to be carried out based on the findings presented here. A second set of *in vivo* experiments needs to be performed using the application-specific cylindrical HIFU transducer and the real-time monitoring system presented in Chapter 8. These *in vivo* experiments should aim to treat a large area of subcutaneous adipose tissue, similar to what was performed *ex vivo*. The thickness of the tissue before and after treatment should be measured and will be used as a means to assess the efficacy of the procedure. In addition, medical

measurements of vital signs, *i.e.* heart rate, SpO2 and ventilator rate, should also be monitored with a veterinary monitoring system during the treatment.

The primary aim of these *in vivo* experiments will be to identify the long-term effects of HIFU-induced lipolysis, the type of inflammatory response that it causes, and the state of the tissue following macrophage activity. This may lead to new treatment guidelines as to the maximum area of adipose tissue that should be exposed during any one treatment, and the appropriate time interval in-between consecutive HIFU treatments. The question of whether the entire targeted area of adipose tissue should be treated, or whether untreated patches of tissue should be left as 'anchors' in between treated areas to avoid detachment of the subcutaneous fat layer from skin and muscle should also be investigated.

Following the outcome of the final *in vivo* set of experiment, clinical trials need to be carried out prior to commercialisation of a HIFU device for non-invasive destruction of adipose tissue based on the experimental parameters defined by the present study.

The long term effect of the treatment is an issue of major medical importance that needs to be fully investigated if this technique is to be clinically used. The two major concerns are the maximum amount of damaged adipose tissue the human body can safely process and the histological and aesthetic appearance of skin and underlying tissues following lipolysis. The work presented here is a firm basis upon which a clinically relevant system can be developed. It is believed that the novel system developed as part of this thesis has identified the treatment parameters which will enable the treatment of large areas of tissue, thus minimizing treatment times, with minimal levels of acoustic energy, thus maximizing treatment safety. It is very much hoped that future studies will address the

remaining medical issues in order for this technique to be used in a clinical environment in the near future.

Appendix A

List of scientific publications and patents

Z.M. Kyriakou, M. Ignasi Corral-Baques, A. Amat, C.-C. Coussios , "HIFU-induced cavitation and heating in subcutaneous fat", Ultrasound in Medicine and Biology (in press)

Z. Kyriakou, J. Collin, T. Ansari, M. Ignasi Corral, A. Amat, C.-C. Coussios, "Instigation and localisation of HIFU-induced cavitation activity in subcutaneous fat and histological assessment of associated tissue damage", 10th International Symposium on Therapeutic Ultrasound, Tokyo, Japan (2010)

Z.M. Kyriakou, M. Ignasi Corral-Baques, A. Amat, C.-C. Coussios, "Characterization of HIFU-induced cavitation activity and heating in porcine subcutaneous fat", 9th International Symposium on Therapeutic Ultrasound, Aix-en-Provence, France (2009)

Inventor in the 08160842.4 – 1240 European patent application

Appendix B

During all calibrations the signal generator output voltage, the input voltage to the matching network and the output voltage of the hydrophone were recorded and compared while the calibration setup was always kept the same to achieve reproducibility and to minimize potential errors.

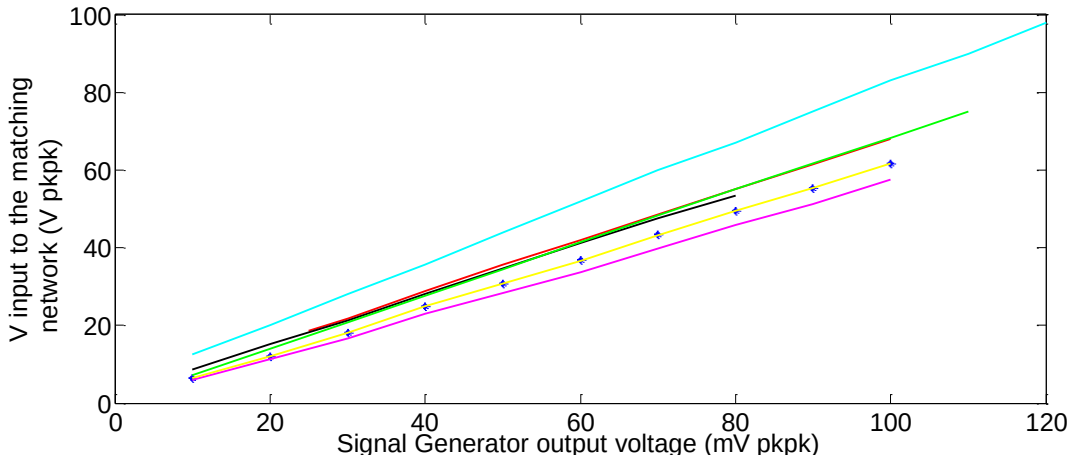

Figure B- 1: The input to the matching network at a given output voltage setting of the function generator at 0.5MHz for short-pulses (10 cycles). Different colors represent different measurements carried out throughout the duration of this research.

According to Figure B-1, which summarizes all the calibrations performed at 0.5MHz, for a given output voltage setting of the function generator the input to the matching network lays within a very narrow range of values and therefore can be at all times estimated. This is a very reasonable and expected result since the amplifier has a constant gain of 55 dB for 0.3-35MHz and the total impedance of the matching network and the transducer at that frequency has a constant value of approximately 50 Ohms. The only exception was the measurement carried out in July 2008 shown in light blue, which gave slightly higher voltages for the same input voltage settings and was therefore not taken into account. The mean average value from the rest of the measurements for the input

voltage to the matching network given a signal generator output voltage setting was used for further reference.

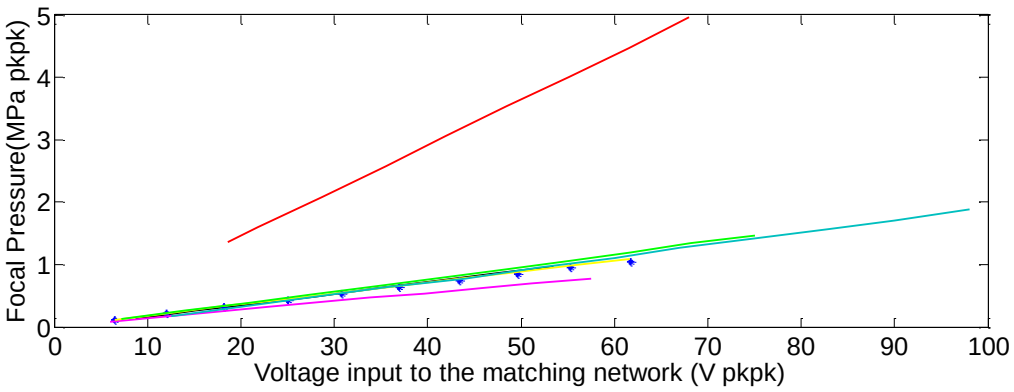

Figure B- 2: The focal pressures of the HIFU transducer at a given output voltage of the matching network at 0.5MHz for short-pulses (10 cycles). Different colors represent different measurements carried out throughout the duration of this research.

Results obtained for the pkpk focal pressure are shown in Figure B-2. With the exception of the October 2007 calibration (shown in red), for which the hydrophone was found to be faulty, all other calibrations are in close.

Identical measurements were carried out *in situ* under the exact same experimental condition in order to calculate the *insertion loss factor* as this is shown in Table 4-2. Taking the mean of non-discarded calibrations and including the effect of the transmission loss due to the propagation of sound through multiple tissue layers resulted in Figure B-3. These calibrations, and associated linear-fit equations as shown in Tables 4-1 and 4-2, were used as the gold standard for all pressures reported.

For the higher frequency, a different matching network is needed and the total input impedance of the matching network and the transducer changes, therefore the exact same measurements were also performed at all higher frequencies used for this research.

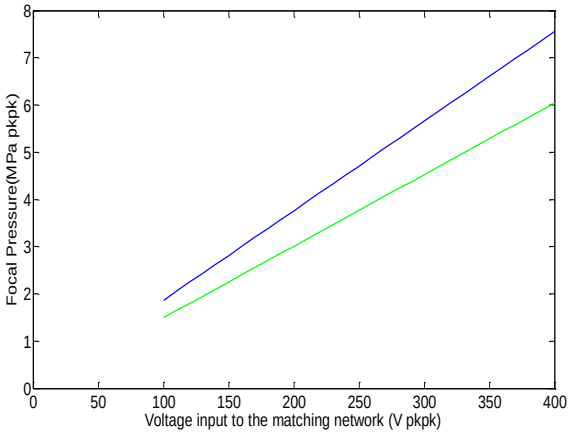

Figure B- 3: Calibration data at 0.5MHz in the free field and *in situ* shown in blue and green respectively.

Bibliography

Ablaza V.J., Gingrass M.K., Larry P.C., Fisher J., Patrick M.G. Tissue temperatures during ultrasound-assisted lipolysis. Plastic and Reconstructive Surgery, Journal of the American Society of Plastic Surgeons 1998;102(2):534-542.

Ablaza V.J., Gingrass M.K., Larry P.C., Fisher J., Patrick M.G. Tissue temperatures during ultrasound-assisted lypolysis. Plastic and Reconstructive Surgery, Journal of the American Society of Plastic Surgeons 1998;102(2):534-542.

Apfel R.E. Acoustic Cavitation, Methods Expt. Physics (ed. PD Edmonds) 1981;19:355–411.

Apfel R.E. Acoustic cavitation series. 4. Acoustic cavitation inception. Ultrasonics 1984;22(4):167-173.

Apfel R.E., Holland C.K. Gauging the likelihood of cavitation from short-pulse, low duty cycle diagnostic ultrasound. Ultrasound in Medicine and Biology 1991;17(2):179-185.

Atchley A.A., Prosperetti A. The crevice model of bubble nucleation. Journal of the Acoustical Society of America 1989;86(3):1065-1084.

Avram A.S., Avram M.M., James W.D. Subcutaneous fat in normal and diseased states 2. Anatomy and physiology of white and brown adipose tissue. Journal of the American Academy of Dermatology 2005;53:671-683.

Bancroft J.D., Cook H.C. Manual of histological techniques and their diagnostic applications. Edinburgh: Churchill Livingstone, 1994.

Barnett S.B., ter Haar G.R., Ziskin M.C., Nyborg W.L., Maeda K., Bang J. Current status of research on biophysical effects of ultrasound. Ultrasound in Medicine & Biology 1994;20(3):205-218.

Bohris C., Jenne J.W., Raster R., Simiantonakis I., Brix G., Spp J., Hlavac M., Nemeth R., Huber P.E., Debus J. MR monitoring of focused ultrasound surgery in a breast tissue model in vivo. Magnetic Resonance Imaging 2001;19(2):167-175.

Brennen C.E. Cavitation and bubble dynamics: New York; Oxford: Oxford University Press, 1995.

Cedidi C.C., Berger A. Severe abdominal wall necrosis after ultrasound-assisted liposuction. Aesthetic Plastic Surgery 2002;26:20-22.

Chivers R.C., Hill C.R. Ultrasonic attenuation in human tissue. Ultrasound in Medicine & Biology 1975;2(1):25-29.

Chivers R.C., Parry R.J. Ultrasonic velocity and attenuation in mammalian tissues. Journal of the Acoustical Society of America 1978;63(3):940-953.

Church C. C. Prediction of rectified diffusion during nonlinear bubble pulsations at biomedical frequencies. Journal of the Acoustical Society of America 1988;83(6):2210-2217.

Church C.C. Spontaneous homogeneous nucleation, inertial cavitation and the safety of diagnostic ultrasound. Ultrasound in Medicine & Biology 2002;28(10):1349-1364.

Cinti S. The adipose organ. Prostaglandins, leukotrienes, and essential fatty acids 2005;73:9-15.

Collin J.R.T. (2009). Detection and interpretation of thermally relevant cavitation during HIFU exposure, Department of Engineering Science, University of Oxford, Doctor of Philosophy.

Cook H.C. Manual of histological demonstration techniques. London: Butterworths, 1974.

Coussios C.C., Collin J.R.T., Muckle A.J. Non-invasive monitoring and control of inertial cavitation dynamics during HIFU exposure in vitro. 6th International Symposium on Therapeutic Ultrasound 2006:316-321.

Coussios C.C., Farny C.H., ter Haar G., Roy R.A. Role of acoustic cavitation in the delivery and monitoring of cancer treatment by high-intensity focused ultrasound (HIFU). International Journal of Hyperthermia 2007;23(2):105 - 120.

Coussios C.C., Roy R.A. Applications of acoustics and cavitation to noninvasive therapy and drug delivery. Annu Rev Fluid Mech 2008;40:395-420.

Datta S., Coussios C.C., McAdory L.E., Tan J., Porter T., De Courten-Myers G., Holland C. K. Correlation of cavitation with ultrasound enhancement of thrombolysis. Ultrasound in Medicine & Biology 2006;32(8):1257-1267.

Eller A., Flynn H.G. Rectified diffusion during nonlinear pulsations of cavitation bubbles. Journal of the Acoustical Society of America 1965;37(3):493-503.

Errabolu R.L., Sehgal C.M., Bahn R.C., Greenleaf J.F. Measurement of ultrasonic nonlinear parameter in excised fat tissues. Ultrasound in Medicine & Biology 1988;14(2):137-146.

Farny C.H. (2006). Identifying and monitoring the roles of cavitation in heating from high intensity focussed ultrasound. Department of Aerospace and Mechanical Engineering, Boston University, PhD.

Ferraro G.A., De Francesco F., Nicoletti G., Rosano F., D'Andrea F. Histologic effects of external ultrasound-assisted lipectomy on adipose tissue. Aesthetic Plastic Surgery 2008;32:111-115.

Fry W.J., Fry R.B. Determination of Absolute Sound Levels and Acoustic Absorption Coefficinets by Thermocouple Probes-Experiment. Journal of the Acoustical Society of America 1954a;26(3):311-317.

Fry W.J., Fry R.B. Determination of Absolute Sound Levels and Acoustic Absorption Coefficinets by Thermocouple Probes-Theory. Journal of the Acoustical Society of America 1954b;26(3):294-310.

Fujishiro S., Mitsumori M., Nishimura Y., Okuno Y., Nagata Y., Hiraoka M., Sano T., Marume T., Takayama N. Increased heating efficiency of hyperthermia using an ultrasound contrast agent: a phantom study. International Journal of Hyperthermia 1998;14(5):495-502.

Gaertner W. Frequency dependence of ultrasonic cavitation. Journal of the Acoustical Society of America 1954;26(6):977-980.

Giuseppe A.Ferraro Francesco De Francesco, Gianfranco Nicoletti, Ferdinando Rossano, Francesco D'Andrea. Histologic Effects of External Ultrasound-Assisted Lipectomy on Adipose Tissue. Aesthetic Plastic Srgery 2007;32:111-115.

Goss S.A., Johnston R.L., Dunn F. Comprehensive compilation of empirical ultrasonic properties of mammalian tissues. Journal of the Acoustical Society of America 1978;64:423-447.

Gyö ngy M., Coussios C.C. Passive spatial mapping of inertial cavitation during HIFU exposure. IEEE Transactions on Biomedical Engineering, 2010;57(1).

Hall T.L., Fowlkes J.B. A real-time measure of cavitation induced tissue disruption by ultrasound imaging bacscatter reduction. IEEE Transactions on Ultrasonics, Ferroeletrics, and Frequency Control 2007;54(3):569-575.

Hamilton M.F., Blackstock D.T. Nonlinear acousics: theory and applications. San Diego, California: Academic Press, 1998.

Hashemi R.H., Bradley W.G., Lisanti C.J. MRI the basics: Lippincott Williams & Walkins.,

Hilgenfeldt S., Lohse D. The acoustics of diagnostic microbubbles: dissipative effects and heat deposition. Ultrasonics 2000;38(1-8):99-104.

Hill C.R. Optimum acoustic frequency for focused ultrasound surgery. Ultrasound in Medicine & Biology 1994;20(3):271-277.

Hill C.R., Bamber J.C., Haar G.R. Physical Principles of Medical Ultrasonics. London: Ellis Horwood, 1986.

Holland C.K., Apfel R.E. Thresholds for transient cavitation produced by pulsed ultrasound in a controlled nuclei environment. Journal of the Acoustical Society of America 1990;88(5):2059-2069.

Holland C.K., Deng C.X., Apfel R.E., Alderman J.L., Fernandez L.A., Taylor K.J.W. Direct evidence of cavitation in vivo from diagnostic ultrasound. Ultrasound in Medicine and Biology 1996;22(7):917-925.

Holt R.G., Roy R.A. Measurements of bubble-enhanced heating from focused, MHz-frequency ultrasound in a tissue-mimicking material. Ultrasound in Medicine & Biology 2001;27(10):1399-1412.

Holt R.G., Roy R.A. (2005). Bubble dynamics in therapeutic ultrasound. Bubble and particle dynamics in acoustic fields: Modern trends and applications. A. Dionikov. Kerala, Transworld Research Network**:** 108-229.

Hynynen K. The threshold for thermally significant cavitation in dog thigh muscle in vivo. Ultrasound in Medicine and Biology 1991;17(2):157-169.

Hynynen K., Martin C. J., Watmough D. J., Mallard J. R. Errors in temperature-measurement by thermocouple probes during ultrasound induced hyperthermia. British Journal of Radiology 1983;56(672):969-970.

Jeffers J., Feng R.Q., Fowlkes J.B., Brenner D.E., Cain C.A. Sonodynamic therapy: activation of anticancer agents with ultrasound. Ultrasonics Symposium, 1991. Proceedings IEEE 1991:1367-1370.

Kennedy J.E. High-intensity focused ultrasound in the treatment of solid tumours. Nature Reviews Cancer 2005;5(4):321-327.

Kennedy P., Arora M., Coussios C.C. Localization and interpretation of bubble activity during HIFU exposure. AIP Conference Proceedings 2009;1113:68-72.

Kerr J.B. Atlas of functional histology: Elsevier Health Sciences, 1999.

Khokhlova V.A., Bailey M.R., Reed J.A., Cunitz B.W., Kaczkowski P.J., Crum L.A. Effects of nonlinear propagation, cavitation, and boiling in lesion formation by high intensity focused ultrasound in a gel phantom. Journal of the Acoustical Society of America 2006;119(3):1834-1848.

Kino G.S. Acoustic waves: Devices, imaging and analog signal processing. Englewood Cliffs,NJ: Prentice-Hall, 1987:189-191.

Law WK, Frizzell LA, Dunn F. Determination of the nonlinearity parameter B/A of biological media. Ultrasound in Medicine & Biology 1985;11(2):307-318.

Lawrence N., Cox S.E. The efficacy of external ultrasound-assisted liposuction: a randomized controlled trial

Dermatologic Surgery 2000;26:329-332.

Leighton T.G., Fedele F., Coleman A.J., McCarthy C., Ryves S., Hurrell A.M., De Stefano A., White R.R. A passive acoustic device for real-time monitoring of the efficacy of shockwave lithothripsy treatment. Ultrasound in Med. & Biol., 2008;34(10):1651-1665.

Leighton TG. The Acoustic Bubble. London: Academic Press, 1994.

Lynn J.G., Zwemer R.L., Chick A.J., Miller A.E. A new method for the generation and use of focused ultrasound in experimental biology. J Gen Physiol 1942;26.

Madanshetty S.I., Roy R.A., Apfel R.E. Acoustic microcavitataion: its active and passive acoustic detection. Journal of the Acoustical Society of America 1991;90(3):1515-1526.

Mast T. D. Empirical relationships between acoustic parameters in human soft tissues. Acoustics Research Letters Online 2000;1:37.

Mast T. Douglas, Salgaonkar Vasant A., Karunakaran Chandrapriya, Besse John A., Datta Saurabh, Holland Christy K. Acoustic Emissions During 3.1 MHz Ultrasound Bulk Ablation In Vitro. Ultrasound in Medicine & Biology 2008;34(9):1434-1448.

McDannold N., Vykhodtseva N., Hynynen K. Targeted disruption of the blood-brain barrier with focused ultrasound: association with cavitation activity. Physics in Medicine and Biology 2006;51(4):793-807.

McLaughlan J., Rivens I., Leighton T., Ter Haar G.R. A study of bubble activity generated in ex vivo tissue by high intensity focused ultrasound. Ultrasound in Medicine & Biology 2010;36(8):1327--1344.

Mellen R. H. Ultrasonic Spectrum of Cavitation Noise in Water. The Journal of the Acoustical Society of America 1954;26:356.

Mendes F.H. External Ultrasound-Assisted Lipoplasty from our own experience. Aesthetic Plastic Surgery 2000;24:270-274.

Mitragotri S. Healing sound: the use of ultrasound in drug delivery and other therapeutic applications. Nature Reviews Drug Discovery 2005;4:255-260.

Morris H., Rivens I., Shaw A., ter Haar G. Investigation of the viscous heating artefact arising from the use of thermocouples in a focused ultrasound field. Physics in Medicine and Biology 2008;53.

Morse P.M., Ingard K. U. Theoretical Acoustics. New York, 1968.

Muir T.G., Carstensen E.L. Prediction of nonlinear acoustic effectc at biomedical frequencies and intensities. Ultrasound in Medicine & Biology 1980;6:345-357.

Neppiras E. A. Acoustic cavitation. Physics Reports 1980;61(3):159-251.

Nyborg W.L. Physical mechanisms for biological effects of ultrasound. DHEW Publication (FDA) 1978;78:8062.

Nyborg W.L. Biological effects of ultrasound: Development of safety guidelines. Part II: General Overview. Ultrasound in Medicine & Biology 2001;27(3):301-333.

O'Neil H.T. Theory of focusing radiators. The Journal of the Acoustical Society of America 1949;21(5):516-526.

Owen N.R., Bailey M.R., Hossack J., Crum L.A. A method to synchronize high-intensity, focused ultrasound with an arbitrary ultrasound imager. IEEETransactions on Ultrasonics Ferroelectrics and Frequency Control 2006;53(3):645-650.

Perez J.A., van Tetering J.P.B. Ultrasound-Assisted Lipoplasty: A review of over 350 consecutive cases using a two-stage technique. Aesthetic Plastic Surgery 2003;27:68-76.

Phelps A.D., Leighton T.G. The subharmonic oscillations and combination-frequency emissions from a resonant bubble: their properties and generation mechanisms Acta Acoustica 1997;83:59-66

Pond C. The fats of life. Cambridge: Cambridge University Press, 1998.

Prosperetti A. Thermal effects and damping mechanisms in forced radial oscillations of gas-bubbles in liquids. Journal of the Acoustical Society of America 1977;61(1):17-27.

Prosperetti A. Acoustic cavitation series.2. Bubble phenomena in sound fields1. Ultrasonics 1984;22(2):69-78.

Rabkin B.A., Zderic V., Crum L.A., Vaezy S. Biological and physical mechanisms of HIFU-induced hyperecho in ultrasound images. Ultrasound in Medicine & Biology 2006;32(11):1721-1729.

Rabkin B.A., Zderic V., Vaezy S. Hyperecho in ultrasound images of HIFU therapy: involvement of cavitation. Ultrasound in Medicine and Biology 2005;31(7):947-956.

Rivens I., Shaw A., Civale J., Morris H. Treatment monitoring and thermometry for therapeutic focused ultrasound. International Journal of Hyperthermia 2007;23(2):121 - 139.

Roberts W.W., Hall T.L., Ives K., Wolf J.S., Fowlkes J.B., Cain C.A. Pulsed cavitational ultrasound: a noninvasive technology for controlled tissue ablation (histotripsy) in the rabbit kidney. Journal of Urology 2006;175(2):734-738.

Rohrich R.J., Beran S.J., Kenkel J., Adams W.P., Di Spaltro F. Extending the role of liposuction in body contouring with ultrasound-assisted liposuction. Plastic and Reconstructive Surgery, Journal of the American Society of Plastic Surgeons 1998;101(4):1090-1102.

Ross M.H., Reith E.J., Romrell L.J., with illustrations by Kibiuk L.V. Histology: a text and atlas: Baltimore ; London : Williams & Wilkins, c1989, 1989.

Roy R.A., Madanshetty S.I., Apfel R.E. An acoustic backscattering technique for the detection of transient cavitation produced by microsecond pulses of ultrasound. Journal of the Acoustical Society of America 1990;87(6):2451-2458.

Sehgal C.M., Bahn R.C., Greenleaf J. F. Measurement of the acoustic nonlinearity parameter B/A in human tissues by a thermodynamic method

Journal of the Acoustical Society of America 1984;76(4).

Sokka S.D., Gauthier T.P., Hynynen K. Theoretical and experimental validation of a dual-frequency excitation method for spatial control of cavitation. Physics in Medicine and Biology 2005;50(9):2167-2179.

Spalding K.L., Arner E, Westermark P.O., Bernard S, Buchholz B.A., Bergmann O, Blomqvist L, Hoffstedt J, Nä slund E, Britton T, Concha H, Hassan M, Rydén M, Frisén J, Arner P. Dynamics of fat cell turnover in humans. Nature Reviews Drug Discovery 2008;453(7196):783-787.

Sternberg S. Histology for pathologists: Lippincott-Raven, 1992.

Sterry W., Paus R., Burgdorf W. Thieme clinical companions. Dermatology.: Thieme, 2006.

Szabo TM. Diagnostic Ultrasound Imaging: Inside Out. London: Elsevier Academic Press, 2004.

ter Haar G. Ultrasound focal beam surgery. Ultrasound in Medicine & Biology 1995;21(9):1089-1100.

ter Haar G., Coussios C.C. High Intensity Focused Ultrasound: Past, present and future. International Journal of Hyperthermia 2007;23(2):85 - 87.

ter Haar G., Coussios C.C. High intensity focused ultrasound: Physical principles and devices. International Journal of Hyperthermia 2007;23(2):89 - 104.

ter Haar G., Sinnett D., Rivens I. High intensity focused ultrasound - a surgical technique for the treament of discrete liver tumours. Physics in Medicine & Biology 1989;34(11):1743-1750.

ter Haar G.R., Daniels S. Evidence of ultrasonically induced cavitation in vivo. Physics in Medicine and Biology 1981;26(6):1145-1149.

Thomas C.R., Farny C.H., Coussios C.C., Roy R.A., Holt R.G. Dynamics and control of cavitation during high-intensity focused ultrasound application. Acoustics Research Letters Online 2005;6(3):182-187.

Tran B.C., Seo J., Hall T.L., Fowlkes J.B., Cain C.A. Microbubble-enhanced cavitation for noninvasive ultrasound surgery. IEEETransactions on Ultrasonics Ferroelectrics and Frequency Control 2003;50(10):1296-1304.

Trayhurn P. Adipocyte biology. Obesity Reviews 2006;8 (Suppl. 1):41-44.

Tung Y.S., Liu H.L., Wu C.C., Ju K.C., Chen W.S., Lin W.L. Contrast-agent-enhanced ultrasound thermal ablation. Ultrasound in Medicine & Biology 2006;32(7):11103-11110.

Umemura S., Kawabata K., Hashiba K., Eds. (2001). Enhancement of ultrasonic absorption by microbubbles for therapeutic application. Ultrasonics Symposium, 2001 IEEE. Arlanta, GA, USA.

Vaezy S., Shi X.G., Martin R.W., Chi E., Nelson P.I., Bailey M.R., Crum L.A. Real-time visualization of high-intensity focused ultrasound treatment using ultrasound imaging. Ultrasound in Medicine & Biology 2001;27(1):33-42.

Walgenbach K.J., Riabikhin A.W., Galla T.J., Bannasch H., Voigt M., Andree C., Horch R.E., Stark G.B. Effect of ultrasonic assisted lipectomy (UAL) on breast tissue: Histologic findings. Aesthetic Plastic Surgery 2001;25:85-88.

Watkin N.A., ter Haar G.R., Rivens I. The intensity dependence of the site of maximal energy deposition in focused ultrasound surgery. Ultrasound in Medicine & Biology 1996;22(4):483-491.

Webb I., Arora M., Roy R.A., Payne S.J., Coussios C.-C. Dynamics of gas bubbles in time-variant temperature fields. J Fluid Mech 2010 - in press.

Wu F., Wang Z.B., Chen W.Z., Zou J.Z., Bai J., Zhu H., Li K.Q., Xie F.L., Jin C.B., Su H.B., Gao G.W. Extracorporal focused ultrasound surgery for treatment of human solid carcinomas: early chinese clinical experience. Ultrasound in Medicine & Biology 2004;30(2):245-260.

Ziskin M.C., Petitti D.B. Epidemiology of human exposure to ultrasound: a critical review. Ultrasound in Medicine & Biology 1988;14(2):91-96.

Zocchi M. Ultrasonic Liposculpturing. Aesthetic Plastic Surgery 1992;16:287-298.